UNIVERSITÀ DEGLI STUDI DI FOGGIA

DOTTORATO DI RICERCA IN
"INNOVAZIONE E MANAGEMENT DEGLI ALIMENTI AD ELEVATA VALENZA SALUTISTICA"
(XXXI CICLO)

COORDINATORE: PROF. MATTEO ALESSANDRO DEL NOBILE

NAD^+ AND AGING: A FOCUS ON NOVEL MOLECULAR MECHANISMS OF WERNER SYNDROME

Dottoranda: Dr. Domenica Caponio

Tutor: Prof.ssa Claudia Piccoli

ANNO ACCADEMICO 2017/2018

INDEX

ABSTRACT

The Werner syndrome (WS) is an autosomal recessive premature aging disease associated with mutation of the *Werner* gene, which encodes the RecQ family DNA helicase WRN. While accumulation of DNA damage in WS is contributed by the loss of DNA repair activity due to WRN dysfunction, mechanisms of other major WS phenotypes, such as mitochondrial dysfunction, impaired mitophagy and stem cell dysfunction, are largely elusive. WS patients exhibit severe metabolic phenotypes, but the underlying mechanisms are unknown and whether the metabolic deficit can be targeted for therapeutic intervention has not been determined. Our data from WS invertebrate models to human WS patient cells show depletion of a fundamental cofactor NAD^+ induces mitochondrial dysfunction and premature aging. WRN also regulates transcription of NMNAT1 (nicotinamide nucleotide adenylytransferase 1), a key enzyme in NAD^+ biosynthetic pathway. NAD^+ repletion improves lifespan and healthspan in our WS animal models, restores metabolic profiles and improves mitochondrial quality through DCT-1 and ULK-1-dependent mitophagy. We further asked whether NAD^+ depletion contributes to stem cell dysfunction in WS. We studied this hypothesis by investigating changes of both germ-line mitotic cells in WS *C. elegans* and intestinal stem cell (ISC) population in WS *Drosophila*. Intriguingly NAD^+ repletion almost completely restored stem cell proliferation in both WS models.

This work highlights a novel role of NAD^+ in healthy aging and suggests a new therapeutic strategy for WS, a disease currently incurable.

INTRODUCTION

I. Aging

Aging is the most fundamental challenge in humans. Since it is associated with an increased risk factor for several diseases, including cardiovascular diseases, neurodegenerative diseases, cancers and diabetes [1], understanding the mechanisms of this physiological process could be the key to delay it and age in the healthiest way. Aging is a very complex process that involves molecular and cellular changes. The "age era" started 30 years ago when the first long-lived strains was isolated in *C. elegans* [2] and to this day nematodes, flies and yeast are the best model for stuffing aging because of their short lifespan. In the last decades several hallmarks of aging have been identified in different organisms: genomic instability, epigenetic alterations, telomere attrition, loss of proteostasis, deregulated nutrient sensing, mitochondrial dysfunction, cellular senescence, stem cell exhaustion, altered intercellular communication [3] and, more recent data include also autophagy/mitophagy impairment [4-6] **(Fig. 1)**.

Fig. 1. The hallmarks of aging. The picture mentions the nine hallmarks of aging described in López-Otín *et al.* 2013 [3]. The concept of "Hallmarks of aging" has been expanded to ten hallmarks with the addition of "mitophagy impairment" [7, 8].

Several forms of **DNA damage** occur spontaneously, for example ones due to DNA replication errors, spontaneous hydrolytic reactions and reactive oxygen species over-production, and accumulate within cells from aged humans and animal models [9]. Moreover

the integrity and stability of DNA are continuously challenged by exogenous physical, chemical, and biological agents [10]. All of these forms of DNA alterations may affect essential genes and transcriptional pathways, resulting in dysfunctional cells. This is especially relevant when DNA damage impacts the functional competence of stem cells, thus compromising their role in tissue renewal [11]. For example, aged HSCs and muscle stem cells show an increased number of nuclear foci that stain for the phosphorylated form of the variant histone H2A.X (γH2A.X), which serves as a marker of DNA double-strand breaks [12, 13]. Causal evidence for the proposed links between lifelong increase in genomic damage and aging has arisen from studies in mice and humans, showing that deficiencies in DNA repair mechanisms cause accelerated aging in mice and underlie several human progeroid syndromes, such as Werner syndrome, Bloom syndrome, xeroderma pigmentosum, trichothiodystrophy, Cockayne syndrome, and Seckel syndrome [10, 14, 15]. Mutations and deletions in aged mtDNA may also contribute to aging [16]. Interestingly, contrary to previous expectations, most mtDNA mutations in adult or aged cells appear to be caused by replication errors early in life, rather than by the oxidative microenvironment of the mitochondria. These mutations may undergo polyclonal expansion and cause respiratory chain dysfunction in different tissues [17]. Wallace well-defined human multisystem disorders caused by mtDNA mutations that partially phenocopy aging [18]. Furthermore, mutations in genes encoding protein components of nuclear lamina have been identified as responsible for accelerated aging syndromes such as the Hutchinson-Gilford and the Néstor-Guillermo progeria syndromes [19-21].

Normal aging is also accompanied by **telomere attrition** in mammals. Because of the lack of telomerase, most mammalian somatic cells undergo progressive and cumulative telomere shortening. Deficiencies in telomerase and other proteins involved in telomere maintenance have been associated to several diseases and accelerated aging [22-26]. Genetically modified animal models have established causal links between telomere loss, cellular senescence, and organismal aging. Thus, mice with shortened or lengthened telomeres exhibit decreased or increased lifespans, respectively [27-30]. However, the premature aging of telomerase-deficient mice can be reverted when telomerase is genetically reactivated in these aged mice [31].

Several **epigenetic changes** contribute to the age-related increase in the risk of most common diseases [32]. Epigenetic changes include alterations in DNA methylation patterns, post-translational modification of histones, and chromatin remodeling. Increased histone H4K16 acetylation, H4K20 trimethylation or H3K4 trimethylation, as well as decreased H3K9 methylation or H3K27 trimethylation, constitute age-associated epigenetic marks [33, 34]. Indeed deletion of components of histone methylation complexes extends longevity in

nematodes and flies [35, 36]. Moreover, histone demethylases modulate lifespan by targeting longevity insulin/IGF-1 signaling pathway [37]. Furthermore, the sirtuin family (SIRTs) of NAD^+-dependent protein deacetylases has been studied extensively as potential anti-aging factors and, in mammals, at least three members of this family, SIRT1, SIRT3 and SIRT6, contribute to healthy aging [38-41]. For example, SIRT6 exemplifies an epigenetically relevant enzyme whose loss-of-function reduces longevity and whose gain-of-function extends longevity in mice [40, 41]. Alterations in these epigenetic factors lead also two more characteristic features of aging, such as changes in chromatin structure and aberrant production and maturation of many mRNAs [42, 43].

Aging is also linked to **impaired protein homeostasis** or proteostasis [44]. Indeed some well-known age-related diseases, such as Alzheimer's, Parkinson's and cataracts, are associated to chronic expression of unfolded, misfolded, or aggregated proteins [44]. Small molecules can enhance proteostasis by binding to and stabilizing specific proteins (pharmacologic chaperones) or by increasing the proteostasis network capacity (proteostasis regulators) [44]. There are also promising examples of genetic manipulations that improve proteostasis and delay aging in mammals [45].

Deregulated nutrient sensing is another hallmark of aging. There are four nutrient-sensing systems: "insulin and IGF-1 signaling" (IIS), involved in glucose sensing; mTOR, for the sensing of high amino acid concentrations; AMPK, which senses low-energy states by detecting high AMP levels; and sirtuins, which sense low-energy states by detecting high NAD^+ levels [46]. Genetic manipulations, for example downregulation of IIS pathway or of mTORC1 activity, extend the lifespan in worms, flies and mice [47, 48]. Dietary restriction (DR) increases lifespan and healthspan in all investigated eukaryote species, including nonhuman primates [48-50]. Further, a pharmacological manipulation that mimics a state of limited nutrient availability, such as rapamycin, extend longevity in mice [50]. Conversely, AMPK and sirtuins, act in the opposite direction to IIS and mTOR, meaning that they signal nutrient scarcity and catabolism instead of nutrient abundance and anabolism. Accordingly, their upregulation favors healthy aging [51, 52].

For years ROS (reactive oxygen species) have been considered accountable for **mitochondrial deterioration** and global cellular damage. More recently the role of ROS in aging has been re-evaluated, since an increase of ROS may prolong lifespan in yeast and *C.elegans* [53-55]. According to these data, ROS can activate compensatory homeostatic responses, but, beyond a certain threshold, they eventually aggravate, rather than alleviate, the age-associated damage [56]. Dysfunctional mitochondria can contribute to aging independently of ROS through other mechanisms, such as reduced biogenesis of mitochondria, impaired

mitophagy and accumulation of mutations and deletions in mtDNA. For example, a reduced biogenesis was assessed as a consequence of telomere attrition in telomerase-deficient mice, with subsequent p53-mediated repression of PGC-1α and PGC-1β [57]. In wild-type mice mitochondrial decline can be rescued by telomerase activation [58]. Moreover, sirtuins, SIRT1 and SIRT3, modulate mitochondrial biogenesis through PGC-1α and the removal of damaged mitochondria by autophagy and targeting many enzymes involved in energy metabolism, respectively [52, 59, 60]. So telomerase and sirtuins may cooperate to delay aging. Interestingly, endurance training and alternate-day-fasting may improve healthspan through their capacity to avoid mitochondrial degeneration [61, 62]. In conclusion it is well-known that mitochondrial dysfunction can accelerate aging in mammals [63], but it is less clear whether improving mitochondrial function can extend lifespan.

Cellular senescence is a state of irreversible growth arrest of primary eukaryotic cells and was firstly described for cells in culture [64]. This arrest can be triggered by multiple mechanisms including telomere shortening, the epigenetic derepression of the *INK4a/ARF* locus (encoding for proteins involved in $p16^{INK4a}$/Rb and $p19^{ARF}$/p53 pathways), and DNA damage. Senescence may contribute to aging not only by net accumulation of senescent cells in tissues, but also by limiting the regenerative potential of stem cell pools [65], which is lower during aging. However, this undervalues the physiological role of senescence which is to prevent the propagation of damaged cells. In support of these complexities, mutant mice with premature aging due to extensive and persistent damage, present dramatic levels of senescence and their progeroid phenotypes are ameliorated by elimination of $p16^{Ink4a}$ or p53 [66]. In contrast to their anticipated pro-aging role, mice with a mild and systemic increase in $p16^{Ink4a}$, $p19^{Arf}$ or p53 tumor suppressors exhibit extended longevity [67]. Therefore, the activation of p53 and *INK4a/ARF* can be regarded as a beneficial compensatory response aimed at avoiding the propagation of damaged cells and its consequences on aging and cancer. However, when damage is consistent, the regenerative capacity of tissues can be exhausted and, under these extreme conditions, the p53 and *INK4a/ARF* responses can become deleterious and accelerate aging.

In many tissues, homeostatic tissue maintenance and regenerative ability is associated to tissue-specific stem cells, endowed with the capacity to both self-renewal and differentiate into mature daughters. A good balance between quiescence and proliferative activity is critical for their survival and maintenance of appropriate physiological and regenerative responses. The life-long persistence of stem cells in the body makes them particularly susceptible to the accumulation of cellular damage, which can derive from cell-intrinsic, environmental and systemic signals that drive the **loss of stem cell functionality** during aging [68]. Recent studies

point out the possibility to reverse the aging phenotype at the organismal level through stem cell rejuvenation [69]. For example, it has been proposed that reprogramming aged somatic cells into iPSCs, followed by redifferentiation to the desired somatic cell types, may help reset the memory of aged somatic cells [70, 71]. This possibility has been supported in part by studies in which aged hematopoietic progenitors were reprogrammed to produce iPSCs. These iPSCs were then used to create new HSCs in a chimeric embryo system and yielded complete rejuvenation of hematopoietic activity [72]. This is a demonstration how genetic and epigenetic "memory" can be erased and re-established to restore stem cell function. Moreover parabiosis experiments have demonstrated that the decline in neural and muscle stem cell function in old mice can be reversed by systemic factors from young mice [73]. These data lead to the discovery of blood-borne circulating factors, which are easy accessible and to manipulate. Finally the availability of nutritional and pharmacological agents that can target derangements in metabolism of aged cells to improve stem cell function and regenerative potential provides another opportunity for a therapeutic approach. Indeed rapamycin has been demonstrated to delay aging by improving proteostasis, by affecting energy sensing and eventually by improving stem cell function in the epidermis, in the hematopoietic system and in the intestine [74-76].

Aging is not an exclusively cell-autonomous phenomenon, but it also involves changes in **intercellular communication** [77, 78]. These alterations are associated firstly to a proinflammatory phenotype ("inflammaging") that accompanies aging in mammals [79]. Inflammaging may result from multiple causes such as the accumulation of pro-inflammatory tissue damage, the failure of an ever more dysfunctional immune system to effectively clear pathogens and dysfunctional host cells, the propensity of senescent cells to secrete pro-inflammatory cytokines, the enhanced activation of the NF-κB transcription factor, or the occurrence of a defective autophagy response [79]. Pharmacological activation of SIRT1 may prevent inflammatory responses in mice [80, 81]. Indeed, SIRT1 can down-regulate inflammation-related genes by deacetylating histones and components of inflammatory signaling pathways such as NF-κB [82]. Consistent with these findings, reduction of SIRT1 levels correlates with the development and progression of many inflammatory diseases [80]. There are several possibilities for restoring defective intercellular communication underlying aging process, including manipulation of blood-borne systemic factors [73, 83] and of the gut microbiome [84], which shapes the host immune system, and long-term administration of anti-inflammatory agents, such as aspirin which may increase longevity in mice and healthy aging in humans [85, 86].

The recent identified hallmark of aging is **autophagy impairment**. Autophagy is an evolutionary conserved intracellular catabolic process that protects cell against stressful conditions [87-89]. Autophagy can refer to the nonspecific, cell-wide degradation of organelles or misfolded proteins in nutrient-starved conditions, as well as the removal of specific damaged or superfluous organelles. These substrates are engulfed in a double-membrane autophagic vesicle, fused to lysosomes, and then degraded. Three types of autophagy have been identified: microautophagy, chaperone-mediated autophagy (CMA), and macroautophagy (autophagy) [90]. Several data support the link between autophagy and aging, while little is known about any correlation between aging and microautophagy and CMA. Aging is associated with a **compromised autophagy** [4] and its subtype mitochondrial autophagy, named **mitophagy** [6]. Indeed emerging evidence suggests that the upregulation of autophagy may delay the onset and ameliorate the symptoms of age-related phenotypes [91]. Mitophagy has been linked to normal physiological aging [5] and to age-related diseases, including neurodegenerative disorders [92] , such as Parkinson's [93], Huntington's [94], and Alzheimer's [95]. Mitophagy can either specifically eliminate damaged mitochondria or clear all mitochondria during specialized developmental stages (fertilization and blood cell maturation) or starvation (phosphoinositide 3-kinase/PI3K-dependent). Molecular mechanisms of mitophagy have been intensively investigated in multiple species, from yeast to mammals. Under nutrient-rich conditions, damaged and superfluous mitochondria are selectively degraded to maintain mitochondrial homeostasis. One of the most studied pathways in clearing damaged mitochondria in mammalian cells is the PINK1/Parkin pathway [96]. PINK1-Parkin-dependent mitophagy is initiated when a decrease in mitochondrial membrane potential caused by mitochondrial damage leads to the stabilization of the ubiquitin kinase (PTEN)-induced kinase 1 (PINK1) on the outer mitochondrial membrane. Here, it phosphorylates ubiquitin, leading to the recruitment of the E3 ubiquitin ligase Parkin. PINK1 phosphorylation activates Parkin, which polyubiquitinates mitochondrial proteins, leading to their association with the ubiquitin-binding domains of autophagy receptors, such as optineurin (OPTN) and NDP52, which bind to both ubiquitin and LC3 (an autophagosomal protein), inducing the formation of the autophagosome. The autophagosome then fuses with the lysosome, leading to degradation of the mitochondria [97]. Alternatively, PINK1 can recruit mitophagy proteins in a Parkin-independent manner, including AMBRA1, Bcl2-L-13, FUNDC1, MUL1, and Nix/BNIP3L. In *C. elegans*, mitophagy plays important roles in lifespan and healthspan. The *C. elegans* mitochondrial protein DCT-1 is a putative orthologue to the human mitophagy protein Nix/BNIP3L. DCT-1 works downstream of the PINK1-Parkin pathway and is upregulated by the oxidative stress

response transcription factor SKN-1 (ortholog of mammalian NRF2) and the FOXO transcription factor DAF-16 (ortholog of mammalian FOXO3) [98]. In the nematode, mitochondria accumulate with age, which may be due to a reduction in the clearing of damaged mitochondria via mitophagy [98]. Moreover, induction of mitophagy is required for the lifespan extension of several *C.elagans* mutants [99]. Sun et al developed the mt-keima mouse to measure mitophagy *in vivo* and demonstrated that mitophagy declines by approximately 70% in the Dentate gyrus between 3 and 21-months old mice [100]. They supposed that it is not due to an increase in mitochondrial damage, but rather to a decline in mitophagic pathway [100]. Mitochondrial recycling is in part regulated by AMP-activated protein kinase (AMPK). AMPK, as already mentioned, serves as an energy sensor, stimulating ATP production and suppressing its consumption in conditions of high cellular AMP/ATP ratio. AMPK phosphorylates ULK1/ULK2 during mitophagy pathway [101]. Since AMPK can increase intracellular NAD^+ levels [102], it may also promote SIRT1-dependent mitophagy [103-105]. SIRT1 activity enhances mitophagy via FOXO signaling and promotes mitochondrial biogenesis by activating PGC-1α [106]. Indeed sirtuins activating compounds, such as resveratrol [107] and metformin [108], and NAD^+ precursors, such as NR and NMN [109], can be considered therapeutic approaches aimed to increase mitophagy (see later). Furthermore, mitophagy can be also induced by bioactive natural compound, such as Actinonin [100] and Urolithin A [110], although the connection between these pathways and mitochondrial homeostasis remains unclear.

II. The importance of nicotinamide adenine dinucleotide (NAD^+)

II.1. *NAD^+ structure and biosynthesis*

Nicotinamide adenine dinucleotide (NAD^+) is an important cofactor for many enzymes involved in several cellular pathways such as energy production, mitochondrial maintenance, DNA repair, stem cell rejuvenation, cell signaling [104, 111-113]. In 1906 it was named as "cozymase" by Harden and Young, a small molecule able to accelerate yeast fermentation [114]. Hans von Euler is generally recognized as the first to establish the chemical structure of NAD^+. It is a dinucleotide which consists of two nucleotides joined through their phosphate groups. One nucleotide carries an adenine base and the other nicotinamide (vitamin B3 or Niacin). It exists in two forms: NAD^+ and NADH with two more electrons, acquired after a redox reaction (**Fig. 2**).

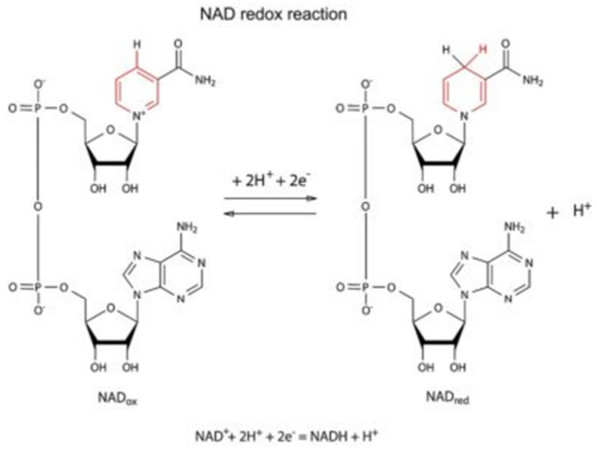

Fig. 2. NAD^+ structure. NAD^+ is a dinucleotide which consists of two nucleotides joined through their phosphate groups. One nucleotide carries an adenine base and the other nicotinamide (vitamin B3 or Niacin). It exists in two forms: NAD^+ and NADH with two more electrons, acquired after a redox reaction. Figure adapted from https://www.selfhacked.com/blog/nad-important-increase/.

NAD^+ is produced in all cells and its levels are continuously modified by cellular activities, including its consuming and synthesis, and also by diet. The basal intracellular concentration is around 800 μM in yeast [115], 100-400 μM in human HEK293 cells [116, 117] and 0.2 mmol/kg in mouse tibialis anterior muscle [102].

NAD^+ is produced from several dietary sources, including NAD^+ itself (it is metabolized in the gut, then synthesized again in cells), and from some of its precursors: tryptophan (Trp), nicotin acid (NA), nicotinamide riboside (NR), nicotinamide mononucleotide (NMN) and

nicotinamide (NAM) [118]. Based on the bioavailability of the precursors, there are three cellular pathways for the synthesis of NAD^+ (**Fig. 3**):

1) from Trp by the ***de novo*** **biosynthesis pathway** or **kynurenine pathway**;
2) from NA in the **Preiss-Handler pathway**;
3) from NAM, NR and NMN in the **salvage pathway**.

First described by Bender in 1983 [119], primary NAD^+ synthesis starts from dietary **Trp**, from which it inherits pyridinic ring. All the steps have been well described by Houtkooper [120]. The first, rate-limiting step in the biosynthesis of NAD^+ is the conversion of tryptophan to N-formylkynurenine by either indoleamine 2,3-dioxygenase (IDO) or tryptophan 2,3-dioxygenase (TDO), both requiring molecular oxygen. In mammals, TDO is the major enzyme contributing to NAD^+ biosynthesis in the liver. In extrahepatic tissues the cytosolic IDO plays an important role, with highest activity reported in lung, spleen, and small intestine [121, 122]. Four enzymatic reactions lead to the formation of the unstable α-amino-β-carboxymuconate-ε-semialdehyde (ACMS), which is a branchpoint in the tryptophan catabolic pathway [119]. ACMS can be enzymatically converted to α-amino-β-muconate-ε-semialdehyde by ACMS decarboxylase directing the pathway to complete oxidation to CO_2 and water. Alternatively, ACMS can undergo spontaneous cyclization forming quinolinic acid, which subsequently serves as a precursor for NAD^+ by taking advantages of enzymes involved in Preiss-handler pathway. This latter nonenzymatic possibility seems to be only relevant when the metabolism of ACMS is limited in the cell, making this step another control point of NAD^+ biosynthesis. This might explain why, in general, Trp is considered a rather poor NAD^+ precursor in vivo, as it will only be diverted to NAD^+ synthesis when its supply exceeds the enzymatic capacity of ACMSD [123]. When it happens, ACMS becomes quinolinic acid, used then by quinolinate phosphoribosyltransferase (QPRT) to form NA mononucleotide (NAMN). This enzyme represents a second rate-limiting step in the biosynthesis of NAD^+. NAMN is then converted to NA adenine dinucleotide (NAAD) using AMP by the enzyme NAM mononucleotide (NMN) adenylyltransferase (NMNAT). This is a key enzyme for NAD^+ synthesis in mammals, irrespective of the precursor used, since it is also needed for NAD^+ salvage. Three NMNAT isoforms (NMNAT1-3) with different tissue and subcellular distributions have been identified in mammals [124]. NMNAT1 is a nuclear enzyme that is ubiquitously expressed, with its highest levels in skeletal muscle, heart, kidney, liver and pancreas and relatively low level in brain [125]. In contrast, NMNAT2 is highly expressed in brain and it is mostly located in the cytosol and Golgi apparatus [126, 127]. Finally, NMNAT3 is highly expressed in erythrocytes with a moderate expression in skeletal

muscle and heart, and has been identified in both cytosolic and mitochondrial compartments [128]. The final step in the primary biosynthesis of NAD^+ includes the ATP-dependent amidation of NAAD by NAD^+ synthase using glutamine as a donor [129].

The dietary NA (nicotinic acid) can be used as a NAD^+ precursor in the short **Preiss-Handler pathway** [130]. Here is converted to NAMN by the NA phosphoribosyltransferase (NAPRT) and then it converges with the previous described ***de novo* pathway**.

The main source of NAD^+ is from **salvage pathway**, which require the uptake of other NAD^+ precursors from the diet, such as NR, NMN and NAM. Extracellularly, NAD^+ or NAM can be converted to NMN, which is then dephosphorylated to NR, likely by CD73. NR is transported into cells by nucleoside transporters [131] and is then phosphorylated by the NR kinases 1 and 2 (NRKs), generating NMN. NMN is then converted in NAD^+ by NMNATs [132].

In mammals, NAM can also be an NAD^+ precursor through its metabolism into NAM mononucleotide (NMN) by the rate-limiting enzyme nicotinamide phosphoribosyltransferase (NAMPT) [133]. NMN can be then converted into NAD^+ through a single additional reaction catalyzed by the NMNAT enzymes. NAM is also the product of NAD^+ degradation by several enzyme families. Therefore, NAMPT is important to not only metabolize circulating NAM, but also to recycle intracellularly-produced NAM via the NAD^+ **salvage pathway**.

Nutritious foods, especially those rich in B-group vitamins, can help to synthetize and use NAD^+. Niacin is abundant in eggs, diary, meat fish, whole grain, brown rice and some vegetables. However, they are delicate and are easily destroyed by cooking or processing. NR is present in cow's milk, while NMN is found in broccoli, avocado and beef.

Recently dietary supplements, such as nicotinamide riboside (NR) and nicotinamide mononucleotide (NMN), have gained credibility as an effective way to boost NAD^+ levels (see later). Moreover diet and exercise affect NAD^+ levels. Studies in both mice and humans have shown than exercise can affect circulating NAD^+ levels in a biphasic way with moderate intensity exercise increasing, and strenuous exercise reducing NAD^+ [134, 135]. It has been demonstrated how exercise and NMN-supplementation can induce reversal of the glucose intolerance induced by obesity, they are associated with tissue-specific effects and differential alterations to mitochondrial function in muscle and liver [134]. High-fat diet decreases NAD^+ in the muscle of HFD-induced obese mice, but 6 weeks of exercise and also caloric restriction improve glucose tolerance and increase muscle NAD^+ in both obese induced and aged mice [136].

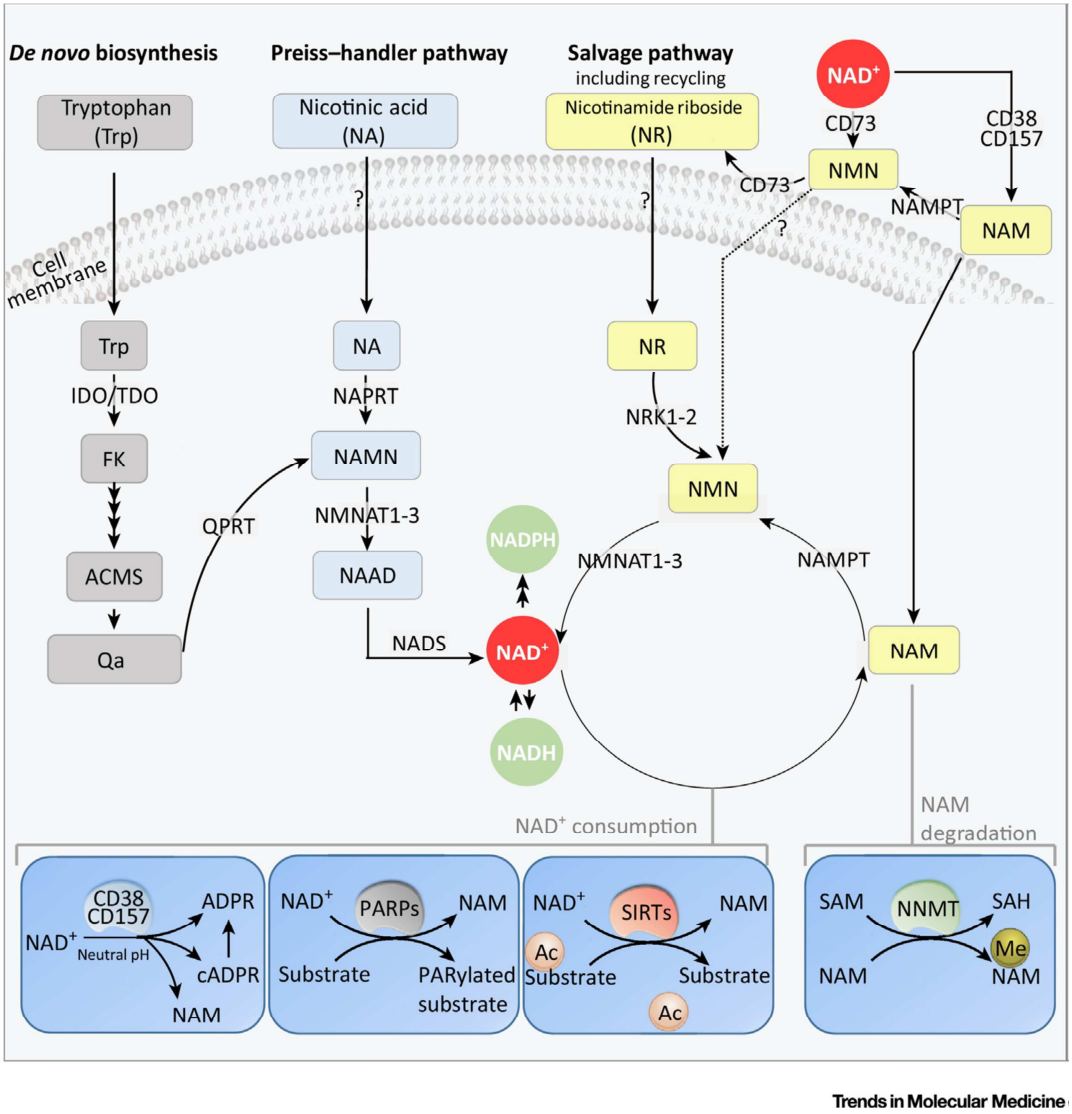

Fig. 3. NAD$^+$ biosynthetic pathways. NAD$^+$ is synthesized via three major pathways in mammals. The lower part shows the major NAD$^+$-consuming enzymes: cADPRSs, PARPs and SIRTs. Figure from Fang *et al.* 2017 [7].

II.2. *NAD$^+$ in metabolism*

As a cofactor NAD$^+$ levels are high in mitochondria, nucleus and cytoplasm. It is responsible for intracellular redox balance and can modulate the activity of compartment specific metabolic pathways. It is involved in pathways such as glycolysis, fatty acid β-oxidation and tricarboxylic acid cycle (TCA).

In the cytoplasm, each molecule of glucose is converted in two molecules of pyruvate by glycolysis. This process requires two NAD$^+$ molecules per molecule of glucose used by GAPDH (glyceraldehyde-3-phosphate dehydrogenase) to reduce NAD$^+$ to NADH and to transform G3P (glyceraldehyde-3-phosphate) into 1-3-biphosphoglycerate.

During mitochondrial fatty acid β-oxidation, a NADH is produced during the reaction catalyzed by hydroxyacyl-CoA dehydrogenase.

The electrons carried by the cytoplasmic NADH are transferred into the mitochondrion by mitochondrial shuttles, such as the malate-aspartate shuttle or glycerol-3-phosphate shuttle.

In the mitochondrion the TCA cycle reduces many NAD^+ molecules. It is the cofactor for dehydrogenases, such as isocitrate dehydrogenase, α-ketoglutarate dehydrogenase and malate dehydrogenase.

The NADH produced during glycolysis, fatty acid β-oxidation and TCA are then used by the electron transport chain to produce ATP. Once in the mitochondria, NADH molecules are oxidized by Complex I (NADH:ubiquinone oxidoreductase) of the ETC. The subsequent two electrons gained by Complex I are relayed along ubiquinone (Coenzyme Q10), complex III (coenzyme Q - cytochrome c oxidoreductase), cytochrome c, and Complex IV (cytochrome c oxidase). In parallel to the oxidation of NADH to NAD^+ by the ETC, the substrate succinate from the mitochondrial TCA cycle, provides additional electrons to ubiquinone in parallel with Complex I. Ultimately, the flow of electrons, generated from NADH and succinate, along the ETC is coupled to the pumping of protons from the mitochondrial matrix to the intermembrane space via Complex I, III and IV, creating a proton gradient. The proton gradient then provides the chemiosmotic gradient to couple the flux of protons back into the matrix via F0F1-ATP synthase with oxidative phosphorylation of ADP to ATP. Overall, the ETC reduces O_2 to water and NADH to NAD^+ for the purpose of generating ATP. Both glycolysis in the cytoplasm and the TCA cycle in the mitochondria are responsible for maintaining metabolic homeostasis by altering cytosolic/nuclear NAD^+ and NADH levels. This balance is important for intracellular redox balance.

Furthermore, even under anaerobic, oxygen-deficient conditions, NADH must be converted back to NAD^+ through anaerobic mechanisms, whether homolactic or alcoholic fermentation.

II.3. *NAD^+-consuming enzymes*

Several enzymes use NAD^+ as cofactor, which can be divided into three groups: deacetylases in the sirtuin family (SIRTs), ADP-ribosyltransferases, including poly(ADP-ribose) polymerases (PARPs), and cyclic ADP-ribose synthases (cADPRSs).

In mammals the **sirtuin family** comprises seven proteins (SIRT1-SIRT7), which vary in tissue specificity, subcellular localization, enzymatic activity and targets [137]. Three sirtuins (SIRT3-5) are located in the mitochondria, while SIRT1, SIRT6 and SIRT7 are mainly found in the nucleus, and SIRT2 is located in the cytoplasm [138, 139]. Since they all use NAD^+ as

cofactor, the bioavailability of NAD^+ is a point of regulation of their activity and SIRTs could be considered as "metabolic sensors" [120]. As already mentioned, during fasting and exercise muscle NAD^+ levels rise, with a concomitant activation of sirtuins [140]. Similarly, caloric restriction increases NAD^+ levels in muscle, liver and white adipose tissue [141]. By contrast, high-fat diet in mice reduces NAD^+/NADH ratio [142].

The sirtuins are mainly involved in removing acetyl moieties from lysines on histones and proteins, releasing NAM and O-acetyl ADP-ribose [120], while some members of this family have also some other enzymatic activities. These enzymes regulate multiple cellular pathways, such as mitochondrial homeostasis, neuronal survival, stem cell rejuvenation, by preventing a series of metabolic and age-related diseases (neurodegeneration, loss of stem cells and mitochondrial dysfunction) [143-146].

Poly ADP-ribose (PAR) polymerases (**PARPs**) family comprises 17 members in mammals [147] which are involved in several cellular pathways, such as DNA repair, inflammation, cell death, neuronal function, endoplasmic reticulum stress and metabolism [147-149]. PARPs transfer the first ADP-ribose unit from NAD^+ to target proteins, followed by the sequential addition of ADP-ribose units to the preceding ones to form poly(ADP-ribose) polymers (PARs) [150].

The **cADPRSs** include CD38 and its homolog CD157 in mammals. CD38 and CD157 are transmembrane proteins, localized to the plasma membrane and to membranes of intracellular organelles, including the mitochondria, nucleus, and endoplasmic reticulum [151]. CD38 is expressed in immune cells, liver, testis, kidney, and brain [151]. Their product cADPR (cyclic ADP-ribose) is involved in Ca^{2+} signaling, cell cycle control, DNA repair, mitochondrial maintenance, and stem cell rejuvenation [104, 113, 152, 153].

II.4. *NAD^+ in aging*

Mounting evidence has indicated that NAD^+ levels decline with age in multiple types of tissues, which include the liver, skeletal muscle, adipose tissue, heart, brain, kidney, pancreas, lungs, spleen, skin, as well as extracellular fluids [7, 154]. Indeed, NAD^+ declines with age in normally elderly (60^+) and the plasma NAD^+ levels are less than 25% of that of normal young people (20-40 years of age) [155]. In addition, an age-dependent decline in NAD^+ levels in *Caenorhabditis elegans* (*C. elegans*), mice, and human post-mortem tissues are reported. All these data indicate an universal age-dependent decrease of cellular NAD^+ across species. Accumulating evidence associate its depletion to nine hallmarks of aging, but there are no

data linking NAD^+ to telomere attrition (**Fig. 4**). However it is still under investigation whether this depletion is due to increased NAD^+ consumption and/or decreased production.

NAD^+ replenishment through its precursors, such as NR, NMN and NAM, have been investigated in animals models. Indeed NAD^+ levels restoration is capable to delay normal aging and to ameliorate both lifespan and healthspan, as shown by several features, including improved mitochondrial health, muscle strength and motor function. One study showed that 10 μM NR could extend the replicative lifespan of wild-type yeast by more than ten generations through two different pathways: the tNrk1 and the Urh1/Pnp1/Meu1 [115]. Similarly, in *C. elegans*, 500 μM NR extended the average lifespan of wild-type worms (N2) via the SIR-2.1 (ortholog to mammalian SIRT1) pathway [106]. For *Drosophila*, no information is available regarding a direct effect of NAD^+ precursors on lifespan, but genetic overexpression of an NAD^+ synthetic enzyme nicotinamidase (D-NAAM) has been reported to extend lifespan [156]. This enzyme is involved in the NAD^+ salvage pathway and converts NAM to NA and, in *Drosophila*, its overexpression can increase the NAD^+:NADH ratio, as well as the mean and maximal lifespan by up to 30% in a Sir2-dependent manner [156]. Moreover, NR has been shown to increase lifespan (5%) in 2 years old C57BL/6J mice [111].

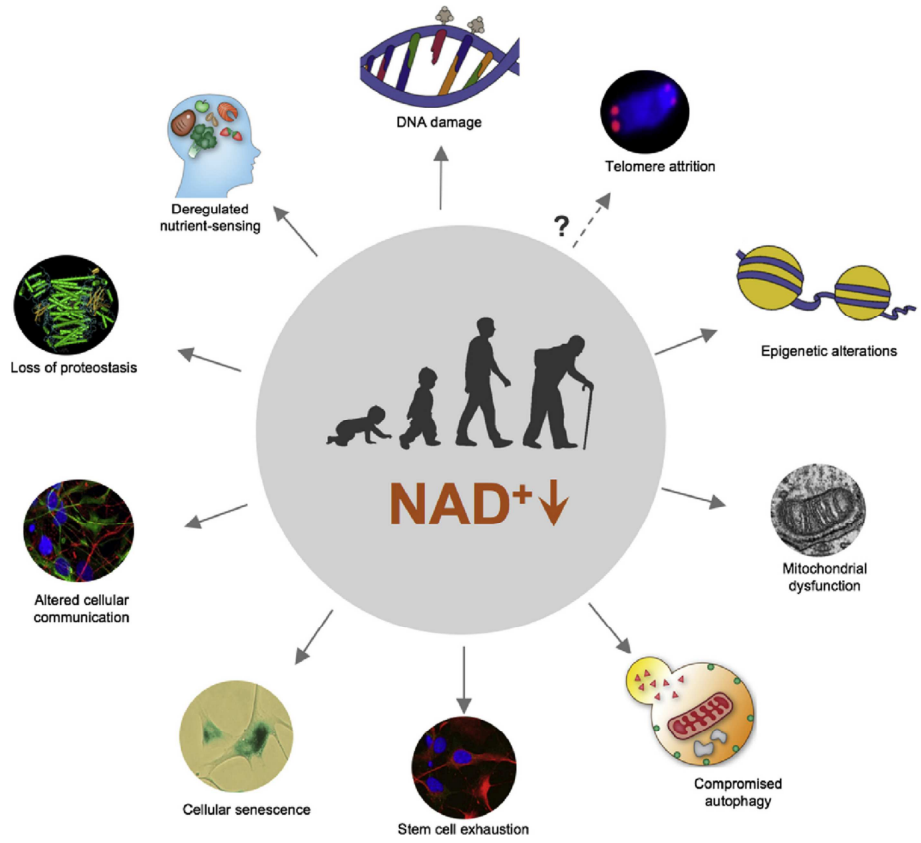

Fig. 4. NAD^+ decline and its correlation with hallmark of aging. A schematic representation of age-dependent decline in NAD^+ levels which correlates with nine hallmaks of aging, namely DNA damage, epigenetic alteration, deregulated nutrient-sensing, loss of proteostasis, altered cellular communication, cellular senescence,

stem cell exhaustion, mitochondrial dysfunction, compromised autophagy. Actually no date are available linking NAD^+ and telomere attrition. Figure from Aman *et al.* 2018 [8].

NAD^+ replenishment can improve **DNA repair** in cells, *C. elegans*, and mice. An early study reported that suitable doses of NAM (~3 mM) significantly enhanced DNA repair in gamma-irradiated XP cells in vitro [157]. In line with this finding, studies in human aortas suggest that the NAM-consuming enzyme NAMPT has a significant role in DNA repair to maintain genome integrity, as demonstrated from an increase in DNA oxidative lesions and DNA DSBs in murine Nampt-deficient murine smooth muscle cells [158]. In addition to NAM, NA and NR also improve DNA repair *in vitro*. Indeed, studies revealed increased DNA repair *in vitro* in peripheral blood mononuclear cells, where NA treatment increased DNA repair efficiency and decreased micronuclei numbers following X-ray irradiation, and in murine Atm-deficient neurons, following NR administration [159]. NAD^+ supplementation can also increase DNA repair *in vivo*, because wild-type mice treated with NR showed decreased DNA damage, as evidenced from lower global PARylation and γ-H2AX foci relative to controls [111, 160]. Both NR and NMN have shown a significant role in delaying the onset of aging in some premature aging disease. These rare diseases, including Xeroderma pigmentosum group A (XPA), Cockayne syndrome (CS) and Ataxia-telangiectasia (A-T), are caused by a deficit in DNA repair pathways. NAD^+ precursors administration improved the lifespan and the healthspan of *C. elegans* models of XPA, CS and A-T [103, 106, 161]. Moreover NR supplementation in drinking water extended lifespan in $Atm^{-/-}$ mice at 10 months (instead of 3-5 months) [106]. In *C. elegans* model of A-T, NAD^+ replenishment has shown an important neuroprotection through an improvement in neuronal DNA repair deacetylation of the DNA repair protein Ku70, and restoration of **mitochondrial homeostasis** via the mitophagy regulator NIX (DCT-1 in *C. elegans*) [106]. Moreover, in mice with hypomorphic BubR1 (a mitotic check-point kinase) exhibited characteristics of premature aging as evidenced by shorter lifespan, which was restored by NMN supplementation. NMN restores deacetylation activity of Sirt2, necessary for BubR1 stabilization [162]. α-amino-β-carboxymuconate-ε-semialdehyde decarboxylase (ACMSD), the enzyme that limits spontaneous cyclization of α-amino-β-carboxymuconate-ε-semialdehyde in the de novo NAD^+ synthesis pathway, has been identified a key modulator of cellular NAD^+ levels, sirtuin activity and mitochondrial homeostasis in kidney and liver [163]. Genetic and pharmacological inhibition of ACMSD in *C. elegans* and mouse boosts de novo NAD^+ synthesis and Sirt1 activity, ultimately enhancing mitochondrial function. These inhibitors may have therapeutic potential for protection of these tissues from injury [163].

NAD^+ precursors ameliorate also **neurodegeneration** in animal models. In AD (Alzheimer's disease) mouse model, 3 months of chronic NR treatment has been demonstrated to attenuate cognitive deterioration through Aβ aggregates degradation by increasing PGC-1α activity and ubiquitin proteasome system induction [164]. Similar results were obtained in SH-SY5Y cells and AD *C. elegans* [164]. NR also improve memory learning, motor function and mitochondrial function as well as protection against neuronal cell death in Parkinson's disease (PD) animal models [165]. In addition, it was able to promote longevity and inhibit/delay cognitive decline in AD *C. elegans* and mice, with the enhanced process of **mitochondrial proteostasis** and modulation of β-secretase 1 (BACE-1) activity via peroxisome proliferator-activated receptor-gamma coactivator 1 (PGC)-1α highlighted as possible underlying mechanisms [164, 166]. Similarly to NR, NMN has also been described to ameliorate mitochondrial dysfunction and neuronal death in APP/PS1 mice, as evidenced from restored oxygen consumption rates, increased levels of Sirt1 and PGC-1α, and normalization of morphology of brain mitochondria from NMN-treated APP/PS1 mice [167]. NMN was also found to protect against Aβ oligomer-induced cognitive impairment, neuronal death, and cognitive dysfunction in a rat model of AD [168].

NAM replenishment in 3xTg AD mice lead to an upregulation of neuronal bioenergetics, including neuroplasticity-involved kinases and transcription factors, as well as by improving autophagy processing [169]. All these data seems to explain that NAD^+ -induced reduction of AD phenotypes is attributable to the upregulation of **autophagy** and/or **mitophagy** because NAD^+/SIRT1 are able to upregulate autophagy through deacetylation of the major autophagy proteins Atg5, Atg7, and Atg8 in human cells, murine neurons, and *C. elegans* [106]. More recently it has been demonstrated that interventions able to stimulate mitophagy therefore have therapeutic potential in the prevention and treatment of AD. Indeed, in both amyloid-β (Aβ) and Tau *C. elegans* models of AD, pharmacological stimulation of mitophagy (through urolithin A, actinonin, and the NAD^+ precursor nicotinamide mononucleotide), reverses memory impairment through a PINK1, PDR-1 or DCT-1 dependent pathway. Mitophagy induction diminishes the levels of insoluble $A\beta_{1-42}$ and $A\beta_{1-40}$ peptide isoforms and prevents cognitive impairment in an APP/PS1 mouse model by a mechanism involving microglial phagocytosis of extracellular Aβ plaques and suppression of neuroinflammation. Furthermore, mitophagy abolishes AD-related Tau hyperphosphorylation in human neuronal cells and reverses memory impairment in transgenic Tau nematodes and the 3xTgAD mice [170].

Moreover, NAD^+ replenishment has been documented to induce **mitochondrial biogenesis** through the NAD^+/Sirt1-PGC1α pathway in aged mice, murine muscle cells and *C.elegans* [111, 171].

A more recent study described further beneficial effects of NR in AD treatment in 3xTg mice. These mice exhibited reduced phosphorylated tau pathology and inhibited cognitive decline, but also, normalized AD-associated neuroinflammation and synaptic dysfunction. More interestingly, DNA damage was reduced, in addition, following chronic administration of NR in a DNA repair deficient 3xTg/Polβ$^{+/-}$ mouse model [172, 173]. This is due to a reduced activity of NAD^+ consuming PARPs which is involved in DNA repair; in this way increase in NAD^+ levels boosts neurogenesis and inhibits AD-associated pathology, neuroinflammation and mitochondrial dysfunction [173]. NAD^+ precursors administration may also counteract age-predisposed metabolic disease. Indeed NR promotes oxidative metabolism, decrease weight gain, improve glucose tolerance and increase survival rate in rodents [174, 175]. Most of these effects are mediated by a Sirt1- and Sirt3-dependent mitochondrial unfolded protein response, thereby improving **mitochondrial metabolism** (increasing mitochondrial complex formation and activity) [176]. Also NMN administration ameliorated impairments in glucose tolerance and promoted insulin secretion/sensitivity in age- or diet-induced diabetic mice, Nampt$^{-/-}$ mice, as well in aged wild type and β cell-specific Sirt1-overexpressing (BESTO) mice [177, 178].

NAD^+ precursors solve also altered **cellular communication**. For example, NR treatment prevented noise-induced hearing loss and led to regeneration of neurite ganglia mediated by NAD^+-dependent SIRT3 activity [179].

Maintaining healthy mitochondria, by replenishing NAD^+ stores, seems furthermore to have beneficial effects also in protecting **stem cells** populations from aging, such as NSC (neural stem cell), MuSC (muscle stem cell) and McSC (melanocyte stem cell) [180, 181]. Indeed in the *mdx* mouse model of Duchenne's muscular dystrophy the reduction of NAD^+ pools blunts the adaptive UPR^{mt} pathway, ultimately leading to a loss of mitochondrial homeostasis with concurrent reduction in the number and self-renewal capacity of MuSCs. Accordingly, NR administration restored proteotoxic resistance due to the activation of the UPR^{mt} pathway, stimulating the prohibitin family of mitochondrial stress sensors and effectors. Then this in turn improved mitochondrial homeostasis, protected against disease progression through preventing MuSC senescence and promoting muscle stem cells function and regeneration [111]. Most importantly, using a MuSC-specific loss-of-function model for *Sirt1*, an essential regulator governing mitochondrial homeostasis [113], the importance and essential nature of the relationship between the NAD^+-SIRT1 pathway, mitochondrial activity and MuSC function

was unequivocally established *in vivo*. Similarly, NR rescued the decline of McSCs in hair follicles of aged mice [111]. NMN also has beneficial effects in aged NSC [182]. Stein and Imai showed that loss of neural stem/progenitor stem cells (NSPCs) is likely due to an age-related decline in the enzyme Nampt and hence its product NMN [182]. Dietary supplementation with NMN in iNSPC-Nampt-KO mice, has indicated that Nampt enzymatic activity is required for NSPC self-renewal. Most notably, in wild-type mice between the ages of 6 and 18 months, dietary NMN supplements prevented the loss of NPSC markers, suggesting that exogenous NMN could be an efficacious strategy to treat or prevent age-related loss of NSPC function [182]. Moreover, Nampt-deficient NSPCs were defective in differentiating into oligodendrocytes, cells responsible for the myelination of neurons in the brain. NAD^+ replenishment, together with redundant SIRT1 and SIRT2 activities, promoted differentiation [182].

III. Werner syndrome

Progeroid syndromes (PSs) are rare genetic disorders mimicking clinical and molecular features of aging. The interest in exploring age-related hereditary disorders is associated both with their severity, leading in many cases to lifespan shortening, and with the expectation that identifying causative genes could help understanding some of the mechanisms underlying the physiological aging. Indeed, all the clinical and biological changes usually observed during normal aging are never totally recapitulated in PSs. To date, most of these diseases, for which genes and pathophysiological mechanisms have been identified are monogenic and fall into the category of segmental PSs. In this context, Werner syndrome and Hutchinson-Gilford progeria syndrome have been the most extensively studied. These syndromes of accelerated aging have been proposed as models to simplify the analysis of the normal aging process, by restricting the focus to a more definable area.

III.1. *Clinical manifestations of Werner syndrome*

Werner syndrome (WS; OMIM# 277700) is a rare autosomal recessive inherited disorder that is characterized by the premature appearance of features associated with normal aging and cancer predisposition [183]. WS was firstly described by a German medical student, Otto Werner, in 1904. Werner reported a family of four siblings, ages 31-40, who presented with "Cataracts in Connection with Scleroderma" as well as short stature and premature graying of hair [184]. WS patients usually develop normally until they reach adolescence and therefore pathological characteristics are not apparent until these individuals reach the third decade of life [185] (**Fig.5**).

Fig.5. Werner syndrome patient with homozygous null WRN mutations. Although apparently normal at age 8, cataracts were removed at age 36 and severe ankle ulcerations were recorded at age 56. Picture from J. Oshima *et al*. (2017) [185]. (Registry#SANAN1010) [186].

The first sign is a lack of a growth spurt and a relatively short stature as adults. Beginning in the early third decade of life patients begin to develop an aged appearance that includes skin

atrophy, loss of subcutaneous fat and graying and loss of hair. Bilateral cataracts requiring surgery are seen in virtually all cases by the late 20s or early 30s [187, 188]. This is accompanied by a series of common age-related diseases that appear during middle age, including type 2 diabetes mellitus, hypogonadism, osteoporosis, atherosclerosis and malignancies. Several studies report that 30-40% of WS cases had children before gonadal atrophy leading to early loss of fertility in their 30s [187, 189]. Indolent deep ulcerations around Achilles tendons and, less frequently, at elbows, are almost pathognomonic to WS. These are associated with extensive subcutaneous calcifications and often lead to amputation of feet or lower extremities [187]. Other features frequently seen in WS include a high pitched hoarse voice (recognizable over the phone), characteristic facial features (a "pinched" facial appearance), thin limbs, truncal obesity, and flat feet. The most common causes of death are atherosclerotic vascular diseases, such as coronary heart disease, myocardial infarction, cerebral vascular diseases and malignancies at a median age of 54 [188-190]. However, the median age of WS patients has been increasing during the last decades, likely due to improved medical care.

Four cardinal signs have been identified to facilitate a diagnosis of WS that appear in over 91% of affected patients. Cardinal signs include bilateral cataracts (present in 100% of WS cases), premature graying and/or thinning of scalp hair (96%), characteristic dermatologic changes (99%) and short stature (95%) [188] (**Tab.1**).

Sign or symptom	Percent frequency
Bilateral cataracts[a]	100 (87/87)
Skin alterations[a]	98.6 (72/73)
Thin limbs	98.4 (60/61)
Premature graying/hair loss[a]	96.3 (79/82)
Pinched facial features	96.1 (49/51)
Short stature[a]	94.7 (71/75)
Osteoporosis	90.6 (48/53)
Voice change	89.0 (65/73)
Hypogonadism	79.5 (35/44)
Type 2 diabetesmellitus	70.8 (46/65)
Soft tissue calcification	66.7 (28/42)
Neoplasm(s)	43.6 (24/55)
Atherosclerosis	39.5(17/43)
All four cardinal signs[a]	90.9 (50/55)

Tab.1. Clinical Features of Werner Syndrome Patients With Molecular Documentation of the Diagnosis. Four cardinal signs facilitate a diagnosis of WS: bilateral cataracts, premature graying and/or thinning of scalp hair, characteristic dermatologic changes, and short stature. Picture from Huang et al. 2006 [188].

There are clinical discordances in the presentation of age-related disorders between WS and normal aging. For example, the most common neoplasms in WS are thyroid follicular

carcinomas, followed by malignant melanoma, meningioma, soft tissue sarcomas, primary bone tumors and leukemia/myelodysplasia. The elevated risk of these neoplasms ranges from 2 to 60-fold higher than population controls [189, 191].

Controversy still exists regarding the degree of brain involvement. Although WS patients may have central nervous system complications due to atherosclerosis, they do not appear to be particularly susceptible to Alzheimer disease or other neurologic alterations different from those atherosclerosis related [192]. Moreover cognitive changes are not typically observed and, when present, they are likely due to co-existing disorders.

This disease is generally rare, but it should be noted that most of the existing patients (845 of the 1200 cases reported worldwide, about two thirds of the total) are Japanese, and also have indicated that 1 in 160 of the Japanese population is a carrier of the disorder [193]. The chronological order of the onset of these complications doesn't change between the populations; in fact, it is similar among Caucasian and Japanese WS patients [189, 190]. In particular, Japan is considered to be a unique model for the analysis of the genetic epidemiology of WS because it is geographically isolated with relatively few population exchanges, and represents the highest frequency of this disease in the world. The prevalence of Werner syndrome varies with the level of consanguinity in populations. In the Japanese population, where this condition could be due to marriage between consanguineous (very often in the past) and to the background high rate of *WRN* mutations, the frequency ranges from about 1:100,000, based upon the frequencies of detectable heterozygous mutations [194]. The global incidence is ranging between 1:1,000,000 and 1:10,000,000 [195].

III.2. *Molecular basis of Werner disease*

Classical WS is caused by homozygous or compound heterozygous loss of function mutations in the *WRN* gene [196]. *WRN* is the only known gene in which mutations cause classical WS, and WS is the only known genetic disorder caused by null mutations of the *WRN* gene. The *WRN* locus is located on human chromosome 8p12, and consists of 34 coding exons spanning 140kb [196]. The encoded WRN protein belongs to RecQ helicase family of proteins. Most mammals possess five RecQ helicases: RECQL1, BLM, WRN, RECQL4, and RECQL5. Defects in human BLM, WRN, or RECQL4 cause monogenic disease syndromes; all RecQ helicases play critical roles in genome maintenance and are often referred to as guardians of the genome [197-199]. RecQ helicases share three highly conserved protein domains [200], the core helicase domain (composed of HD1 and HD2), the RecQ C-terminal

(RQC) domain, and the helicase and RNase D–like C-terminal (HRDC) domain. In addition, they possess unique protein regions and motifs that direct subcellular localization. WRN is unique among RecQ helicases in possessing also exonuclease activity [201]. Indeed, WRN protein is a 1,432-amino acid, 160 kDa multifunctional nuclear protein with a 3'→5' exonuclease domain in its N-terminal region [201], an ATP-dependent 3'→5' helicase in its central region [202] and a nuclear localization signal in its C-terminal region [203, 204]. Structural analysis and biochemical studies demonstrated that RQC, with its winged-helix (WH) domain, is critical for substrate-specific DNA binding to initiate unwinding [205-207]; whereas the HRDC domain also plays a role in DNA binding, particularly for recruiting WRN protein to dsDNA breaks (DSBs) [207-209]. The region between RQC and HRDC was also shown to possess single strand-DNA annealing activity and may influence oligomerization of the WRN protein [210] (see **Fig. 6** for a schematic illustration of WRN protein).

More than 80 different disease mutations have been identified in classical WS patients from all over the world [185, 211, 212] and they have been catalogued by the International Registry of WS (Seattle, WA, USA) and the Japanese Werner Consortium (Chiba, Japan) [195]. The majority of the mutations lead to premature stop codons or deletions, most of which result in truncations of nuclear localization signals at the C-termini and/or nonsense mediated decay of mutant mRNAs, therefore often referred to as null mutations [185, 213]. Other mutations include splicing mutation, missense mutations, intragenic large deletion, and genomic rearrangement extending beyond the *WRN* locus. Particularly interesting were the genomic rearrangements involving *WRN* and neighboring loci, deep intron mutations, and missense mutations, all of which are rare among Werner syndrome patients [211].

In addition to mutations in the *WRN* locus, heterozygous mutations in the *LMNA* gene have also been associated with WS, and is referred to as atypical WS (AWS) [214].

Currently, no clear correlation has been identified between the location of the mutation and the disease severity, thus further studies are needed to clarify this link.

Single nucleotide polymorphisms (SNPs) in the *WRN* gene have also been identified, and several polymorphisms have been linked to both longevity and disease risks though not all findings have been replicated in multiple cohorts [215]. The three different polymorphisms, the L1074F, C1367R, and 1133A have been linked to longevity, though only the association between S1133A and longevity was significant [216, 217]. Additionally, C1376R, S1133A and M387I have been associated to cardiovascular diseases [216-218], while L1074F and C1367R have been connected to the risk of ischemic stroke [219, 220]. *WRN* gene SNPs have also been linked dyslipidemia (V114I and S1133A) [217, 221] and diabetes (C1367R) [222]. Additionally, *WRN* gene SNPs have been associated to various types of cancers including bone and soft

tissue sarcomas (C1367R), breast cancer (C1367R and V114I) and lung cancer (L1074F) [223-225]. In addition, the C1367R has been associated with both bipolar disorder, schizophrenia and increased risk of Creutzfeldt-Jakob disease [226, 227]. Furthermore, SNPs in the 5' upstream region and 5' flanking areas of *WRN* have been associated with cognitive function (rs2251621, rs2725335, and rs2725338) despite mental impairment not being a typical feature of WS patients [228].

WRN helicase specifically unwinds only structures involving DNA metabolic intermediates; these include forked and flap structures (intermediates in DNA replication and repair), bubble structures (intermediates in DNA repair and transcription), Holliday junction structures (intermediates in DNA recombination) and G-quadruplex DNA and D-loop structures (associated with telomere DNA), all of which represent intermediates in DNA replication and repair processes [229-231]. The exonuclease activity of WRN preferentially digests single strands in complex DNA structures, such as double-stranded DNA (dsDNA) with mismatched ends or bubbles [232]; it can also degrade blunt-end and various other normal DNA structures in addition to those that contain bubbles and mismatches [233], or initiate DNA degradation from a nick or a gap in dsDNA.

Several studies demonstrated that the *in vivo* role of WRN in resolving complex intermediate DNA structures, generated either normally or accidentally, in various events, including DNA repair, replication, transcription and telomere maintenance, maintain genomic stability.

Moreover, WRN has been shown to have several interaction partners involved in DNA maintenance. These include proteins central for replication such as replication protein A (RPA), proliferating cell nuclear antigen (PCNA) and topoisomerase I [234]. WRN also interacts with multiple proteins involved in the DNA repair pathways including base excision repair (APE1, PARP-1, FEN1, Polβ) [235], non-homologous end-joining (RAD51, RAD52, Mre11/Rad50/Nbs1) and homologous recombination (BRCA1, MRN, BLM) [236] (see later for a more detailed description).

III.3. *WRN in relation to aging*

Due to a series of premature aging features WS has been considered as a great model for aging research [237, 238]. When comparing characteristics of WS to the hallmarks of aging previously described, WS has been linked with 7 hallmarks of aging: including epigenetic alterations [239], telomere attrition [240-242], changes in DNA damage and repair [236, 243], deregulated nutrient sensing [244-246], loss of proteostasis [247, 248], altered cellular

communication due to inflammation-induced elevated cytokine levels [249] and cellular senescence [250-252]. Conversely, the linkages between WRN dysfunction and stem cell exhaustion, imbalanced autophagy, and mitochondrial dysfunction, respectively are largely elusive and need further investigation (**Fig. 7**).

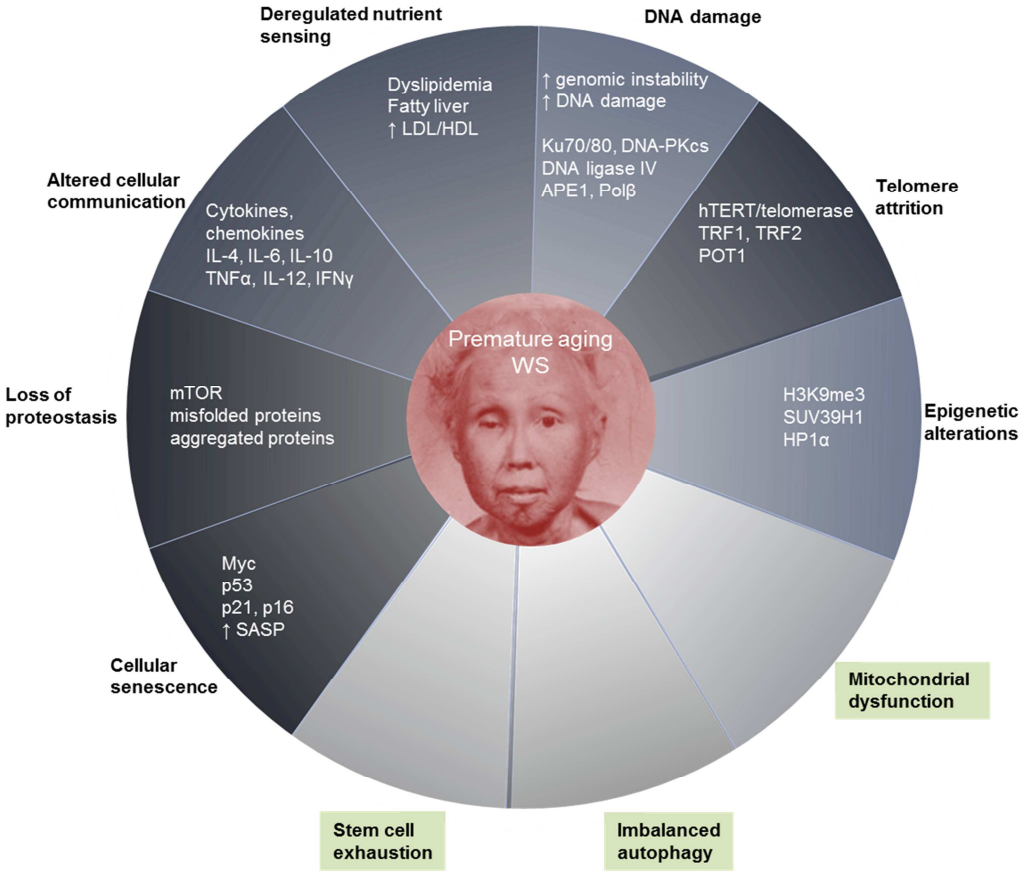

Fig. 7. WS and its relation to the 10 hallmarks of aging. WS can be related to many of the hallmarks of aging indicated outside the circle. Within the colored areas, clinical characteristics, metabolites and proteins involved in the links between WS and the hallmarks of aging are shown. While the linkages between WRN dysfunction and many of the hallmarks of aging are extensively studied, the linkages between WRN dysfunction and stem cell exhaustion, imbalanced autophagy, and mitochondrial dysfunction, respectively (boxed) are largely elusive and need further investigation. For detailed information, please see the text and references found here. Image credit of the WS patient (48 years old): *William and Wilkens publishing Inc*. Figure from Lautrup S. and Caponio D. *et al.* [253].

As already mentioned, WRN has an important role in **DNA maintenance**. To confirm this, the two major characteristics of cells from WS patients are genomic instability and limited cell replicative lifespan [254-256]. At the chromosomal level, genomic instability of WS fibroblasts has been described as variegated translocation mosaicism, with characteristic multiple, variable, predominantly stable chromosomal aberrations [257].

Double Strand Breaks Repair pathway (DSBR) is induced by external insults (*e.g.,* ionizing radiation) as well as internal causes (*e.g.,* endogenous oxygen radicals) and repaired by either non-homologous end joining (NHEJ) or homologous recombination (HR) processes. Recent advances in DSB repair suggest the existence of two distinct mechanisms of NHEJ: classical/canonical (c)-NHEJ and alternative (alt)-NHEJ [258]. The choice of DNA repair pathway is tightly regulated and associated with the cell cycle. While NHEJ is active throughout the cell cycle, DSBs in S and G_2 phases are preferably repaired by HR using the intact sister chromatid. WRN recruits to DSB sites in G_1 as well as in S and G_2 phases [259]. WRN mainly localizes to the nucleolus, and then translocates to DSBs, when occurred. The acetylation of WRN by CBP/p300 affects its subcellular distribution, and deacetylation mediated by Sirt1 affects its translocation to the nucleolus [260, 261]. WRN is known to physically and functionally interact with key proteins involved in NHEJ: Ku70/80, DNA-PKcs and DNA ligase IV/XRCC4 [262, 263]. Ku70/80 and Ligase IV/XRCC4 stimulate WRN exonuclease but not WRN helicase activity, again suggesting a specific requirement of WRN in NHEJ [264, 265]. Alt-NHEJ mainly acts as a backup pathway to c-NHEJ and operates as a major pathway of DSB repair in Ku70/80-deficient cells and ligase IV-deficient cells [266]. MRE11, PARP1, CtIP, DNA ligase I, and DNA ligase III all promote alt-NHEJ [267] and WRN have been demonstrated to interact with some of them, such as PARP1, DNA ligase I, DNA ligase III, and MRN [268-271].

The Ku70/80 heterodimer in association with DNA-PKcs initiates a cascade of events that constitutes the c-NHEJ pathway [272]. WRN has two putative Ku-binding motifs, one in the N-terminus and another in the C-terminus, which accelerate DSB repair. The N-terminal Ku-binding motif mediates Ku-dependent stimulation of WRN exonuclease activity [273]. DNA-PKcs, which gains robust kinase activity by interacting with DSB-bound Ku70/80, phosphorylates WRN at S440 and S467 positions and regulates WRN's enzymatic activities [262, 270]. With its nuclease activity, WRN processes DNA ends and generates substrates suitable for ligation mediated by the X4L4 complex [263]. Ku-mediated c-NHEJ dominates over all other DSB repair pathways, while alt-NHEJ is the default DNA repair pathway in Ku-deficient cells or under conditions that inhibit c-NHEJ [274]. WRN's role in DSB repair pathways is complex; however, findings clearly demonstrate that WRN stimulates c-NHEJ with its enzymatic activities and inhibits alt-NHEJ with its non-enzyme functions [259].

More recently, WRN was shown to participate in 5'→3' DNA end resection in human cells, which is important for the accurate repair of DSBs. This step occurs during HR and creates a substrate for RAD51 binding and subsequent D-loop formation and strand exchange [275].

WRN carries this function in cooperation with the DNA2 endonuclease, likely using its helicase activity to generate a substrate for DNA2. In this role, WRN is redundant with its close homolog, BLM, though it is conceivable that different cell lineages may preferentially utilize one or the other RECQ helicase. Indeed, end resection is carried out in a two-step process: initial resection (short-range), which is regulated by MRN complex with CtIP, and extended resection (long-range) performed by DNA2/BLM or EXO1 [276]. End resection during HR and alt-NHEJ is initiated by MRE11 in association with CtIP. Interestingly, WRN actively restrains 5′-3′ end resection by inhibiting the recruitment of MRE11 and CtIP to DSBs, specifically in G_1 phase. Consequently, alt-NHEJ is upregulated in WS cells and WRN-deficient cells, resulting in telomere fusions. Consistent with this finding, the inhibition of alt-NHEJ by downregulation of CtIP suppresses telomere fusions in WRN-deficient cells [259]. WRN has also recently been shown to inhibit MRE11/Exo1-dependent end resection and generation of single-stranded DNA in camptothecin (CPT)-treated cells [277]. CPT is an anti-cancer agent which blocks replication and induces WRN degradation [278]. Replication fork progression in CPT-treated (low-dose) WS cells was rescued by expressing wild-type WRN [262], and the exonuclease activity of WRN was required to protect DSBs at replication forks from MRE11-dependent processing [277]. WRN and DNA2 physically interact with each other and coordinate their enzyme activities to promote double-stranded DNA degradation and resection at stalled forks [279]. This facilitates fork restart when conditions become permissive for resumption of DNA synthesis. Both WRN helicase and exonuclease activities are implicated in preserving replication forks for restart. WRN may also have an additional role in facilitating DNA synthesis for the first moments after fork restart [280, 281], which is thought to involve its functional interaction with specialized polymerases, such as polymerase eta [282].

Lastly, replication fork phenotypes of WRN deficiency are not limited to cases where replication progression is severely disrupted by genotoxic agents. An early study demonstrated increased stalling of nascent forks during an unperturbed S phase in primary fibroblasts deficient in WRN [283], and later work noted a subtle reduction in fork progression rate during a normal S phase in WRN-depleted transformed human fibroblasts [280]. Chronic low-grade destabilization of forks that can drive the genomic instability phenotype of WRN deficiency, is also suggested by the increased common fragile site expression in WRN-deficient cells [284, 285].

WRN may also participate in base excision repair through the interactions with APE endonuclease and DNA polymerase β [235]. There is a single publication showing the

interaction of WRN and XPG, suggesting an involvement of WRN in nucleotide excision repair [286].

WRN has also a role in **telomere maintenance**. In mammals, telomeres are composed of double-stranded tandem repeats of TTAGGG sequence followed by a single-stranded short 3'-overhang, which invades the double-stranded region to create a T-loop structure. Loss of telomeric repeats or loss of protection by telomere associated proteins triggers telomere dysfunction. Telomeric DNA is bound by several proteins to form the shelterin complex. These proteins include TRF2, TRF1, POT1, TPP1, Rap 1 and TIN2 [287, 288]. In normal cells, the shelterin components TRF2, TRF1 and POT1 directly bind to WRN protein and modulate its enzymatic activities [289, 290]. Indeed, several studies showed that TRF2 regulates the exonuclease activity of WRN; Machwe *et al.*[291] showed that TRF2 recruits WRN to process telomeric ends that form into T-loops, a proposed loop-back structure in which the G-rich single stranded end invades internal telomeric sequences to generate a three-stranded structure (a form of D-loop). Dissociation of D-loop structures is required for release the invading strand and for DNA replication at telomeric regions [291]. Furthermore, POT1 is able to bind the single-stranded G-rich portion of telomeres; it plays a role in capping telomeric ends, preventing them being recognized as DNA damage, and also enhances D-loop unwinding of WRN by maintaining the unwound strands in a melted state. Since WRN helicase has a role in restart of stalled replication forks, an important mechanism for continuing the replication process following DNA damage, WRN and POT1 can cooperate with each other to resolve the G4 structures at telomeres [292]. Several lines of evidence suggest that telomere dysfunction contributes to WS pathology. Cells from WS patients and WRN-deficient cells undergo early replicative senescence and display telomere loss and chromosomal rearrangements. Telomere fusions and chromosome translocations are also well documented in WS patient and WRN-deficient mouse cells [241]. Importantly, re-introduction of telomerase activity into WS cells prevents senescence and telomere loss [241]. Additionally, although the WRN protein is ubiquitously expressed, WS patient cells preferentially display premature aging of mesenchymal cells [293]. In the absence of telomerase, cells maintain their telomeres via recombination mechanisms termed alternative lengthening of telomeres (ALT). ALT cells and cells without WRN protein show increases in telomere-sister chromatid exchanges [259, 294, 295]. This may in part explain that the absence of WRN facilitates the activation of ALT as telomere maintenance mechanism [259] and link with the tumor spectrum of WS patients. Indeed, the development of malignant neoplasm require a mechanism of telomere elongation, such as ALT [295].

The genome-wide distribution of **histone methylation marks** changes during aging [296]. Consistent with this, patients with WS display increased epigenetic age as measured by DNA methylation of known aging biomarkers [239]. In humans, H3K9 trimethylation (H3K9me3) denotes constitutive heterochromatin and is mainly methylated by SUV39H1/2 histone methyltransferase (HMTase) [297]. Though not fully characterized, loss of heterochromatin is considered to increase the susceptibility of genomic DNA to mutations and reduce transcriptional precision, both of which promote genomic instability during aging [296]. Interestingly, Zhang *et al.* [252] reported that WRN exists in complex with SUV39H1, HP1α, and LAP2β, which together are responsible for the epigenetic histone mark H3K9me3. WRN also interacts with the chromatin remodeling chaperone chromatin assembly factor 1 (CAF-1) [298], which deposits histones H3 and H4 onto newly replicated DNA [299]. In response to DNA damage, WRN recruits CAF-1 and participates in chromatin structure restoration [298]. A role of WRN in chromatin regulation has also been suggested by a recent study indicating that treatment with Vitamin C likely rescues many features of premature aging seen in WRN-deficient MSCs via altered expression patterns of a series of genes involved in chromatin condensation, cell cycle regulation, DNA replication and DNA damage and repair [300], though it needs further verification.

In vitro, premature **cellular senescence** is a striking feature of WRN-deficient cells [301]. Collectively, WS patient cells and WRN knock-down cells have been related with premature senescence. The clinical manifestations of WS, including a bird-like appearance, alopecia/gray hair, skin hyperpigmentation, hoarseness, diffuse arteriosclerosis, juvenile bilateral cataracts and osteoporosis, are all associated to premature senescence [302]. Furthermore, primary skin fibroblasts from WS patients and WRN-deficient cells undergo early replicative senescence. Additionally, cells depleted for WRN show increased senescence-associated beta-galactosidase (SA-β-gal) staining, activation of the senescence-associated secretory phenotype (SASP) [303, 304] and accumulation of DNA damage foci [251]. The premature senescence seen in WRN-deficient cells is related to the observed telomere shortening; overexpression of telomerase (hTERT) inhibits premature senescence at the same level as rescue with WRN protein [241, 250]. WRN-null human embryonic stem cells (hESCs) differentiated to mesenchymal stem cells (MSCs) recapitulate features of premature cellular aging including changes of heterochromatin architectures in addition to altered epigenetic marks *e.g.* global loss of H3K9me3, all signs of premature senescence. Interestingly, MSCs from older individuals display decreased levels of WRN in addition to altered heterochromatin marks resembling the alterations seen in the WRN-null MSCs [252]. All these

data demonstrate that deficit in DNA repair, telomere shortening and epigenetic alteration due to WRN loss promote premature cellular senescence.

WRN also links with an impairment of **protein homeostasis** and a deregulation of proteolytic system. Cataracts are one of the most common features observed in WS patients. WRN expression is severely affected by promoter hypermethylation in age-related cataract lens cells [248]. Furthermore, in cultured WS fibroblasts, there is an increase in cytosolic aggregates, which is indirectly related to an excess activation of the mTOR (mammalian target of rapamycin) pathway, leading to the formation of protein aggregates in the cytosol with increasing levels of oxidative stress [247]. Since the expression levels of the two main H_2S producing enzymes, cystathionine β synthase and cystathionine γ lyase, are lower in WS cells compared to normal, the authors evaluated the effect of administration of H_2S as sodium hydrosulfide (NaHS) [247]. NaHS treatment blocked mTOR activity, abrogated protein aggregation and normalized the phenotype of WS cells. Similar results were obtained by treatment with the mTOR inhibitor rapamycin. These data suggest that hydrogen sulfide administered as NaHS restores proteostasis and cellular morphological phenotype of WS cells [247].

WRN may also have a role in regulating **nutrient-sensing mechanisms**. Reduced insulin sensitivity with increased visceral adiposity [302] is the hallmark of both WS and normal aging. Indeed, adipocytes secrete a number of hormones (or adipocytokines), such as tumor necrosis factor-α (TNF-α), leptin, adiponectin, and resistin, thereby regulating insulin sensitivity [305]. The accumulated intra-abdominal visceral fat [306] suggests an altered production of adipocytokines. To investigate the role of adipocytokines in the pathophysiology of WS, Yokote *et al*. [245] examined the serum levels of TNF-α and adiponectin. The serum level of TNF-α, a mediator of insulin resistance, was significantly elevated in WS regardless of having diabetes or not having diabetes compared with the healthy control group. Adiponectin levels in diabetic WS patients was significantly lower than in nondiabetic WS patients or control subjects [245]. These data indicate insulin sensitizing as well as antiatherogenic actions of adiponectin and the association of decreased serum adiponectin with insulin resistance, obesity, and type 2 diabetes [305, 307]. They also reported the successful improvement of glycemic control and insulin sensitivity by pioglitazone in diabetic WS patients. Indeed, the treatment significantly elevated adiponectin levels, while TNF-α and HbA_{1c} levels showed a tendency to decline. According to these data, adipocyte function may be a key element linking *WRN* mutation and the metabolic abnormalities observed in WS and pioglitazone administration could extend the lifespan of WS patients by improving metabolism and preventing early cardiovascular death. Furthermore, Maity *et al*. [308] found that WS cells

respond very weakly to starvation induced autophagy and that this was complemented by transfection with full length WRN which restored the expression of genes responsible for the induction of autophagy. Similarly, depletion of WRN from normal cells results in diminished autophagy and down regulation of autophagy related genes [308]. Deficiency of autophagy in WS cells is primarly due to a downregulation of proteins involved in autophagic initiation process, such as Beclin-1, Atg5 and LC3B. WRN enhances autophagy perhaps by two different pathways. WRN suppresses mTOR, a negative regulator of autophagy. On the other hand and probably more significantly WRN interacts with RNA pol II and subsequently trans-activates autophagic genes including LC3B, Beclin-1, and Atg5 under starvation [308]. However, the exact mechanisms by which WRN induces autophagy are speculative. These results indicate that lack of autophagy is one of the possible reasons for the premature aging in WS cells.

As already mentioned, aging is associated with "inflammaging", an increased production of pro-inflammatory agents, associated with tissue damage and **altered intercellular communication**. Patients with WS have elevated levels of inflammation-driven aging-associated cytokines (IL-4, IL-6, IL-10, granulocyte macrophage colony-stimulating factor [GM-CSF], IL-2, TNF-α, interferon gamma [IFNγ], monocyte chemoattractant protein-1 [MCP-1], and granulocyte colony-stimulating factor [G-CSF]) compared with normal individuals [249].

III.4. *WS model systems*

Most of the data available concerning the underlying mechanisms of WS are based on three model systems: fibroblasts and lymphoblastic cell lines derived from WS patients and two animal models, *Caenorhabditis elegans (C. elegans)* and *Drosophila melanogaster (Drosophila)*. Due to the well-known conservation of evolutionary pathways between the species, both *C. elegans and Drosophila* can be used for drug development against human diseases. Despite mice being the generally most common animal model used for studying human diseases, it must be kept in mind that mice are more expensive to maintain in the laboratory, relatively long-lived and they require a very long process for genetic manipulation. In contrast, *C. elegans* and *Drosophila* models are cheaper to maintain, easy to manipulate and short-lived enabling large-scale lifespan and healthspan studies. One complication in studying the functions of WRN is its unique double DNA repair activities, where it functions both as an exonuclease and a helicase. Similar as the human WRN, the mouse WRN (mWRN) protein contains both the helicase and exonuclease domains, making a

difficulty to disentangle the distinctive biological functions of the two domains. When modifying either one or both domains in mWRN, the mice lack a premature aging phenotype. This might be due the extended telomeres in mice compared to humans, since a premature aging phenotype appears in the telomerase-WRN double null mouse model [309]. Therefore, the WS mouse models are not a preferable choice when studying WS. Unlike mammals, the WRN activities are separated on different proteins in both flies and worms, enabling the separation of these activities and likely helping to understand its involvement at an organismal level.

III.4.a. *WS C. elegans*

In *C. elegans,* four RecQ family DNA helicases have been identified by comparing the genomic DNA sequences. These include the open reading frame T04A11.6, homologous with mammalian RecQL; HIM-6, corresponding to BLM; RCQ-5, equivalent to RecQ5; and the open reading frame F18C5.2 homologous with human WRN and therefore named WRN-1 in WormBase (https://www.wormbase.org/). No homolog of RecQ4 has been predicted in *C. elegans*. WRN-1 possesses only the helicase motif with a DEAH box which shares 43% identity in the amino acid sequence with that of the human WRN helicase domain. Moreover, the RQC (RecQ helicase conserved) domain and the HRDC (Helicase and RNase D, C-terminal conserved) domain share 27% identity with human WRN [310] (**Fig. 6**). In *C. elegans*, WRN-1 lacks the exonuclease domain, although the exonuclease domain of MUT-7 shares 29% identity with human WRN (**Fig. 6**) [310]. Despite the homology, MUT-7 cannot be considered a functional homolog of WRN exonuclease, since it is involved in RNA interference and gene silencing [311, 312], while the helicase activity has been shown to unwind various DNA structures [313]. WRN-1 and also mWRN are non-uniformly distributed in the nucleoplasm at different cellular stages [310], whereas human WRN is mainly localized in the nucleolus [204, 314].

The *wrn-1* in *C. elegans* recapitulates several major phenotypes of WS patients, but also shows some distinctive features. The WRN-1 protein level has been shown to decrease with age in all tested tissues in adult worms [310]. Notably, it has been shown that by silencing *wrn-1* using RNAi knockdown, worms have a shortened lifespan (from 13.6 of WT to 11.0 days in the *wrn-1*(RNAi) at 25°C), they accumulate lipofuscin faster than wild type worms and show phenotypes similar to clinical manifestations in human WS such as small body size, the formation of a “bag of worms” (where the parent’s cuticle surrounds it’s progeny), ruptured body, dumpy shape, growth arrest at larval stages and a transparent body [310]. *Wrn-1* (RNAi)

worms also show an acceleration of larval growth and surprisingly early *wrn-1* (RNAi) embryos exhibit a shorter S-phase, which is in contrast to an elongated S-phase seen in WS patient cells [310]. Indeed, mitotically proliferating germ cells in *wrn-1* (RNAi) worms show an ineffective checkpoint for DNA replication arrest even after hydroxyurea-induced stress. Moreover γ-radiation exacerbates the WS phenotype of *wrn-1* (RNAi) worms, while the faster growth rate is independent of ionization, suggesting that WRN-1 is involved in cellular responses to DNA damage [310]. Additionally, WRN-1 has been proposed to be responsible for extensive end-resection. When WRN-1 is absent, it causes hyper-accumulation of RPA resulting in a failure of recruitment and phosphorylation of RAD-51, leaving the cells with an inefficient double strand break repair system [311, 315].

The *wrn-1 C. elegans* serves as a useful model for drug screening towards WS. By the application of the *wrn-1 C. elegans*, it has been shown that vitamin C extends lifespan in these WS worms [316, 317]. In *wrn-1* worms, vitamin C treatment altered the expression of genes involved mainly in locomotion and anatomical structure in addition to carbon metabolism (sugars and lipids), likely involved in the premature aging phenotype [310, 317]. Importantly, vitamin C has been verified to be effective in the WS mice [318] as well as in a human mesenchymal stem cell model of WS [319]. All in all, the current data suggest that *wrn-1* worms recapitulate some primary phenotypes of WS patients, and can serve as a powerful model for anti-WS drug screening.

III.4.b. *Drosophila models of WS*

In flies, an orthologue of the exonuclease domain of human WRN has been identified. Proteins encoded by the CG7670 and CG6744 loci have been identified as homologous to the human WRN exonuclease domain [320]. CG7670 displays 34% homology, while CG6744 displays 33% homology with human WRN, respectively. CG6744 shares homology with the ATP-binding domain, the RQC region and C-terminal region of human WRN [320, 321]. Additionally, CG6744 also shows 40% identity and 59% similarity with the exonuclease 3'-5' domain-like 2 protein (**Fig. 6**) [320]. Thus, CG6744 has been assigned as the orthologue of human WRN, termed DmWRNexo [320]. The helicase domain of human WRN has been found to share a high percentage amino acid identity and similarity (80%) with DmBLM encoded by the *mus309* locus (**Fig. 6**) [320, 322].

Although lack of a helicase domain, the DmWRNexo reserves some important functions of human WRN. DmWRNexo is involved in restarting stalled replication forks, and mutations in its locus lead to hyper-recombination and camptothecin hypersensitivity, as already shown in human WS cells [321, 323]. Studies have also demonstrated how DmWRNexo plays a key role already in the early embryogenesis. Indeed, fly embryos carrying a mutation in the exonuclease domain of DmWRNexo, undergo slower replication. This causes replicative fork arrest leading to accumulation of DNA damage, resulting in improper nuclear division and embryonic development [324]. Similar features have already been observed in WS and WRN–depleted human cells [325-327].

III.4.c. *WS mice*

mWRN shares ~70% amino acid identity with that of the human WRN protein and it exhibits both helicase and exonuclease activity [328] (**Fig. 6**). There are at least three WS mouse models available. These models include mice lacking the entire WRN protein (*Wrn null* or $Wrn^{-/-}$ mice), mice carrying a deletion in the helicase domain ($Wrn^{\Delta hel/\Delta hel}$ mice) and transgenic mice expressing human WRN with a dominant-negative mutation (K577M-WRN) [328-331]. $Wrn^{-/-}$ *and* $Wrn^{\Delta hel/\Delta hel}$ mice have been well-characterized. The $Wrn^{-/-}$ mice show increased DNA damage sensitivity, but surprisingly they do not exhibit accelerated aging features, possibly due to the long telomeres compared to humans [309]. Indeed, Chang *et al*. showed that combined telomere dysfunction and *WRN* depletion in mice faithfully manifests human WS [332]. Thus the $Terc^{-/-}$ $Wrn^{-/-}$ mice recapitulate many of the phenotypes of human WS, showing a key role of telomere maintenance in WS and the aging process [309].

Conversely, the $Wrn^{\Delta hel/\Delta hel}$ mice recapitulate most of the WS phenotypes, such as abnormal hyaluronic acid secretion, higher systemic ROS levels, dyslipidemia, heart failure, increased genomic instability and different types of cancers [329, 333, 334]. Moreover, these mice have a shorter mean lifespan (reduced 10-15% when compared to wild type). As also seen in human cells and *C. elegans* models, vitamin C increases the lifespan and healthspan of $Wrn^{\Delta hel/\Delta hel}$ mice [318, 330]. Mislocalization of WRN mutant protein to organelles including peroxisomes, endoplasmic reticulum and autophagosomes, rather than to the nucleus, likely is responsible for the premature aging phenotypes [331].

WRN K577M mice show abolished ATPase and helicase activity but a retained exonuclease activity. In addition, tale fibroblasts from K577M-WRN transgenic mice exhibit

hypersensitivity to the genotoxic agent 4-nitroquinoline-1-oxide (4NQO) and slower proliferative capacity, even though these mice do not show any pathophysiological feature linked to WS [335].

III.4.d. *Human WS iPSC*

The availability of WS iPSCs has provided a new and powerful approach to study WS, through the provision of isogenic background and the differentiation of any types of cells of interest. Generation of WS iPSCs allows researchers to unveil pathophysiological mechanisms and also test the newest pharmacological treatments in a human matrix. Currently, most of the data on WS are limited to patient-derived fibroblasts and lymphocytes. *WRN*$^{-/-}$ hESCs have been established and differentiated to MSCs as explained earlier. The *WRN*$^{-/-}$ MSCs exhibited features of premature cellular aging, including premature loss of proliferative potential and epigenetic and chromatin structure alterations [336]. Although these cells provide a reasonable model of WS, a human iPSCs line would allow the *in vitro* reconstruction of the disease. Currently, the generation of human iPSCs from WS patients are limited to three cases, describing a successful generation of iPSCs through the introduction of several pluripotency genes and the gene encoding human telomerase reverse transcriptase (hTERT) [337-339]. When fully reprogrammed to iPSCs, the cells completely lost the WS related phenotype and showed restored telomerase levels, opposite to the original WS patient fibroblasts. Additionally, the karyotype of the iPSCs remained stable over multiple passages [340]. A strong interplay between WRN and telomere maintenance has previously been observed, confirming the importance of telomere maintenance. Induction of hTERT in the reprogramming process from WS patient fibroblasts to iPSCs recovers the telomerase activity, which causes elongation of telomeres and hereby an extended cellular lifespan [340]. These data demonstrate that the premature senescence observed in WS fibroblasts likely is due to an insufficient activity of telomerase, and that expression of hTERT recovers the phenotype when generating iPSCs [337, 338]. Results from these iPSC studies suggest that WS is a stem cell dysfunction-associated disease. However, since WS is a segmental progeroid syndrome, features associated with aging (such as dementia) do not completely overlap with WS. Despite the apparent aging phenotypes observed in mesenchymal stem/progenitor cells and fibroblasts, lack of premature senescence is observed in neural stem cells, keratinocytes [293] and endothelial cells [341]. It raises the question whether *WRN* mutation equally affects all the lineages and tissues. Besides senescence, other hallmarks of aging have not been

systematically examined in different adult stem/progenitor cells. Thus, more studies are needed to differentiate the effects of WRN depletion in various iPSC-derived cell types.

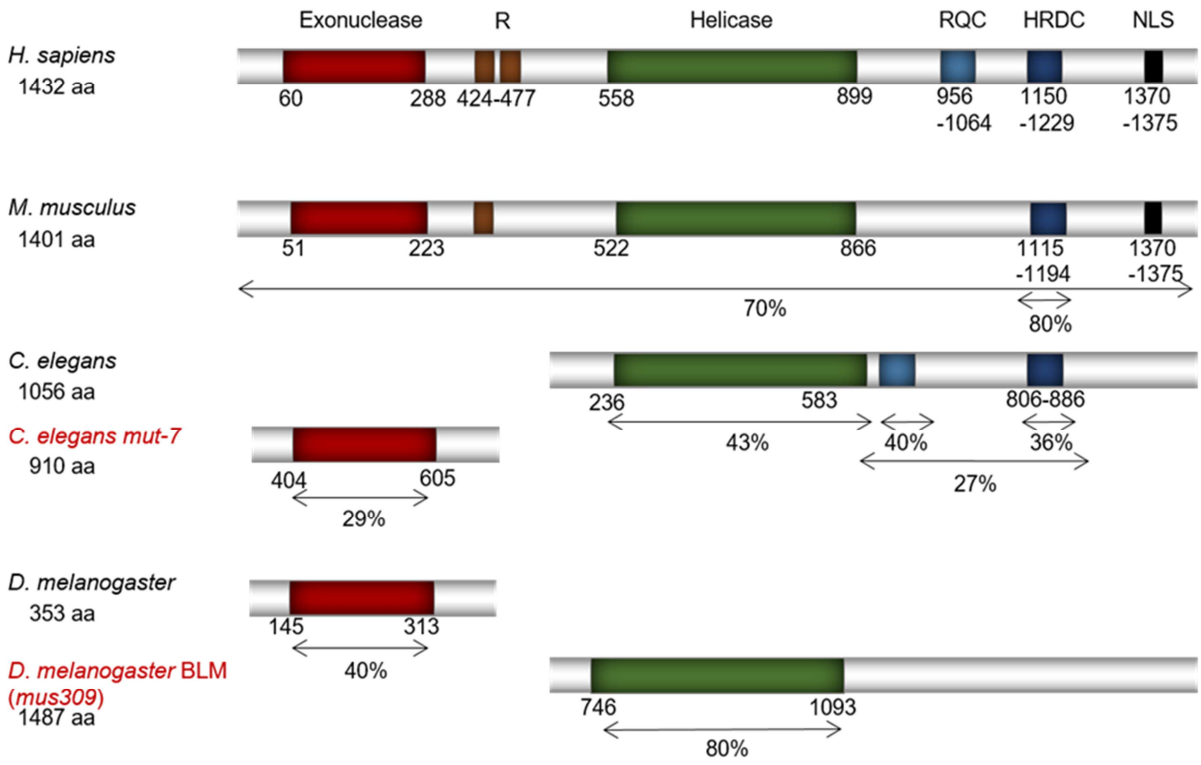

Fig. 1. Comparison of conserved regions of WRN in WS humans and animal models. Amino acid identities with human WRN are indicated below WS model proteins. R = acidic repeats; RQC = RecQ conserved domain; HRDC = helicase Rnase D conserved domain; NLS = nuclear localization signal. The numbers just below the illustration of the various domains refer to the amino acids in the protein sequence. The domains are drawn based on *H. sapiens*: UniProtKB – Q14191 and [215]; *M. musculus*: UniProtKB - O09053 and [342]; *C. elegans* wrn-1: UniProtKB - Q19546 and [310, 311]; C. elegans mut-7: UniProtKB - P34607 and [310]; *D. melanogaster* WRN: UniProtKB - Q9VE86 and [320, 321]; *D. melanogaster* BLM encoded by mus309 locus: UniProtKB - Q9VGI8, [320, 322]. RecQ5 and RecQ4 also show high similarity to human WRN, but lower than that of DmBLM [320]. Figure from Lautrup S. and Caponio D. *et al.*[253].

AIM OF THE THESIS

Nowadays aging is the major challenge in human medical care. During the last decades, ten hallmarks of aging have been well-characterized. These hallamarks are: genomic instability, telomere attrition, epigenetic alterations, loss of proteostasis, deregulated nutrient-sensing, mitochondrial dysfunction, cellular senescence, stem cell exhaustion, altered intercellular communication, and defective autophagy/mitophagy. More recently, NAD^+ replenishment has been considered as a novel approach to improve health and slow and even reverse the aspects of aging and delay the progression of age-related diseases, such as metabolic disorders, cancer and neurodegenerative diseases. Indeed, also NAD^+ depletion has been linked to all the hallmarks of aging and may underlie a wide-range of age-related diseases. From this perspective, boosting NAD^+ levels may arise as a promising therapeutic strategy to counter aging-associated pathologies and/or accelerated aging, such as Werner syndrome (WS). WS is a segmental progeroid syndrome, which mimics aging at an accelerated rate and, for this reason, has provided cues in understanding the hallmarks of aging. Indeed, WS has been linked to most of hallmarks of aging, such as genomic instability, telomere attrition, epigenetic alterations, loss of proteostasis, deregulated nutrient-sensing, cellular senescence, altered intercellular communication. The linkages between WRN dysfunction and stem cell exhaustion, imbalanced autophagy, and mitochondrial dysfunction, respectively are largely elusive and need further investigation.

Exploration of the interconnected networks between NAD^+ depletion and WRN dysfunction could provide new angels to understand the sophisticated aging process.

This thesis aims to clarify the connection between WRN and stem cell exhaustion, imbalanced autophagy, and mitochondrial dysfunction respectively and to investigate a possible involvement of NAD^+ depletion in molecular pathology in WS. Moreover, it explores the possibility that bolstering cellular NAD^+ levels may counteract WS phenotypes.

MATHERIALS AND METHODS

Cell Culture, RNAi knockdown, and mitochondrial parameters. The primary fibroblast cell lines HT01 (#AG09599) and the WS01 (#AG03141) cells were acquired from Coriell Institute. The WRN-KD cells were siRNA knockdown in HT01 cells using WRN human siRNA ologo duplex (CAT#: SR322215, Origene). Briefly, siRNAs were incubated in Optimem with 4 ml RNA Interferin (siRNA transfection reagent, Polyplus) per 1 ng RNA for 15 min and added to complete media for a final concentration of 30 nM siRNA. After 3-day incubation, cells were applied for further experiments. Knockdown efficiency was examined by western blot. All other primary human fibroblasts (detailed in Table S1) were generated with approval by the ethics committee of the Chiba University Graduate School of Medicine, and signed informed consent obtained from the patients. The mouse embryonic fibroblasts (MEFs) were generated from *Wrn*$^{-/-}$ embryos with MEFS from the wild type littermates as controls. All cells were maintained in GIBCO MEM medium supplemented with 15% FBS, 1% P&S, 1xVitamin C, 1xGlutamin, and 1xNEAA, and grown in 20% O_2/5% CO_2 at 37 °C. Cells of 6-10 passages were used for the experiments. Flow cytometery was used mitochondrial parameters, electron microscopy for mitochondrial morphology, a XFe96 for mitochondrial oxygen consumption rate (OCR), and a luminescent assay for ATP quantification. First, human primary cells (HT01, WRN-KD, WS01) or MEFs (WT and *Wrn*$^{-/-}$ cells) were stained with designated dyes followed by flow cytometry to quantify relative mitochondrial ROS (using mitoSOX dye 3 μM for 30 min), mitochondrial membrane potential/MMP (TMRM dye, 10 nM for 15 min), or relative mitochondrial content (MitoTracker Green, 50 nm for 30 min) [103]. All reagents were from Life Technologies. Data was analyzed using FCS Express 4 software (De Novo Software). ATP levels in the primary human fibroblasts were examined using a commercial kit (abcam#ab113849).

Mice and mitochondrial functions. Mice carrying *Wrn*$^{-/-}$ allele [309] were maintained under standard laboratory conditions at the NIA with free access to water and standard diets. All animal experiments were approved by the NIA animal care and use committee. High resolution respirometry was performed on the Oxygraph-2k (O2k, OROBOROS Instruments, Innsbruck, Austria) according to previous report [343]. Mice were sacrificed by cervical dislocation and brain, heart and liver tissues were rapidly dissected and homogenized by 10-15 strokes of a 15mL dounce homogenizer in Mir05 respiration buffer (110 mM sucrose, 60 mM K-lactobionate, 0.5 mM EGTA, 3 mM $MgCl_2$, 20 mM taurine, 10 mM KH_2PO_4, 20 mM HEPES, and 0.1% BSA essentially fatty acid free, pH 7.1 at 37°C). Protein was quantified by BCA assay and 1 mg/mL homogenate loaded for respiration measurements at 37°C. Malate

(2.5mM), pyruvate (5mM) and ADP (2.5mM) addition results in complex I mediated state 3 respiration. Subsequently, complex I inhibitor rotenone (0.5μM) was added and then complex II substrate succinate (10mM) injection initiates complex II mediated state 3 respiration. Complex III inhibitor antimycin A (2μM) was then added followed by the artificial complex IV substrate ascorbate + TMPD (4mM +1mM, respectively). Fatty acid metabolism of the heart homogenate was also performed using malate plus palmitoyl-carnitine (5mM each) followed by state 3 respiration initiate with 2.5 mM ADP.

Fly lines, lifespan and i*n vivo* stem cell proliferation assays. To temporally control WRN knockdown, we used GeneSwitch lines expressing an inactivated form of Gal4 that is activated in the presence of the drug RU486 [344]. We used *w;DaGeneSwitch-Gal4* for ubiquitous knockdown and *w;5961GeneSwitch-Gal4, UAS-nlsGFP/CyO* (a gift from Benjamin Ohlstein [345]) for intestinal stem cell-specific knockdown. We used *y,v,sc;Wrnexo*$^{\text{RNAi}}$*;* (Bloomington line #38297) for knockdown, and *w;LacZ* RNAi (a gift from Masayuki Miura) as controls for non-specific RNAi effects.

Flies were maintained at 25°C on a 12 hr light/dark cycle, using the following food recipe: 1L distilled water, 13g agar, 22g molasses, 65g malt extract, 18g brewer's yeast, 80g corn flour, 10g soy flour, 6.2ml propionic acid, 2g methyl-p-benzoate in 7.3ml of EtOH. For treatment food, RU486 was dissolved in the EtOH for 200 μM final concentration. Lifespan experiments were performed as previously described [346]. Briefly, female offspring of *DaGeneSwitch* and *Wrnexo*^{RNAi} lines were allowed to mate for 2-3 days, then transferred to vials with food ± RU486 and/or NMN at 5mM final concentration. Up to 70 flies per vial were flipped thrice weekly, with dead flies counted visually. The Kaplan-Meier lifespan curves were generated using Prism. For statistics, multiple condition experiments were evaluated by one-way ANOVA with statistics using Peto's log-rank test (Cox-Mantel test).

The *5961GeneSwitch-Gal4, UAS-nlsGFP* line was crossed to *Wrnexo* or *LacZ* RNAi to evaluate stem cell proliferation in response to pathogenic insult. After allowed to mate for 2 days after eclosionfemale offspring were transferred to food with/without RU486 (200 μM), ± NR supplementation (0.78 mM). At six days of age (after four days of RNAi), they were transferred to 5% sucrose ± *Erwinia carotovora carotovora 15* from 15 mL of overnight culture. After 24 h, guts were dissected in 1x phosphate-buffered saline (PBS), fixed for 45 min at room temperature (100 mM glutamic acid, 25 mM KCl, 20 mM $MgSO_4$, 4 mM sodium phosphate, 1 mM $MgCl_2$, and 4% formaldehyde), washed for 1 h at 4°C (1x PBS, 0.5% bovine serum albumin and 0.1% Triton X-100), and then incubated with rabbit anti-phospho-

Histone H3 Ser 10 (Upstate, 1:1,000) overnight at 4°C. Secondary antibody staining was done at room temperature for 2 h, using fluorescent antibody from Jackson Immunoresearch at 1:500. DAPI was used to stain DNA (1:1000). Guts were washed 3x 10 min after each antibody. pH3 positive cells were counted manually on a Zeiss dissecting fluorescent microscope, with representative images captured on a Zeiss LSM 700 confocal microscope and processed using Adobe Photoshop/Illustrator. The *UAS-nlsGFP* construct was used to evaluate the total number of intestinal stem cells, to rule out cell death as a factor in the proliferative response. Comparisons between proliferation counts were done by one-way ANOVA, using Sidak's post hoc test.

***C. elegans* strains, and lifespan/healthspan studies.** Standard *C. elegans* strain maintenance procedures were followed in all experiments [347]. Nematode rearing temperature was kept at 25°C, unless noted otherwise. N2: wild type Bristol isolate was from Caenorhabditis Genetics Center and the *wrn-1(gk99)* was a gift from Dr. Hyeon-Sook Koo (Yonsei University, Korea) [310]. RNAi knockdown of designated genes was performed using standard protocol and verified by PCR [348]. Lifespan examination was performed at 25°C on NGM plates containing 100 μM 5-FudR and seeded with 100 μL E. coli OP50 strain. Worms were scored every other day and scored as dead when they stopped pharyngeal pumping and were unresponsive to touch. Lifespan experiments were performed with 100-150 worms/group. Kaplan Meier survival curves of pooled populations were generated and the log-rank test was used for statistics. Swimming and pharyngeal pumping were used for healthspan evaluation following established methods [348], with 10-30 worms/group (3 biological repeats). Drug or vehicle treatment began at L4 stage, unless noted otherwise. Drugs used were the NAD^+ precursors NR and NMN (both at 1 mM), a SIRT1activator SRT1720 (10 μM), and a PARP inhibitor Olaparib (500 nM). Two to seven biological repeats were performed for all experiments. OCR of *C. elegans* was measured using Seahorse XFe96 instrument [349, 350]. *wrn-1* and N2 *C. elegans* strains were synchronized by standard egg lay and L4 stage nematodes were transferred to plates +/- NR (1mM). At days 2 and 10, worms were washed three times with M9 buffer and allows to digest gut bacteria for 30 minutes prior to the start of respiration. Worms were plated in XFe96 seahorse plates in M9 buffer (15-30 worms per well). Instrument was started with 6 measurements of each respiratory state. First, baseline respiration was measured followed by injection of FCCP (10μM, final concentration) to elicit maximal respiration. Then, sodium azide (40mM, final concentration) was injected to account for non-mitochondrial respiration. Number of nematodes per well were counted for normalization.

Quantification of mitotic cells in the germ line region of *C. elegans*. For quantification of mitotic cells, immunostaining was performed as described previously [351]. Briefly, worms were treated with NR (1 mM) at L4 stage and germlines were isolated on adult day 1 and adult day 6 worms. Germlines were isolated on poly-L-lysine-coated slides in egg buffer (containing 25 mM HEPES, pH 7.4, 118 mM NaCl, 48 mM KCl, 2 mM CaCl2, 2 mM MgCl2) supplemented with 0.1% Tween-20 and 0.2 mM levamisol. The slides were mounted with 7 µl mounting solution containing ProLong Gold (Thermo Fisher) and 0.5 µg/ml DAPI (Sigma), followed by imaging in a confocal microscope. Number of mitotic cells was measured using ZEN 2.3 software. The distal edge of the transition zone border was defined as the first cell diameter in which two or more nuclei displayed the characteristic crescent shape.

***C. elegans* imaging.** We performed imaging for mitochondrial network, mitophagy levels, and fat staining. To evaluate mitochondrial network in worm muscle cells, a *myo-3::gfp* reporter strain was imaged with Zeiss confocal microscopy, with 5 images/worm and 15 worms/group/experiment. Mitochondrial network was scored in a double-blinded manner on an arbitrary scale from 1 to 5. A score of 5 denotes a perfectly organized mitochondrial network with healthy mitochondria running parallel with the myofilament lattice. For highly fragmented and disorganized mitochondrial network morphology, we gave a score of 1 [348]. The mitophagy reporter strain *N2;Ex(pmyo-3::dsred::lgg-1;pdct-1::dct-1::gfp)* (a gift from Dr.Tavernarakis [98]) was crossed with the *wrn-1(gk99)*, followed by evaluation of mitophagy as detailed previously [348]. For imaging of mitophagy signals, we randomly took over 5 images/worm with 15 worms/group/ experiment with at least two biological repeats.

Fat staining in *C. elegans*. Oil Red O staining was carried out as previously described with some modifications [352, 353]. Day 7 old worms (100-200 adults) were washed three times with PBS then fixed in 200 µl of 1xPBS, 10% PFA and 2XMRWB (KCl 160 mM, NaCl 40 mM, NaEGTA 14 mM, 30 mM PIPES pH 7.4, 0.4 Spermine 1 mM, 1 mM Spermidine, 0.2% beta-mercaptoethanol) buffer for 1 hour in an end over end mixing at room temperature. Fixed worms were washed 3 times with 100 mM Tris-HCl (pH 7.4). After the washes, the worms were incubated with 250 µl 40 mM DTT for 30 minutes at RT, followed by 3 washes in 1xPBS and a 15 minutes incubation with 70% isopropanol. Isopropanol was removed, and 1 ml of 60% Oil-Red-O dye (Sigma-Aldrich Cat. No. O9755) was added. Oil-Red-O solution was prepared by dissolving the dye in isopropanol at 5 mg/ml and equilibrating for several days. The solution was then freshly diluted with 40% water to obtain a 60% stock, allowed to sit 10 minutes at room temperature and filtered before using to remove insoluble material.

Stained animals were incubated overnight with rocking at room temperature. The dye was then removed and 200 µl of 1x PBS with 0.01% TritonX-100 was added. Oil-Red-O absorbs light at 510 nm [353]. Using ImageJ we measured the average pixel intensity for a 40 pixel radius in an area behind the pharynx of each animal. A minimum of 40 animals were measured for each strain.

Mass spectrometric analysis of PAR levels. For quantitation of PAR levels in *C. elegans*, around 3,000 worms were collected at an adult age of 7 days and snap frozen in liquid nitrogen. Thereafter, worm pellets were resuspended in 1 ml 10% TCA and subjected to 5 freeze-thaw cycles using liquid nitrogen and a 37°C water bath. Then, samples were centrifuged at 3,000 × *g* for 10 min at 4°C. The TCA pellets were washed twice in 500 µl ice-cold 70% EtOH, air-dried, and stored at -20°C until further processing. Afterwards PAR was purified and analyzed by mass spectrometry as described previously [354, 355].

Microarray and proteomics using *C. elegans* samples. For both experiments, N2 and wrn-1(gk99) were treated with NR (1 mM final concentration) from L4 stage, followed by collection of the worms tissues from adult day 1 and adult day 7, with fresh drugs administered at adult day 4. The worms were washed with M9 buffer 3 times and flash frozen. The samples were then subjected to microarray as well as proteomics with detailed methods mentioned previously [348].

Electron microscopy (EM). EM was used to examine ultrastructure of mitochondrial morphology which was performed by a US Certified Electron Microscopist Dr. J. Bernbaum. 25-30 images were randomly taken for each sample. Quantification of mitochondrial parameters in different cell types was performed using ImageJ plugin ObjectJ (length, diameter, and area). Percentage of damaged mitochondria as well as mitophagic-like events were calculated. All quantifications were performed in a double-bind manner with two-way ANOVA used for the comparison between multiple groups.

NAD^+ quantification and metabolomics for NAD^+ metabolites. Measurement of NAD^+ levels was performed using two methods, including a commercial kit and liquid chromatography-mass spectrometry (LC-MS) [356, 357]. For the commercial kit (#ab65348), cells were freshly collected (5 million cells/group), quickly washed with 1xPBS (cold), followed by NAD^+ detection per manufacter's protocol. All the procedures were performed on ice or at 4°C to minimize NAD^+ metabolism. To detect intracellular NAD^+ metabolites (including NMN, NAD^+, NAAD, ADPR, MeNAM, NA, Inosine, IMP, NADP, cytidine, AMP, ADP, NAM etc), cells were treated with NR for 24 h, followed by collection of cells

for LC-MS as detailed elsewhere [356]. Snap frozen cells from three biological repeats were collected for LC-MS. The experiments were performed at Dr. Charles Brenner's laboratory.

Extracellular metabolites. To detect extracellular metabolites, cells were treated with NR for 24 h followed by collection of cell culture media. Cell culture media from 3 biological repeats/group was used to run LC-MS (including Label-free QqQ metabolomics and post-processing and bioinformatic analysis). Plain MEM media (incubated that had been in cell culture incubator for 24 h) was used as internal background control. Agilent 1290 UHPLC and 6490 Triple Quadrupole (QqQ) Mass Spectrometer (LC-MS) were used in this study. Agilent MassHunter Optimizer and Workstation Software LC/MS Data Acquisition for 6400 Series Triple Quadrupole B.08.00 was used for standard optimization and data acquisition. Agilent MassHunter Workstation Software Quantitative Analysis Version B.0700 for QqQ was used for data analysis. For reversed-phase chromatography (RPC), a Waters Acquity UPLC BEH TSS C18 column (2.1 x 100mm, 1.7µm) was used with mobile phase (A) consisting of 0.5 mM NH4F and 0.1% formic acid in water; mobile phase (B) consisting of 0.1% formic acid in acetonitrile. Gradient program: mobile phase (B) was held at 1% for 1.5 min, increased to 80% in 15 min, then to 99% in 17 min and held for 2 min before going to initial condition and held for 10 min. For hydrophilic interaction chromatography (HILIC), a Waters Acquity UPLC BEH amide column (2.1 x 100mm, 1.7µm) was used with mobile phase (A) consisting of 20mM ammonium acetate, pH 9.6 in water; mobile phase (B) consisting of acetonitrile. Gradient program: mobile phase (B) was held at 85% for 1 min, decreased to 65% in 12 min, then to 40% in 15 min and held for 5 min before going to initial condition and held for 10 min. Both columns were at 40℃ and 3 µl of each sample was injected into the LC-MS with a flow rate of 0.2 ml/min. Calibration of TOF MS was achieved through Agilent ESI-Low Concentration Tuning Mix. Optimization was performed on the 6490 QqQ in the positive or negative mode for the RPC or HILIC respectively for each of 220 standard compounds to get the best fragment ion and other MS parameters for each standard. Retention time for each of 220 standards was measured from a pure standard solution or a mix standard solution. The LC-MS/MS method was created with dynamic MRMs with RTs, RT windows and MRMs of all 220 standard compounds. Key parameters of AJS ESI in both the positive and the negative acquisition modes are: Gas temp 275℃, Gas Flow 14 l/min, Nebulizer at 20 psi, SheathGasHeater 250℃, SheathGasFlow 11 l/min, and Capillary 3000 V. For MS: Delta EMV 200V or 350V for the positive or negative acquisition mode respectively and Cycle Time 500ms and Cell Acc 4V for both modes.

The QqQ data was pre-processed with Agilent MassHunter Workstation Software Quantitative Analysis and post-processed for further quality control in the programming language R. We calculated coefficient of variation (CV) across replicate samples for each metabolite given a cut-off value of peak areas in both the positive and the negative modes. We then compared distributions of CVs for the whole dataset for a set of peak area cut-off values of 0, 1000, 5000, 10000, 15000, 20000, 25000 and 30000 in each mode. A noise cut-off value of peak areas in each mode was chosen by manual inspection of the CV distributions: 5000 for the positive mode and 5000 for the negative mode. Each sample is then normalized by the total intensity of all metabolites to reflect the same protein content as a normalization factor. We then retained only those metabolites with at least 2 replicate measurements. The remaining missing value in each condition for each metabolite was filled with the mean value of the other replicate measurements. Finally, the abundance of each metabolite in each sample was divided by the median of all abundance levels across all samples for proper comparisons, statistical analyses, and visualizations among metabolites. The statistical significance test was done by a two-tailed t-test with a significance threshold level of 0.1. The p-values were not adjusted in favor of subsequent manual inspection and more flexible biological interpretation. Those metabolites with p-value < 0.1 and CV < 1 were defined to be differential metabolites. Pathway analysis of differential metabolites was done using the webtool of MetaboAnalyst with default settings (metaboanalyst.ca). All other bioinformatics analyses including graphs and plots were also done using R/Bioconductor.

Real-time PCR. Cells were treated with/without NR (1 mM) for 24 h. Total RNA was extracted with TriZol (Invitrogen, Carlsbad, CA, USA) reagent, reverse-transcribed using iScript cDNA Synthesis Kit (BIO-RAD, Hercules, CA, USA). mRNA levels were quantified by real-time PCR using a SYBR Green quantitative PCR kit (Thermo Fisher Scientific, Waltham, MA USA) on the MyiQ iCycler real-time PCR detection system (BIO-RAD, Hercules, CA, USA), and then normalized to GAPDH using the $2^{-\Delta\Delta CT}$ calculation method [358]. Primer sequences used in this study are as follows: NMNAT1 forward, 5'-TCTCCTTGCTTGTGGTTCATTC and reverse, 5'-TGACAACTGTGTACCTTCCTGT; GAPDH forward, 5'-GAGTCAACGGATTTGGTCGT and reverse, 5'-GACAAGCTTCCCGTTCTCAG [359]. For the real-time PCR in worms, we collected 50 worms/group and performed PCR using samples from three biological replicates. Primers used for the PCR were detailed elsewhere [98, 360]. Values are the means of at least three independent experiments, and standard deviations are indicated as error bars.

Western Blots. Western blotting was used to examine protein expression following methods detailed previously [348]. Briefly, primary human cells (HT01, WRN-Kd, WS01 cells) were collected and prepared using 1x RIPA buffer (Cell Signaling, #9806S) containing protease inhibitors (Bimake, #B14002) and phosphatase inhibitors (Bimake, #B15002). Proteins were separated on 4-12% Bis-Tris gel (ThermoFisher Scientific, #NP0336BOX) and probed with antibodies. Chemiluminescence detection was performed using a ChemiDoc XRS System. Antibodies used were: β-actin (Santa Cruz, #sc-1616), WRN (Santa Cruz, # sc-5629), CD38 (Santa Cruz, # sc-374650), CD157 (R&D systems, #AF4736), CD73 (R&D systems, #AF5795), PAR (TREVIGEN, #4336-BPC-100), PARP1 (Cell signaling, #9542), AMPK (Cell signaling, #5831), pAMPK (Thr172) (Cell signaling, #2535), pULK1 (Ser555) (Cell signaling, #5869), ULK1 (Cell signaling, #6439), p62 (Cell signaling, #39749), Bcl2L13 (ThermoFisher, # PA5-15043), LC3 (Novus, #NB100-2220), PSD95 (Cell signaling, #3450). All other antibodies were obtained from Cell signaling. Gamma adjustment was used to reduce dark background when necessary. Quantification was performed using ImageJ.

Data collection and statistical analysis. Double-blinded methods were used in the *C. elegans* studies (including lifespan, healthspan) and experiments requiring imaging. We used two-tailed unpaired t-test for comparison between two groups, or One-Way ANOVA or Two-way ANOVA (followed by Tukey's test) for comparison among multiple groups. All data were presented as mean ± S.E.M. as indicated with p value < 0.05 considered statistically significant. For lifespan studies, p values were derived from log-rank calculations.

RESULTS

I. Mitochondrial alterations in WS patient cells and *wrn-1 C. elegans*

WS patients develop diabetes (70%) and dyslipidemia (60%) [187] following an abnormal glucose and lipid metabolism. However, no data explain clearly the relationship between *WRN* mutation and dysregulation of energy metabolism. Here we hypothesized that this link could be based on mitochondrial dysfunction and, for this purpose, we evaluated a series of mitochondrial parameters using primary fibroblasts from a 30-year WS patient (termed WS01). These were compared to primary fibroblasts from a sex- and age-matched healthy control subject (termed HT01) (**Table S1**). We also created an isogenic cell line by using siRNA to deplete *WRN* in normal control fibroblasts (termed WRN-KD). WS01 and WRN-KD cells had higher mitochondrial ROS, lower mitochondrial membrane potential, increased mitochondrial content, and decreased cellular ATP levels compared to HT01 cells (**Fig. 1A-D**).

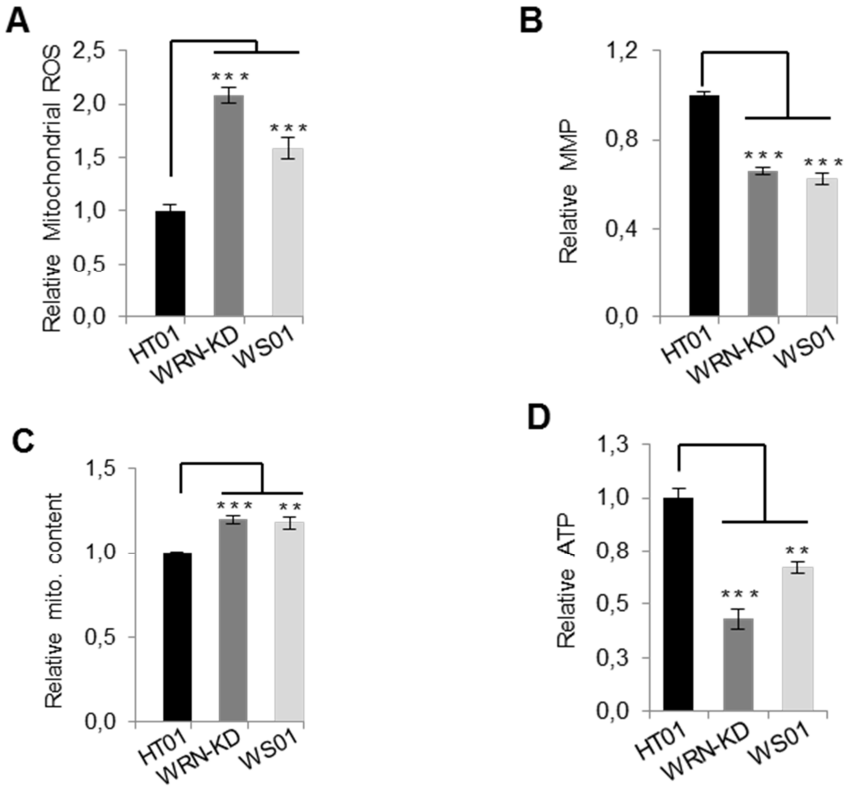

Fig. 1. Mitochondrial dysfunction in WS human cells. A WS patient primary fibroblast cell line (WS01) and a sex- and age-matched fibroblast line from a healthy donor (HT01), as well as a WRN-KD fibroblast line (generated through siRNA-WRN KD in the HT01 cells) were used to evaluate mitochondrial function. For siRNA control, siRNA-Vector was added to HT01 and WS01 cells.

(A-C) Flow cytometry was used to quantify relative mitochondrial ROS (A, using mitoSOX dye), mitochondrial membrane potential/MMP (B, TMRM dye), and relative mitochondrial content (C, MitoTracker Green). n= 3 biological repeats.

(D) An ELISA assay showing relative cellular ATP levels. Data are shown in mean ± S.E.M, n = 3 biological repeats.

One-way-ANOVA or student *t*-test was used for data analysis with *, p<0,05, **, p<0,01, ***, p<0,001. Primary cells were used at the same passage for experiments.

To explore the underlying causes of abnormal mitochondria in WS, first we evaluated mitochondrial ultrastructure using electron microscopy and, as shown in **Fig. 2A-B**, WRN deficient cells exhibited a nearly 3-fold increase in damaged mitochondria relative to HT01 cells.

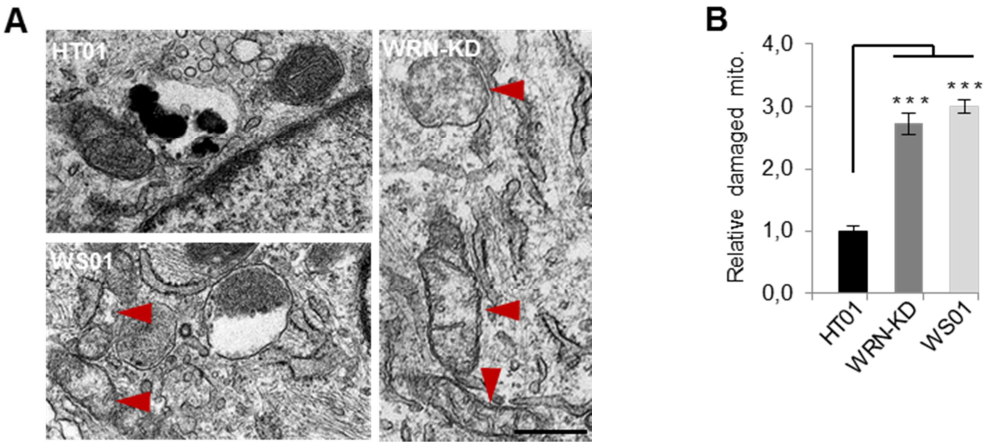

Fig. 2. Mitochondrial ultrastructure evaluation in WS human cells. A WS patient primary fibroblast cell line (WS01) and a sex- and age-matched fibroblast line from a healthy donor (HT01), as well as a WRN-KD fibroblast line (generated through siRNA-WRN KD in the HT01 cells) were used to evaluate mitochondrial quality. For siRNA control, siRNA-Vector was added to HT01 and WS01 cells.

(A-B) Changes of mitochondrial ultrastructure were evaluated through electron microscopy (A) with percentage of damaged mitochondria quantified (B). Data are shown in mean ± S.E.M (n = 100-150 mitochondria). Red arrows denote damaged mitochondria.

One-way-ANOVA or student *t*-test was used for data analysis with *, p<0,05, **, p<0,01, ***, p<0,001. Primary cells were used at the same passage for experiments.

We then asked whether mitochondrial dysfunction is conserved across animal models of WS. We started with a *C. elegans* model of WS, *wrn-1(gk99)* [310, 315]. Similar to the WS cells, we found reduced mitochondrial network complexity (42 % reduction of the score, **Fig. 3A-B**), and increased oxidative stress (**Fig. 3C**) in *wrn-1(gk99)* compared to wild type (WT) N2 worms. Consistent with these findings, both young (adult Day 2/D2) and old (D10) *wrn-1(gk99)* worms exhibited decreased basal and maximal mitochondrial oxygen consumption (OCR) rates compared to N2 worms (**Fig. 3D**).

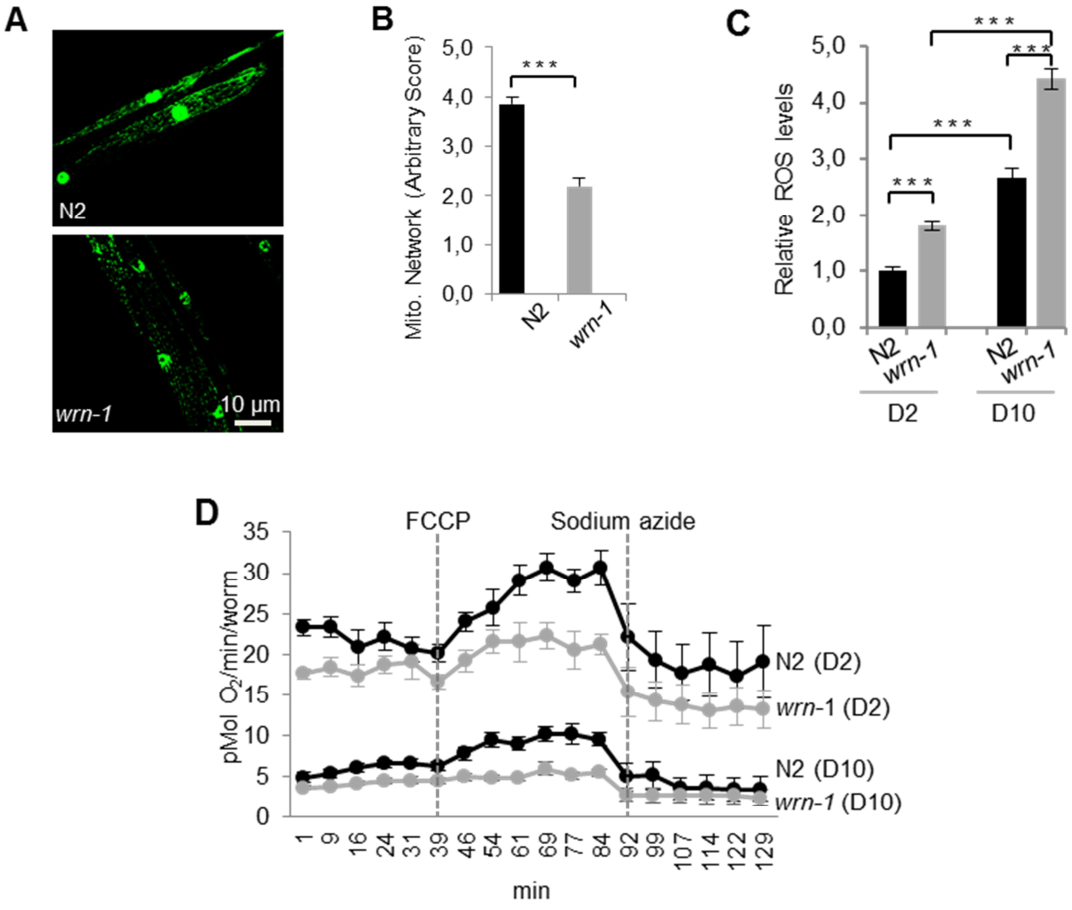

Fig. 3. Mitochondrial dysfunction in WS *C. elegans*. A *C.elegans* model of WS *wrn-1(gk99)* was used to evaluate mitochondrial function/quality.

(A-B) A *myo-3::gfp* reporter was expressed in both the nucleus and mitochondria to mark non-pharyngeal body wall muscle cells in the N2 and *wrn-1*(*gk99*) worms. Representative images (A) and quantified scores (B) of muscle mitochondrial morphology of adult D2 N2 and *wrn-1*(*gk99*) worms. Data are shown in mean ± S.E.M (n = 20 worms).

(C) Relative levels of ROS in adult D2 and D10 worms. Data are shown in mean ± S.E.M (n =10 worms/group).

(D) The XFe96 was used to evaluate oxygen consumption rate (OCR) in adult D2 and D10 worms (n =15-30 worms/well, 3 biological repeats).

One-way-ANOVA or student *t*-test was used for data analysis with *, p<0,05, **, p<0,01, ***, p<0,001.

Thus, WRN deficiency induces mitochondrial damage in primary WS patient cells/WRN-KD human cells and dysfunction in *wrn-1(gk99) C. elegans*. There was no detectable mitochondrial impairment in mouse embryonic fibroblasts (MEFs), brain, liver, or heart tissue from *Wrn*$^{-/-}$ mice compared with samples from matched WT littermates (**Fig. S1A-E**). This is not surprising because the *Wrn*$^{-/-}$ mice do not exhibit accelerated aging features [309], as WS patients.

II. NAD$^+$ depletion in WS

As already mentioned, mitochondrial dysfunction and NAD$^+$ reduction have been linked to aging and metabolic disorders including obesity, insulin resistant diabetes and fatty liver disease [113, 118]. NAD$^+$ levels in WS01 or WRN-KD cells were 30-40% lower than in HT01 cells (**Fig. 4A**). To verify this finding, we examined NAD$^+$ levels in additional primary fibroblasts and plasma from WS patients and healthy controls (**Tables S1 and S2**). NAD$^+$ levels in 4 different WS cell lines (WS2-WS5) ranged from 20-70% lower than matched healthy controls (HT2-HS5, **Fig. 4B**). We further examined NAD$^+$ in plasma from 10 WS patients (WS02-WS11) and 12 healthy controls (HT2-HT13). Although NAD$^+$ levels varied within each group, the average NAD$^+$ was 58% lower in WS than healthy control fibroblasts (**Fig. 4C-D**). Notably, the three WS plasma samples with the highest NAD$^+$ levels were from patients that did not exhibit diabetic phenotypes (**Fig. 4D and Table S2**), suggesting a possible negative correlation between NAD$^+$ and the severity of metabolic dysfunction in WS patients.

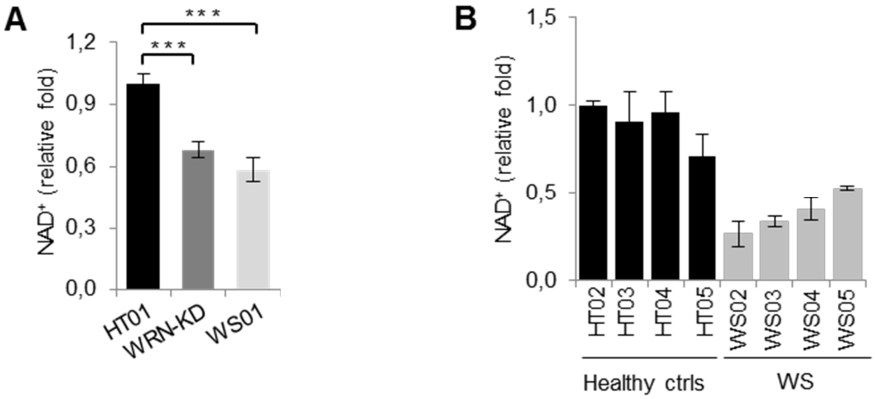

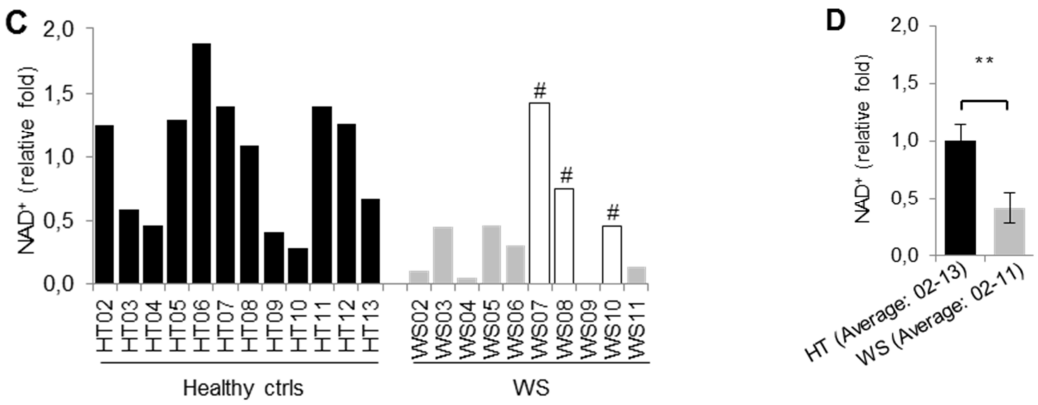

Fig. 4. NAD$^+$ reduction in WS human cells. (A-B) Relative NAD$^+$ levels in human WS patient cells compared with samples from matched healthy controls. Data are shown in mean ± S.E.M (n = 3 biological repeats).
(C-D) Relative NAD$^+$ levels in plasma samples from human WS patients and samples from matched healthy controls. Data of (D) were mean ± S.E.M from all samples of (C). #, samples from WS patients without obesity (also see Table S2). One-way-ANOVA or student *t*-test was used for data analysis with *, p<0,05, **, p<0,01, ***, p<0,001. Primary cells were used at the same passage for experiments.

We also detected NAD$^+$ levels in *wrn-1 (gk99) C.elegans* and NAD$^+$ levels were lower in *wrn-1 (gk99)* compared to N2 worms (**Fig. 5**). In summary, these results indicate NAD$^+$ depletion across species in WS.

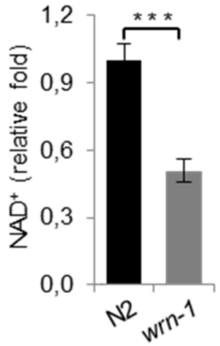

Fig. 5. NAD$^+$ reduction in WS *C.elegans*. Relative NAD$^+$ levels in adult D2 worms. Data are shown in mean ± S.E.M (n = 3 repeats).

III. NAD$^+$ replenishment normalizes NAD$^+$ biosynthetic machinery

After observing a reduction of NAD$^+$ in WS patient cells and plasma, and in a *C. elegans* model of WS, we wondered whether this alteration drove the accelerated aging phenotypes in WS. To test this hypothesis, we pharmacologically increased cellular NAD$^+$ levels by

incubating the HT01 and the WRN-KD cells with the NAD^+ precursor nicotinamide riboside (NR, 1 mM for 24h), followed by systematic evaluation of intra- and extracellular NAD^+ metabolic profiles using liquid chromatography-mass spectrometry (LC-MS) [357, 361]. NAD^+ and its precursor nicotinamide mononucleotide (NMN) were both decreased in WRN-KD cells relative to HT01 cells (**Fig. 6A-B**). NR treatment robustly increased NMN and NAD^+ levels in both WRN-KD and HT01 cells (**Fig. 6A-B**). According to recent studies NAAD (nicotinic acid adenine dinucleotide, the substrate of glutamine-dependent NAD^+ synthetase) [7] has been identified as an efficient sensitive biomarker for effective NAD^+ supplementation [361]. Indeed, NAAD was undetectable in fibroblasts not treated with NR and increased to approximately 7 and 12 pmol/mg protein in NR-treated WRN-KD and HT01 cells, respectively (**Fig. 6C**). NR treatment also led to increased ADPR (**Fig. 6D**).

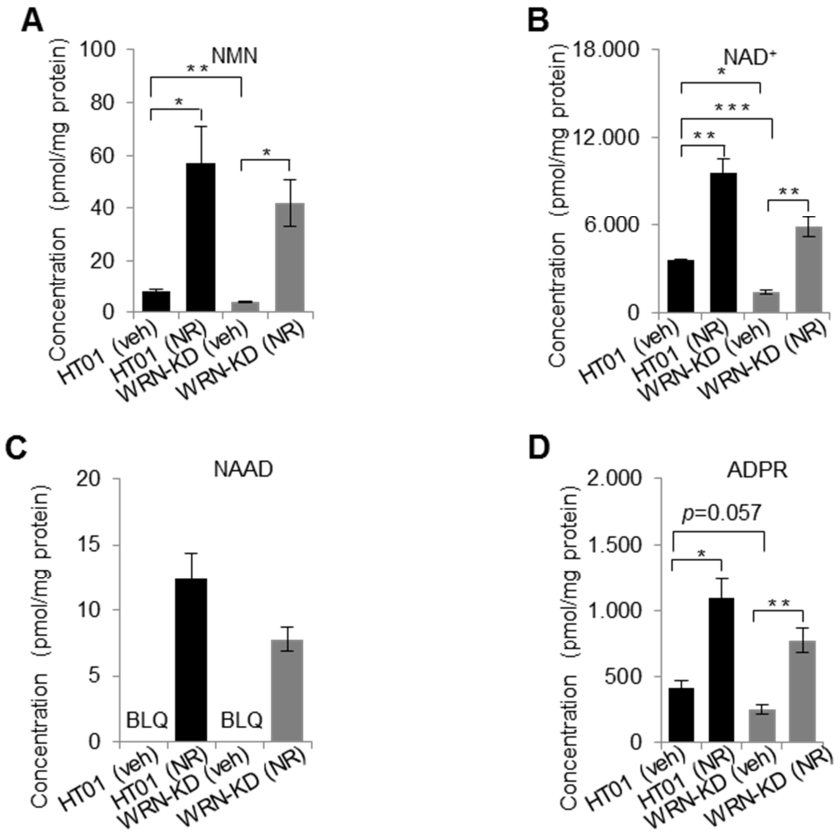

Fig. 6. Impaired NAD^+ amount in human WS cells.

(A-D) Liquid chromatography-mass spectrometry (LC-MS) data showing changes of nicotinamide mononucleotide (NMN) (A), NAD^+ (B), Nicotinic acid adenine dinucleotide (NAAD) (C), and ADP-ribose (ADPR) (D) in HT01 and WRN-KD cells before and after NR treatment (1 mM, 24 h). Data are shown in mean ± S.E.M (n = 3).

One-way-ANOVA or student *t*-test was used for data analysis with *, p<0,05, **, p<0,01, ***, p<0,001. Primary cells were used at the same passage for experiments.

There was a significant decrease in methylated nicotinamide (MeNAM) in WRN-KD cells vs. WT, however, no significant change after NR treatment was observed (**Fig. S2A**). There were no clear differences in other NAD^+ related metabolites, such as inosine, inosine 5'-monophosphate (IMP) and NADP in the NR-treated WRN-KD cells compared with WRN-KD (veh) cells (**Fig. S2B-I**). We further examined extracellular NAD^+ metabolic profiles using medium from cells that had been treated with NR for 24 h NR. The extracellular metabolomic data show that nicotinamide (NAM) and nicotinate levels were dramatically increased after NR treatment by ~3- to 20-fold relative to the medium from vehicle-treated control cells, indicating increased NAD^+ metabolism in the cells although we do not exclude a possibility of partial NR degradation (**Fig. S3**).

Cellular NAD^+ balance depends on a series of enzymes involved in NAD^+ synthesis and consumption [7, 113, 118]. To further dissect the underlying mechanisms of NAD^+ depletion in WS cells, we examined the protein expression levels of these enzymes. Nicotinamide nucleotide adenylyltransferase 1 (NMNAT1) is a key NAD^+ biosynthetic enzyme which catalyzes the formation of NAD^+ from NMN [7, 118]. Compared with HT01 cells, the nuclear-localized NMNAT1 was decreased in WRN-KD primary cells (**Fig. 7A** and quantification in **Fig. S2J**). NMNAT1 was also decreased in other cells with WRN KD, e.g., in the U2OS cells (**Fig. S2K**). We further asked whether WRN regulates NMNAT1 at the transcriptional level. We then knocked down *WRN* in human U2OS cells, which resulted in a 40% decrease in *NMNAT1* (**Fig. 7B**). mRNA and protein levels of NMNAT1 increased in response to NR treatment (**Fig. 7A-B**, and in quantification of protein expression in **Fig. S2J**). Nicotinamide phosphoribosyltransferase (NAMPT) is the rate-limiting enzyme in the NAD^+ salvage pathway which recycles NAM to NMN for NAD^+ biosynthesis [7, 118]. Surprisingly, the protein levels of NAMPT in the WRN-KD cells were higher than in the HT01 cells, suggesting a compensatory cellular feedback to improve NAD^+ synthesis (**Fig. 7A**).

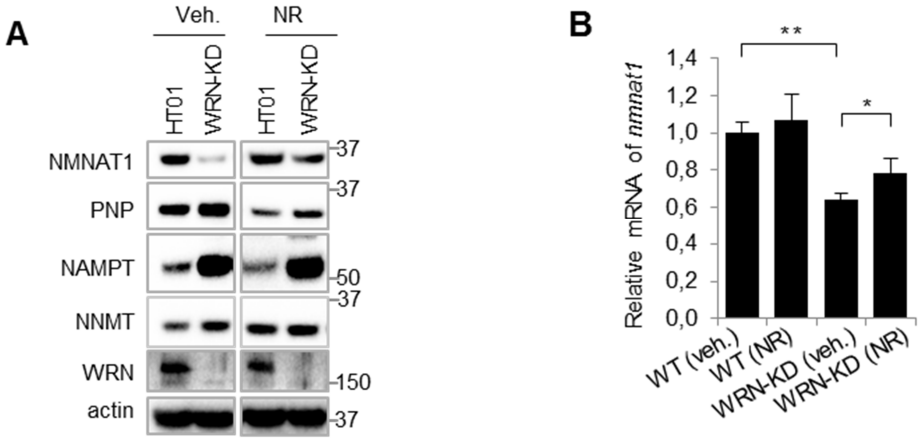

Fig. 7. Correlation between WRN and NAD$^+$ biosynthetic machinery.

(A) Western blot showing changes of designated proteins in HT01 and WRN-KD cells.

(B) WRN regulates NMNAT1 at transcriptional level. mRNA levels of *nmnat1* in different conditions were performed using real-time PCR. Data are shown in mean ± S.E.M (n = 3 biological repeats).

One-way-ANOVA or student *t*-test was used for data analysis with *, p<0,05, **, p<0,01, ***, p<0,001. Primary cells were used at the same passage for experiments.

There were no significant changes in levels of the cyclicADP-ribose synthases (e.g., CD38 and CD157) in the WRN-KD cells. The protein and activity levels (as shown by PARylation) of poly(ADP-ribose)polymerases (PARPs) in the WRN deficient cells were higher compared with HT01 (veh) cells (**Fig. S2L-M**). In worms, there was also a trend of increased PARylation in the *wrn-1(gk99)* worms relative to N2 controls; however, there was no significant difference of PARylation in *wrn-1(gk99)* worms (**Fig. S2N**).

Consistently, NAD$^+$ repletion reduced mitochondrial oxidative stress and mitochondrial content in the WRN-KD and WS01 cells (**Fig. 8A-B**).

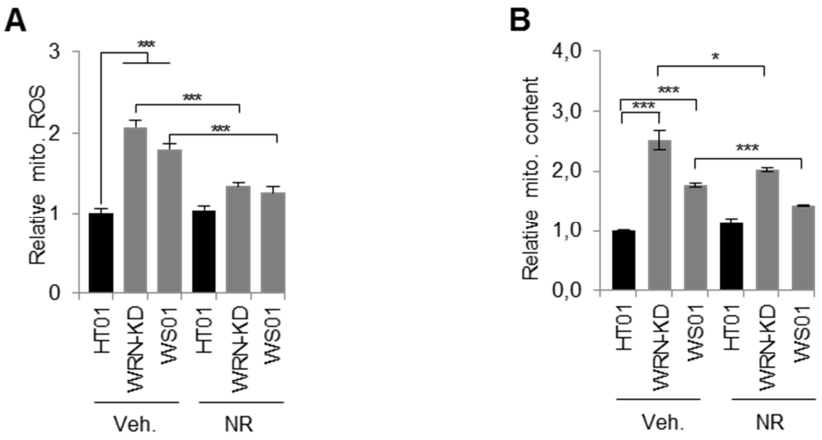

Fig. 8. Effects of NR on mitochondrial ROS and mass.

(A-B) Effect of NR (1 mM, 24 h) on the relative levels of mitochondrial ROS (mitoSOX dye) and mitochondrial content (mitoGreen dye) of the designated cells. Data are shown in mean ± S.E.M (n = 3 biological repeats).

One-way-ANOVA or student *t*-test was used for data analysis with *, p<0,05, **, p<0,01, ***, p<0,001. Primary cells were used at the same passage for experiments.

A summary of the changes in NAD$^+$ metabolites and in related enzyme levels before and after NR treatment is shown in **Fig. S2O**.

Collectively, these results suggest that WRN depletion induces NAD$^+$ depletion and an imbalance of the NAD$^+$ synthesis machinery, while NR treatment corrects these defects.

IV. NAD^+ replenishment inhibits accelerated aging in WS cells and animal models

Given that NAD^+ replenishment improves mitochondrial parameters in human WS cells, we further examined whether it increased lifespan in the *wrn-1(gk99) C. elegans*. We treated the *wrn-1(gk99)* worms and the WT N2 worms with NR (1 mM) from the L4 stage, and tested lifespan and healthspan parameters. NR increased the lifespan in the N2 worms by 10% (**Fig. S4A**), in line with previous studies [103, 106, 360]. The NAD^+ level was 38% lower in *wrn-1(gk99)* compared to N2, *and* NR treatment increased organismal NAD^+ 2.2 times compared with vehicle-treated groups (**Fig. 5**). Interestingly, we found that NR dramatically extended the mean lifespan of the *wrn-1(gk99)* worms from 13.9 days to 18.1 days, similar to that of the lifespan of untreated N2 worms (20.6 days) (**Fig. 9A-B** and quantification in **Fig. S4A**).

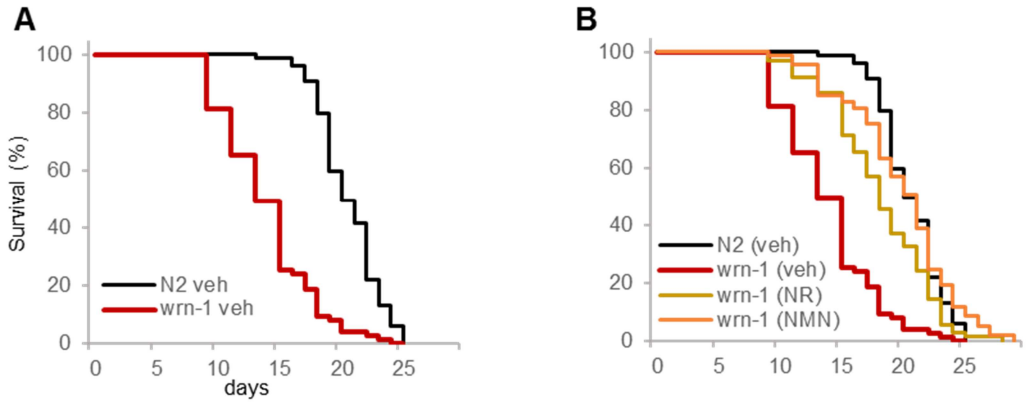

Fig. 9. NAD^+ replenishment increases lifespan in WS worms.

The N2 and *wrn-1*(*gk99*) worms were treated with NR/NMN (1 mM) from L4 stage followed by detection of designated parameters.

(A) Lifespan curves in the N2 and *wrn-1*(*gk99*) worms at 25 °C.

(B) Effects of NR/NMN on the lifespan curves in the *wrn-1*(*gk99*) worms at 25 °C. Experiments were repeated 7 times, with one representative set of data are shown. Summarized data, including the effects of NR/NMN in the N2 worms, were in Fig. S4A.

NR treatment also significantly improved healthspan in the *wrn-1(gk99)* worms, as detected by increased pharyngeal pumping (**Fig. 10**). There was no difference in maximum velocity of movement in the worms between the genotypes or after NR treatment (**Fig. S4B**).

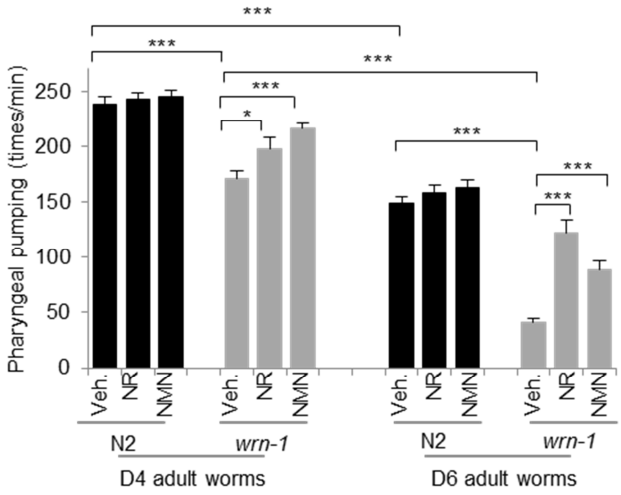

Fig. 10. NAD$^+$ replenishment improves healthspan in WS worms. The N2 and *wrn-1*(*gk99*) worms were treated with NR/NMN (1 mM) from L4 stage followed by detection of designated parameters. Effects of NR/NMN on pharyngeal pumping in the N2 and the *wrn-1*(*gk99*) worms. Data are shown in mean ± S.E.M (n = 3 biological repeats with 10-20 worms for each condition).

Another hallmark of aging is stem cell dysfunction, which occurs prematurely in human WS cells [252]. Thus, we further examined whether NR could affect stem cell viability in WS by assaying the number of germ line-localized mitotic cells [362]. The *wrn-1(gk99)* worms without treatment had 18% fewer mitotic cells than middle aged N2 worms at D6. After NR treatment, the number of cells increased from 75 cells/worm to 132/worm in *wrn-1(gk99)* worms (**Fig. 11A**, and a representative set of images in **Fig. 11B**). The number of proliferating cells can be quantified by staining for phosphorylated Histone 3 (pH3) [363].

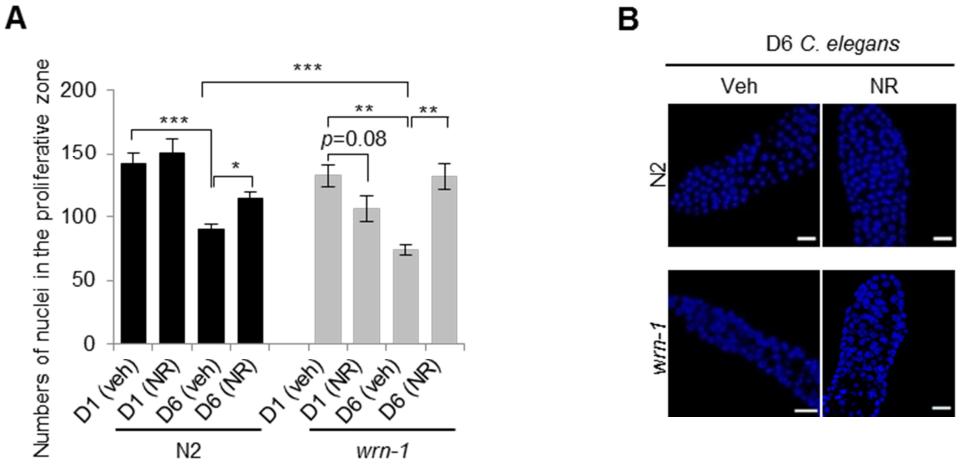

Fig. 11. NAD$^+$ replenishment increases the number of germ line-localized mitotic cells in WS worms.
The N2 and *wrn-1*(*gk99*) worms were treated with NR/NMN (1 mM) from L4 stage followed by detection of designated parameters.

(A) Changes of the numbers of germ line-localized mitotic cells in the designated groups of worms. Data are shown in mean ± S.E.M (n = 10-20 worms per condition).
(B) A representative set of images on the changes of the numbers of germ line-localized mitotic cells in the designated groups of D6 worms.
Comparisons between proliferation counts were done by one-way ANOVA, using Sidak's post hoc test: ***, p<0.001.

When worms were treated with 90 Gy of γ-radiation to induce genomic stress, there were less proliferative cells in the *wrn-1(gk99)* worms than in the WT worms. While NR treatment had no significant effect on the numbers of $pH3^+$ cells in N2 worms, it dramatically increased $pH3^+$ cells in *wrn-1(gk99)* worms (**Fig. 12A**, and a representative set of images in **Fig. 12B**).

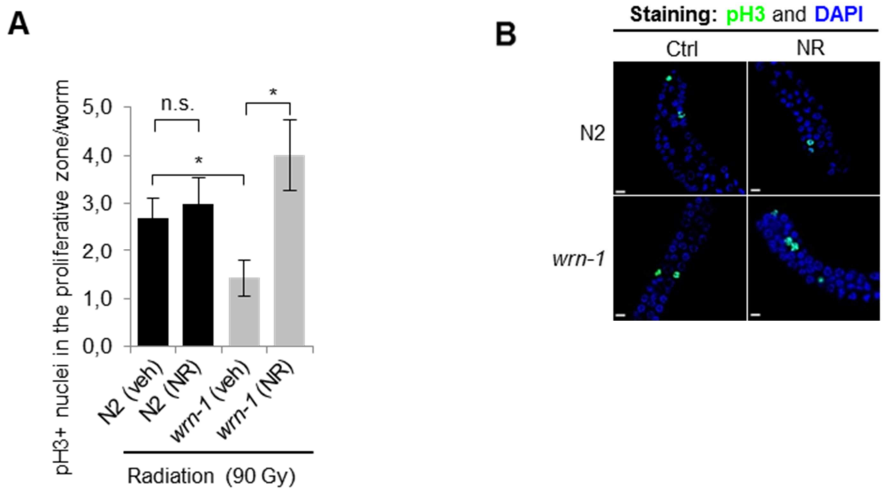

Fig. 12. NAD^+ replenishment increases the number of germ line-localized mitotic cells in WS worms. The N2 and *wrn-1*(*gk99*) worms were treated with NR/NMN (1 mM) from L4 stage followed by detection of designated parameters.
(A) Differences of the numbers of $pH3^+$ mitotic cells in the designated groups of worms after exposure to 90 Gy ionizing radiation. Data are shown in mean ± S.E.M (n = 6-13 worms per condition).
(B) A representative set of images on the changes of the numbers of $pH3^+$ mitotic cells in the designated groups of D6 worms. Quantification was in Fig. 3F. All the worms were exposed to 90 Gy γ-radiation.
Comparisons between proliferation counts were done by one-way ANOVA, using Sidak's post hoc test: ***, p<0.001.

Collectively, the data suggest NAD^+ repletion extends lifespan and healthspan, and improves the numbers and proliferative potency of mitotic cells in the *wrn-1(gk99) C. elegans*.

To test whether these benefits of NAD^+ replenishment were conserved across species, we moved to a *Drosophila melanogaster* model of WS through RU486-dependent induction of

RNAi knockdown of *Wrnexo*, hereafter termed *Wrnexo*^{RNAi} flies [320]. Compared with WT control (veh) flies, *Wrnexo*^{RNAi} had a significantly shorter lifespan (**Fig. 13**). Importantly, boosting NAD^+ (though NMN administration) significantly extended the lifespan in both WT and *Wrnexo*^{RNAi} flies, indicating a role of NAD^+ in maintaining lifespan (**Fig. 13**).

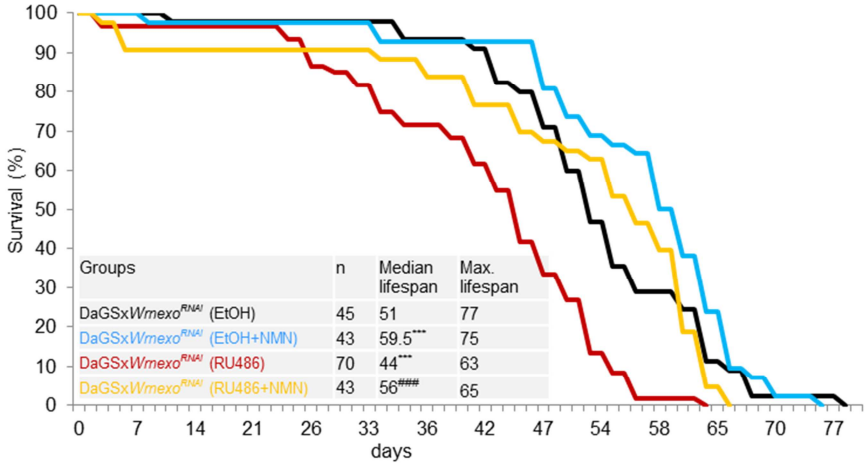

Fig. 13. NAD^+ replenishment extends lifespan in WS flies. Effects of NAD^+ supplementation on the lifespan curves in *w;DaGeneSwitch-Gal4;y,v,sc;Wrnexo*^{RNAi} (EtOH) (WT), and the *w;DaGeneSwitch-Gal4;y,v,sc;Wrnexo*^{RNAi} (RU486) (WRN-KD) flies at 25 °C. Female offspring of *w;DaGeneSwitch-Gal4* and *y,v,sc;Wrnexo*^{RNAi} lines were allowed to mate for 2-3 days, then transferred to vials with food ± RU486 and/or NMN at 5mM final concentration. The *Wrnexo*^{RNAi} was activated in the presence of the drug RU486. A representative set of data from two biological repeats is shown. Log-rank test was used for statistics: ***,p<0.0001 compared with *w;DaGeneSwitch-Gal4;y,v,sc;Wrnexo*^{RNAi} (WT) (EtOH), ###,p<0.0001 compared with *w;DaGeneSwitch-Gal4;y,v,sc;Wrnexo*^{RNAi} (RU486) (WRN-KD) (EtOH).

As the number of germline mitotic cells is not a direct measure of stem cell function, we validated and explored NAD^+-dependent restoration of stem cell function in the *Wrnexo*^{RNAi} flies. In response to injury from pathogenic bacteria, *Drosophila* intestinal stem cells (ISCs) proliferate to regenerate the intestine [363]. In *WRNexo*^{RNAi} flies, infection failed to induce a proliferative response. This effect was rescued by boosting NAD^+ during the period of RNAi, which had no effect on WT controls (**Fig. 14A** and **Fig. 14B**). This *Wrnexo* KD-induced reduction of proliferation in ISCs is not due to loss of stem cells in *Wrnexo*^{RNAi} flies (**Fig. 14C**).

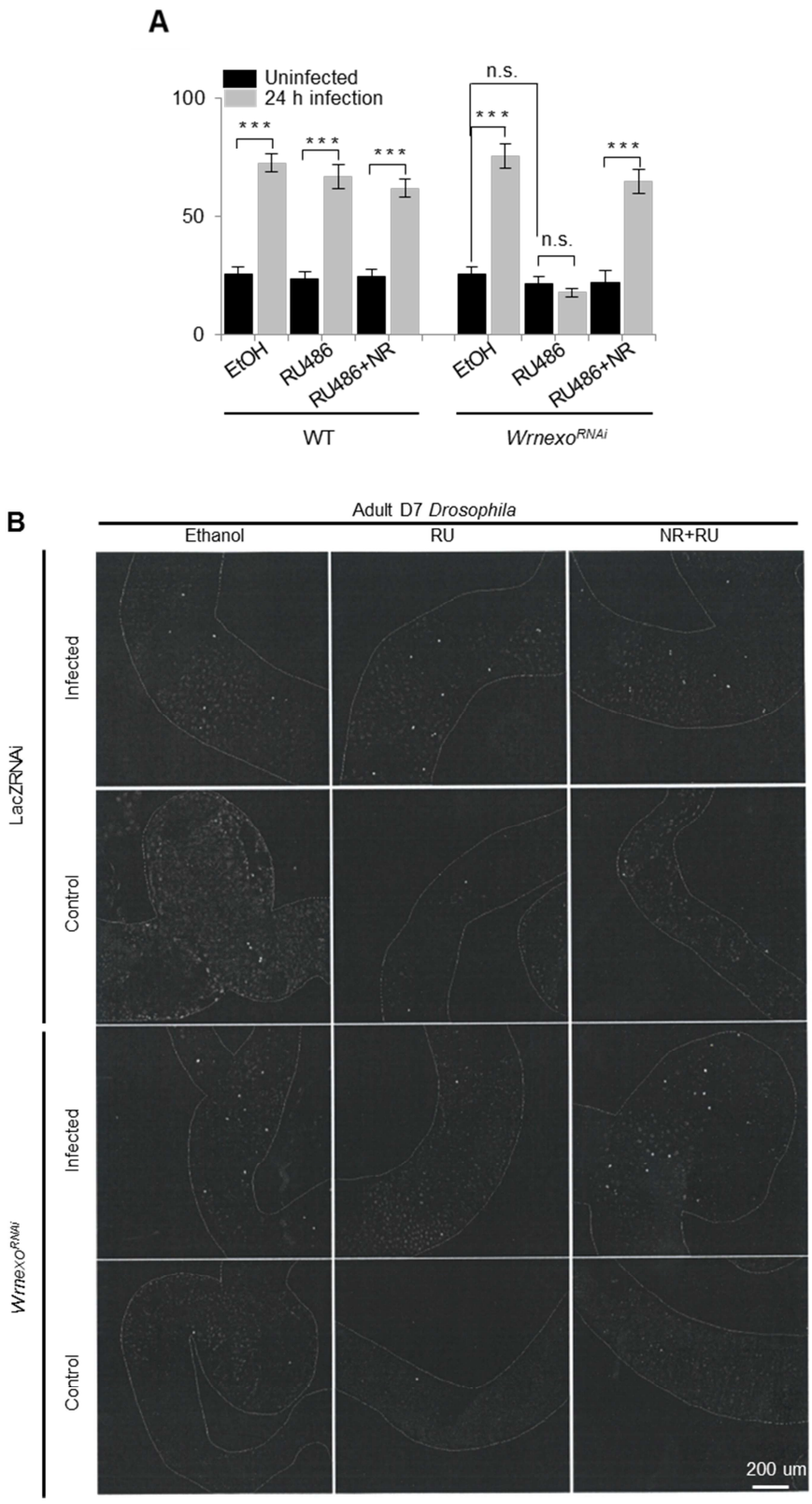
A
Uninfected
24 h infection
100
50
0
***
***
***
n.s.
***
n.s.
***
EtOH
RU486
RU486+NR
EtOH
RU486
RU486+NR
WT
Wrnexo^RNAi
B
Adult D7 Drosophila
Ethanol
RU
NR+RU
LacZRNAi
Infected
Control
Wrnexo^RNAi
Infected
Control
200 um

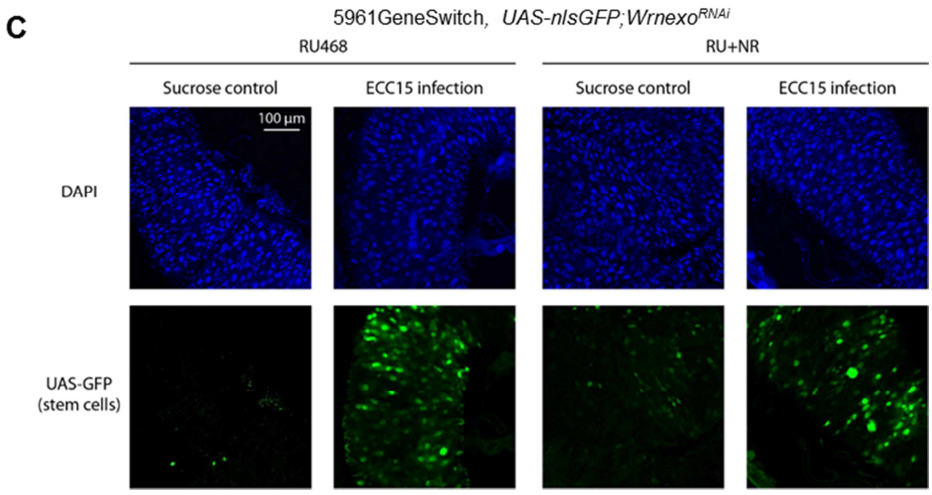

Fig. 14. NAD$^+$ replenishment restores proliferation potency in WS flies.

(A) Average numbers of proliferating intestinal stem cells (ISCs)/fly in designated groups. Total numbers of pH3$^+$ cells/gut in the adult Day 7 flies were counted. Female flies were used for experiments with data are shown in mean ± S.E.M (n = 10-20 flies for each condition, two biological repeats).

(B) The WT and the *Wrnexo*^{RNAi} flies were treated with vehicle or NR and the total numbers of the pH3$^+$ gut stem cells (i.e., dividing stem cells) were counted on adult day 7. The 5961GeneSwitch-Gal4 line was used for the study. This line expresses an inactivated form of Gal4 in intestinal stem cells, which is activated in the presence of the drug RU486. A set of representative images are shown here with quantified data shown in Fig. 14A.

(C) The *UAS-nlsGFP* construct was used to evaluate the total number of intestinal stem cells, to rule out cell death as a factor in the proliferative response. Intestinal stem cells were still present in *Wrnexo*^{RNAi} flies, before and after infection. Also, infection stimulated stem cell numbers.

Comparisons between proliferation counts were done by one-way ANOVA, using Sidak's post hoc test: ***, $p<0.001$.

According to these data, we speculated that NAD$^+$ supplementation with multiple different precursors should show similar beneficial effects. Indeed, NMN (1 mM) treatment gave very similar anti-aging benefits in *wrn-1(gk99)* as did NR treatment (**Fig. 5, Fig. 9A-B, Fig. 10**, and **Fig. S4C**). NAD$^+$ alone also extended the lifespan in the *wrn-1(gk99)* worms (**Fig. S4C**). NAM treatment extended the lifespan one more day but this did not reach statistic difference (**Fig. S4C**). We further explored the effect of treatment with NAD$^+$ precursors at different ages on lifespan in *wrn-1(gk99)*. Exposure to NR beginning at the egg, L4 (last developmental stage), or young adult (D3) stages all had similar effects in extending lifespan. However, NR's benefit was significantly reduced when exposure began at D5 (**Fig. S4D-J**).

Taken together, these data suggest that NAD$^+$ depletion is a driver of accelerated aging in WS.

V. Restoration of impaired mitophagy by NAD^+ repletion in WS

To explore the cellular and molecular mechanisms of WRN and NAD^+ in aging, we measured whole genome gene expression study of N2 and *wrn-1(gk99)* worms with/without NR (from L4, using 1 mM NR) (**Fig. S5** and **Table S3**). Principal component analysis (PCA) revealed a separation between N2 (veh) and *wrn-1(gk99)* (veh), while NR treatment led to a shift of the *wrn-1(gk99)* transcriptomic profile towards the N2 (veh) profile (**Fig. S5A**). GO term analysis indicated changes in the *wrn-1(gk99)* worms of many pathways related to development and metabolism, such as larval development, lifespan, redox regulation and mitochondria (**Fig. S5C**, a full list in **Table S3**), in line with aging phenotypes [310]. NR treatment increased over 50 GO terms in the N2 worms, including AMPK, mTOR inhibition (which increases autophagy) and the endoplasmic reticulum unfolded protein response, but there was no significant difference of some of these GO terms between *wrn-1(gk99)* (veh) and N2 (veh) groups (**Fig. S5D**). These GO terms are related to energy expenditure, autophagy, cellular stress and aging [4, 364]. Interestingly, NR treatment changed many GO terms in the *wrn-1(gk99)* worms, especially signal transduction, lifespan, and metabolic process (**Fig. S5E** and **Table S3**). Consistent with impaired mitochondrial function by WRN-1 dysfunction (**Fig. 3D**), heat map analysis of the GO terms suggested a reduction of many mitochondria-related pathways, including oxidoreductase activity pathways, metabolic process, cellular lipid metabolic process, among others; NR treatment activated many of these pathways in the *wrn-1(gk99)* worms (**Fig. S5F-G**).

Collectively, our transcriptomic analysis suggests that WRN dysfunction impacts metabolism, autophagy, cellular stress responses, development and aging in the *wrn-1(gk99)* worms, and NAD^+ repletion normalizes many of these pathways at the transcript level. Mitochondrial autophagy, termed mitophagy, is the process of clearance of damaged/superfluous mitochondria.

Dysfunction of mitophagic machinery has been recently listed as an hallmark of aging [103, 143]. Our data in WS patients and in the *C. elegans* models of WS indicate mitochondrial dysfunction and accumulation of damaged mitochondria (**Fig. 1-2-3**), and we supposed that these could be caused by impaired mitophagy. To test this hypothesis, we crossed the *wrn-1(gk99)* worms with a mitophagy reporter worm strain to visualize the colocalization of LGG-1 (the worm homologue of mammalian LC3) and DCT-1 (the worm homologue of mammalian NIX/BNIP3L), a well-established indicator of mitophagy [98, 106]. The basal level of mitophagy in muscle cells of the *wrn-1(gk99)* worms was 41% lower than in N2 worms,

while two independent NAD^+ replenishment strategies (NR, NMN) restored mitophagy in *wrn-1(gk99)* to that of N2 (**Fig. 15A-B**).

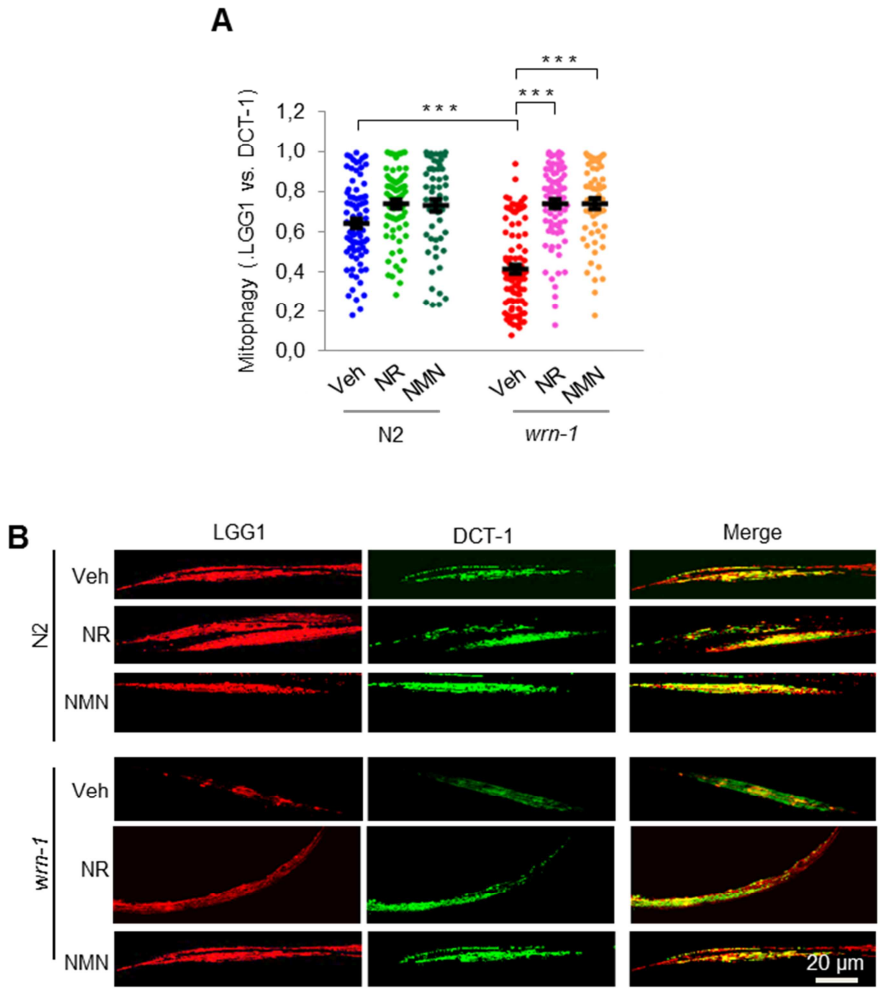

Fig. 15. NAD^+ replenishment restores mitophagy in WS worms.

(A-B) Relative mitophagy rate in the adult D7 N2 and the *wrn-1*(*gk99*) worms under designated conditions. Mitophagy events were calculated by the colocalization between the autophagic marker DsRed::LGG-1 and the mitophagy receptor DCT-1::GFP in muscle cells. Data are shown in mean ± S.E.M. (n = ~20 worms for each condition).

Two-way ANOVA followed by Tukey's post hoc tests: *, $p<0.05$, **, $p<0.01$, ***, $p<0.001$.

To identify mitophagy proteins involved in NAD^+-induced mitophagy and related healthspan improvement (e.g., pharyngeal pumping), we knocked down a list of known mitophagy genes through RNAi feeding and analyzed the changes in pharyngeal pumping. Two mitophagy genes, *dct-1* (mammalian *NIX*) and *unc-51* (mammalian *ULK1*) were involved in NAD^+-induced improvement in pharyngeal pumping in both N2 and the *wrn-1(gk99)* worms (**Fig. 16A**). Indeed, the mRNA levels of *dct-1* and *unc-51* were lower in the *wrn-1(gk99)* worms,

and two NAD^+ replenishment strategies significantly increased *dct-1* and *unc-51* expression (**Fig. 16B-C**).

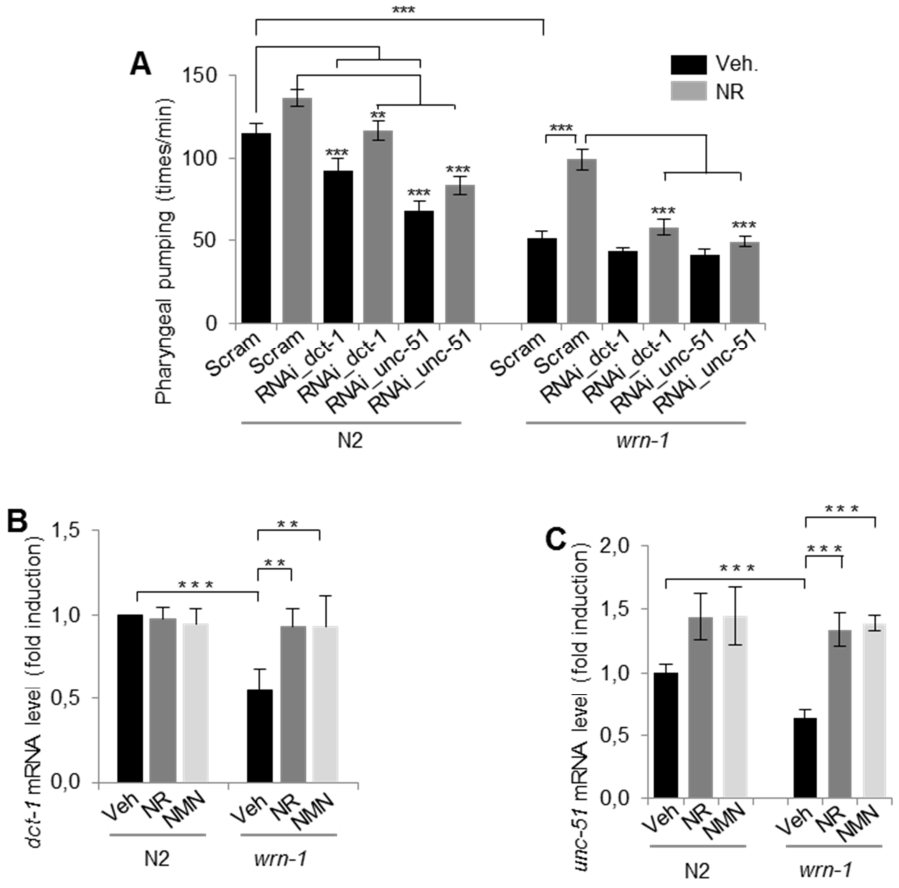

Fig. 16. NAD^+ ameliorates premature aging in WS through DCT-1 and ULK1-dependent mitophagy.

(A) Pharyngeal pumping rates in adult D7 worms of designated groups. Data are shown in mean ± S.E.M (n = 20-40 worms/group).

(B-C) mRNA levels of *dct-1* (B) and *unc-51* (C) in adult D7 worms. Data are shown in mean ± S.E.M (n = 3 biological repeats).

Two-way ANOVA followed by Tukey's post hoc tests: *, $p<0.05$, **, $p<0.01$, ***, $p<0.001$.

NAD^+ replenishment had no detectable transcriptional effect on other mitophagy genes, such as *pink1* and *pdr-1* (*Parkin* in mammals), although WRN dysfunction also decreased *pink-1* mRNA (**Fig. S6A**). The two NAD^+ replenishment strategies improved the muscle mitochondrial network (**Fig. 17**) and mitochondrial size (**Fig. S6B-C**).

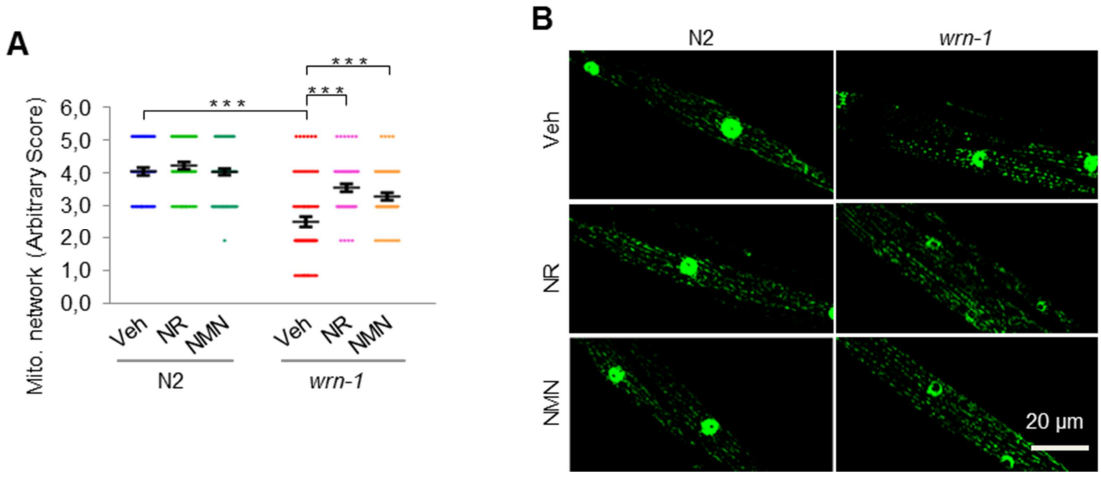

Fig. 17. NAD$^+$ replenishment improves the muscle mitochondrial network in WS worms.

(A) Quantified scores of muscle mitochondrial morphology of adult D7 N2 and *wrn-1*(*gk99*) worms under different conditions. A *myo-3::gfp* reporter gene was expressed in body wall muscles for imaging. Data are shown in mean ± S.E.M (n = 20 worms/group).

(B) Representative images of muscle mitochondrial morphology of adult D7 N2 and *wrn-1*(*gk99*) worms under different conditions. A *myo-3::gfp* reporter gene was expressed in body wall muscles for imaging. Data shown in mean ± S.E.M (n = 10-20 worms/condition).

Two-way ANOVA followed by Tukey's post hoc tests: *, p<0.05, **, p<0.01, ***, p<0.001.

We further confirmed that mammalian NIX and ULK1 were necessary for NAD$^+$-dependent mitophagy in WS1 and WRN-KD cells (**Fig. 18**).

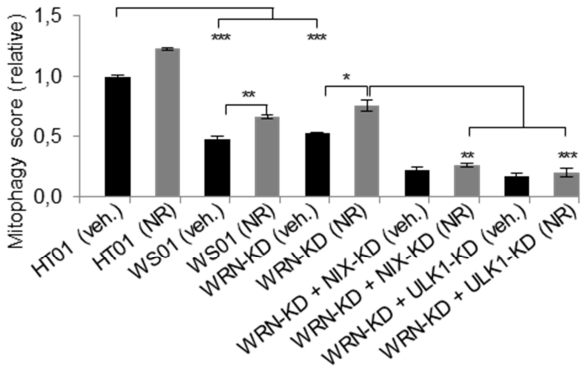

Fig. 18. NAD$^+$-dependent mitophagy in WS cells is regulated by NIX and ULK1.

Flow cytometry quantification of relative mitophagy incidence in the HT01, WS01, and WRN-KD cells under different conditions. For siRNA control, siRNA-vector was added to HT01 and WS01 cells. Data are shown in mean ± S.E.M (n = 3 biological repeats).

Two-way ANOVA followed by Tukey's post hoc tests: *, p<0.05, **, p<0.01, ***, p<0.001.

It has been shown that AMPK regulates energy expenditure through phosphorylation of ULK1 at Ser555 [101]. Indeed, AMPK activity, as detected using antibodies specific for phosphorylated forms of AMPKα (p-Thr127) and its downstream target p-ULK1 (p-Ser555), was lower in WRN deficient cells, and NAD^+ replenishment restored AMPKα activity (**Fig. 19**, and quantification in **Fig. S6D**). In the WRN-KD cells there were no impairments of the macro-autophagic machinery, and the basal level of macro-autophagy was increased (**Fig. S6E**), in line with previous work [365].

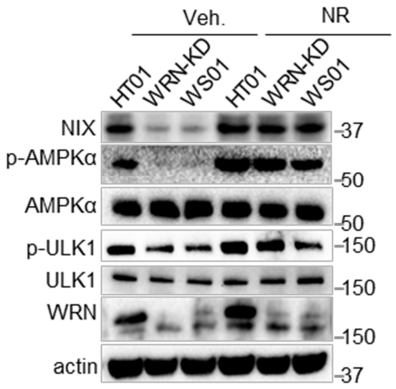

Fig. 19. NAD^+ replenishment restores AMPKα activity in WS cells.
Western blot data showing changes of expression of designated proteins.
Two-way ANOVA followed by Tukey's post hoc tests: *, $p<0.05$, **, $p<0.01$, ***, $p<0.001$.

In summary, our data from *C. elegans* and human cells consistently indicate impaired mitophagy in WS, and that NAD^+ replenishment restores mitophagy by a mechanism involving DCT-1 (NIX) and UNC-51 (ULK1).

VI. NAD^+ restores fat metabolism in the *C. elegans* animal model of WS

Mitochondrial turnover is important for fat metabolism regulation [366]. We focus on detecting a role of WRN in premature atherosclerosis and insulin-resistant diabetes and identifying whether NAD^+ replenishment could improve fat metabolism in the *wrn-1(gk99)* worms. We performed transcriptomic and proteomic analyses using whole bodies from adult D1 and adult D7 worms. At the transcriptional level, WRN-1 dysfunction inhibited almost all of the lipid metabolism-related pathways, including cellular lipid metabolic process, lipid transport, and lipid transporter activity (**Fig. S5G**). NR treatment increased the activity of some of these pathways (**Fig. S5G**). At the protein level, we used our proteomic data to evaluate the changes

in fat-metabolism-related molecular pathways, including mitochondrial β-oxidation, peroxisomal β-oxidation, lipolysis, glycolysis, fatty acid transport, as well as fatty acid desaturation and elongation. Comparing Day1 and Day7, there was an age-dependent decrease of many proteins which are involved in fat metabolism in both N2 and *wrn-1(gk99)* worms (**Figs. 20-21**). Within the same age, many fat-metabolism/catabolism-related proteins were differentially expressed in the *wrn-1(gk99)* worms compared to the N2 worms, e.g., acyl-coenzyme A oxidase (ACOX-1), POD-2, and carnitine palmitoyl transferase 2 (CPT-2), and acyl-CoA dehydrogenase family member 11 (ACDH-11) (**Figs. 20-21**). Notably, ACDH-11 plays important roles in stress resistance (e.g., heat adaptation) and fat catabolism through transcriptional inhibition of the stearic CoA desaturase FAT-7 [367]. In adult D1 worms, ACDH-11 was high in the N2 worms, but it was undetectable in the *wrn-1(gk99)* worms. NR treatment remarkably increased ACDH-11 to over 2-fold higher than that of the N2 group (veh) (**Fig. 20**).

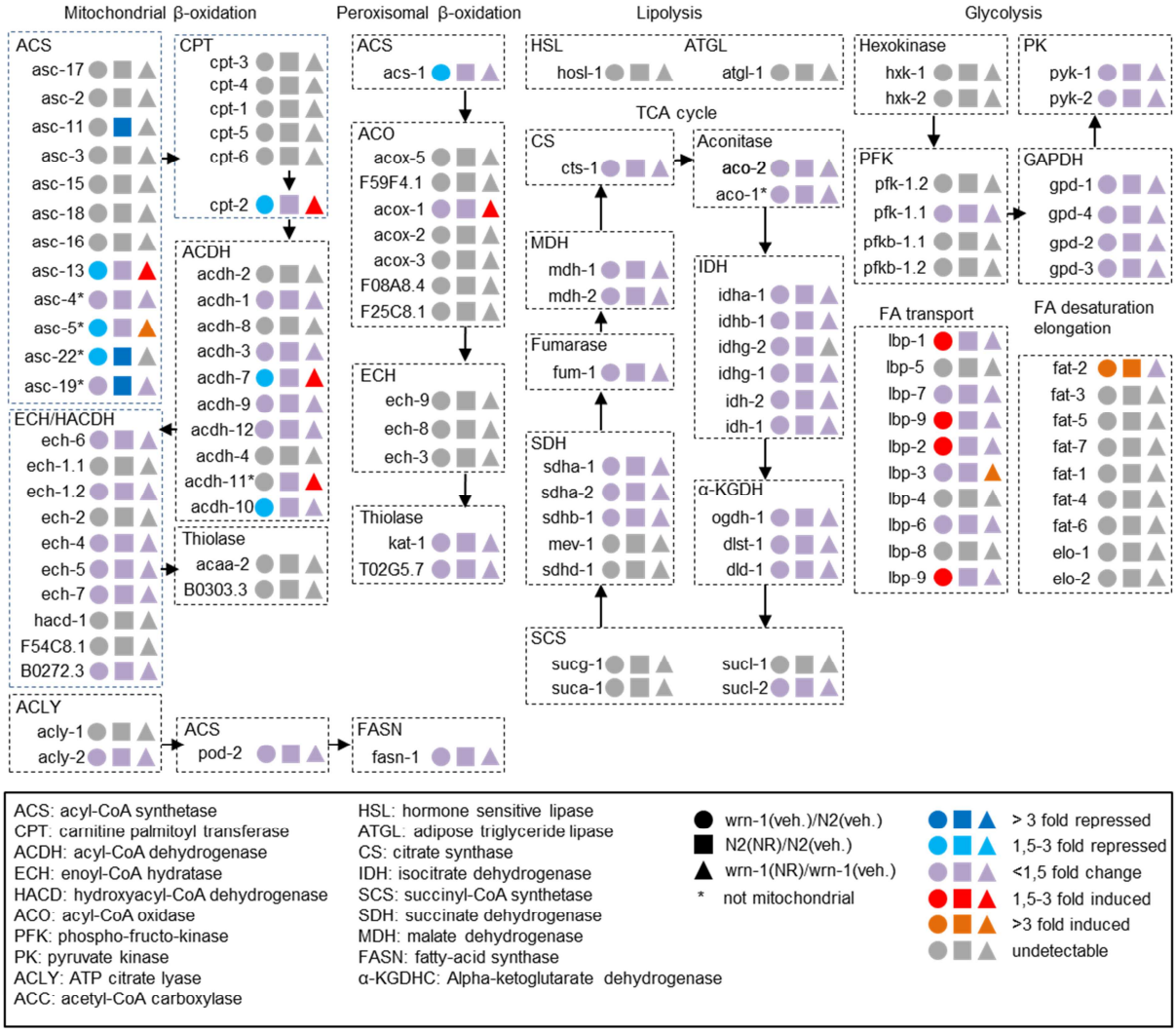

Fig. 20. Effects of NAD$^+$ replenishment on fat metabolism in adult Day 1 *wrn-1 C. elegans*.

We performed systematic proteomic analysis using mass spectrometry with samples from the whole-body tissues from adult D1 worms (n= 4 replicates). We then comprehensively evaluated the changes of fat-metabolism-related molecular pathways, including mitochondrial β-oxidation, peroxisomal β-oxidation, lipolysis, glycolysis, fatty acid transport, as well as fatty acid desaturation and elongation (reference from Yong Yu et al., Nature Communications 2017).

Summary of fat metabolism network is shown.

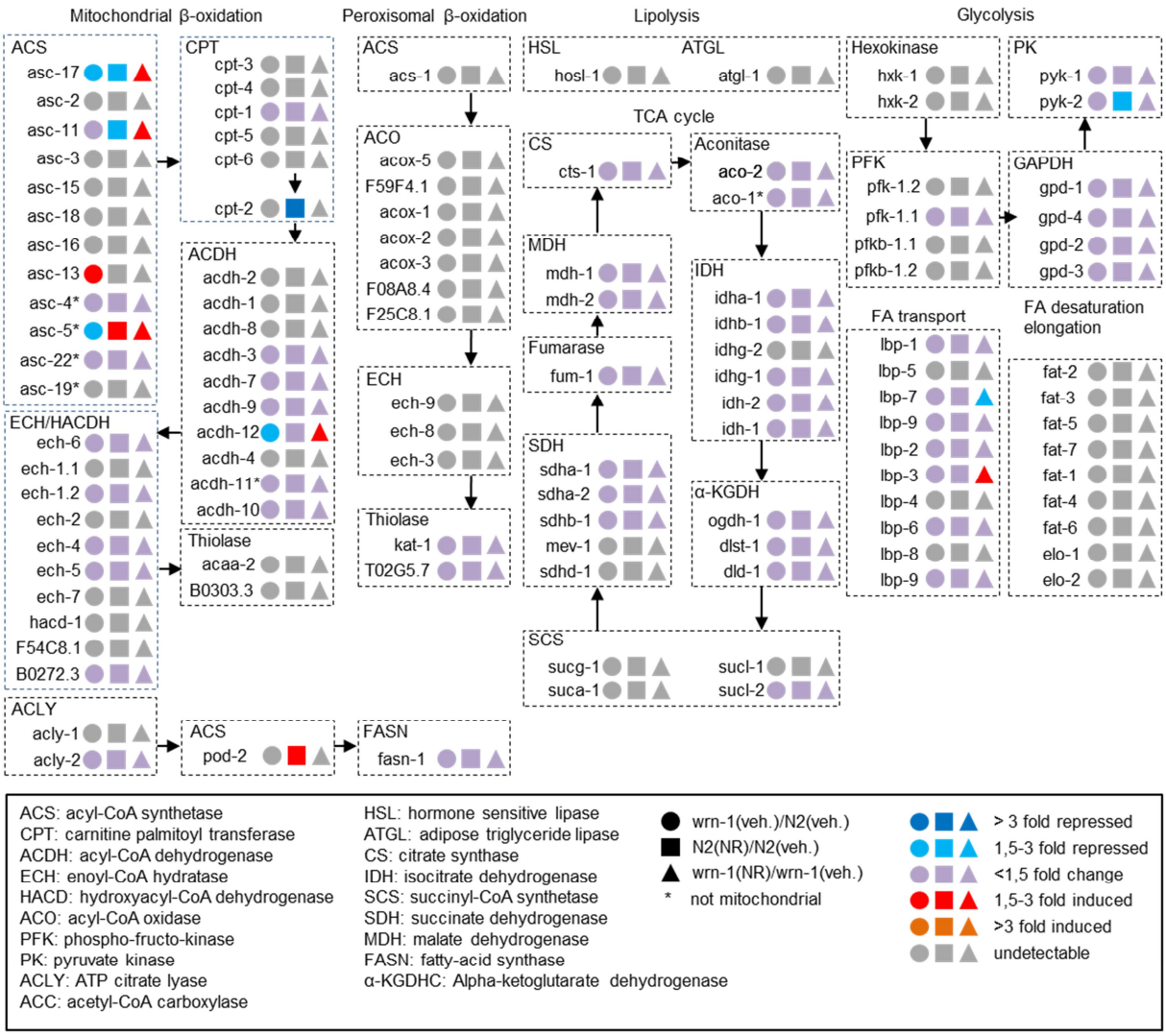

Fig. 21. Effects of NAD$^+$ replenishment on fat metabolism in adult Day 7 *wrn-1 C. elegans*.

We performed systematic proteomic analysis using mass spectrometry with samples from the whole-body tissues from adult D7 worms (n= 4 repeats). We then comprehensively evaluated the changes of fat-metabolism-related molecular pathways, including mitochondrial β-oxidation, peroxisomal β-oxidation, lipolysis, glycolysis, fatty acid transport, as well as fatty acid desaturation and elongation (reference from Yong Yu et al., Nature Communications 2017).

A summary of fat metabolism network is shown.

We finally asked whether NR could affect lipid storage at the organismal level in the *wrn-1*(*gk99*) worms. We stained lipids using oil red in Day7 worms. While WRN-1 dysfunction significantly increased the amount of whole body lipid content (*wrn-1* veh. vs. N2 veh), NR treatment decreased whole organismal lipid levels to 80% of itself in the *wrn-1*(*gk99*) worms (*wrn-1* NR vs. wrn-1 veh) (**Fig. 22A-B**).

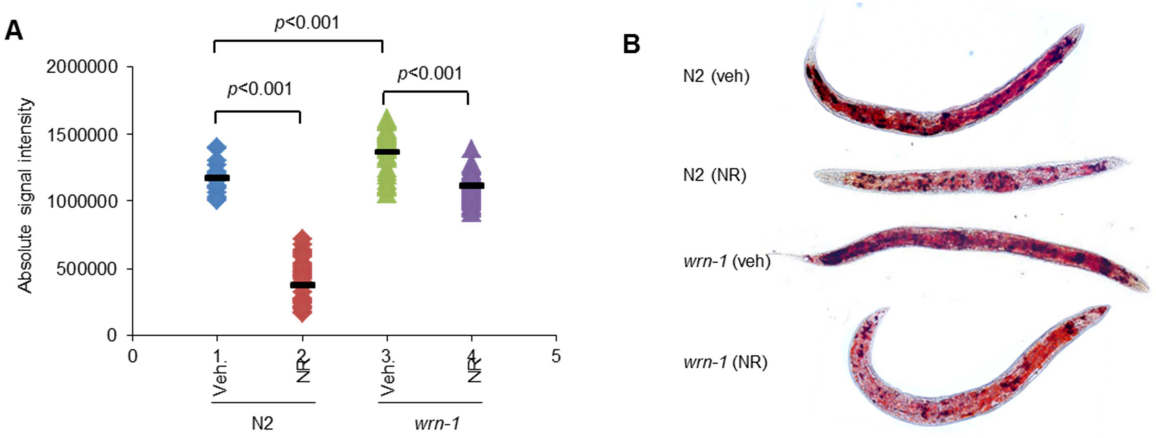

Fig. 22. Effects of NAD$^+$ replenishment on lipid storage in adult Day 7 *wrn-1 C. elegans*.

(A) Changes of fat content in the adult D7 worms treated with/without NR from L4. Oil Red staining was used for imaging with quantification using ImageJ. n= 30-40 worms/group.

(B) A representative set of oil red-stained images are shown.

However, we did not detect any increase of OCR in the NR-supplemented young (adult day 2) and old (adult day 10) wrn-1 worms (**Fig. S7**), possibly due to NR's dominant role in mitophagy rather than mitochondrial biogenesis.

Collectively, our combined transcriptomic, proteomic, and fat staining data support a novel role of WRN in fat metabolism, and NR treatment may partially improve the abnormal fat metabolism in the *wrn-1(gk99)* worms.

VII. NAD$^+$ replenishment improves DNA repair in *C. elegans*

Because DNA repair deficiency is prominent WS [238], we explored whether NR was able to improve DNA repair in WS. WRN mutation causes defect in homologous recombination (HR) [368], we thus performed an embryonic HR capacity assay by exposing early stage embryos to ionizing radiation (90 Gy) [369]. Compared with N2 worms, the *wrn-1(gk99)* worms were more sensitive to ionizing radiation (90 Gy) as indicated by less embryonic survival (**Fig. S8A**). While NR had no significant effect of HR in the N2 embryos, it significantly improved embryonic survival in the *wrn-1(gk99)* worms (**Fig. S8B**). WRN plays a role in RAD51-dependent HR [368], we thus checked RAD-51 filament formation in the *wrn-1(gk99)* germline after 90 Gy ionizing radiation. Compared with N2 worms, there were increased numbers of RAD-51-positive foci/mitotic region in the *wrn-1(gk99)* worms (**Fig. S8B-C**). Consistently, NR had no significant effect in the N2 worms, but it dramatically

decreased numbers of RAD-51 cells in the mitotic region in the *wrn-1(gk99)* worms (**Fig. S8B-C**).

Altogether, these data indicate that NR is able to improve HR DNA repair in the WS *C. elegans*.

DISCUSSION

WS has been linked to seven hallmarks of aging. Here we report the recent discovered relationship between WRN and remaining hallmarks of aging: mitochondrial dysfunction, compromised mitophagy and stem cell exhaustion.

Indeed, by the fourth decade of life, WS patients develop abnormal glucose and lipid metabolism which is often accompanied by type II diabetes mellitus [185]. We supposed that this phenotype could be caused by mitochondrial dysfunction. For this purpose, we observed that both WS cells and *wrn-1(gk99)* worms show reduced mitochondrial network complexity, increased ROS content and decreased basal and maximal mitochondrial oxygen consumption rate. Accumulation of abnormal and dysfunctional mitochondria could derive from a defective mitophagy. Mitophagy has been recently linked to aging [5]. It can either specifically eliminate damaged mitochondria or clear all mitochondria during specialized developmental stages (fertilization and blood cell maturation) or starvation (phosphoinositide 3-kinase/PI3K-dependent) [6]. Data from *C. elegans* and cells indicated a consistent reduction of mitophagy in WS.

Mitophagy-dependent mitochondrial quality control regulates fat metabolism [366]. Indeed, we detect defects in fat metabolism, which may contribute to diabetes. Transcriptomic and proteomic data in *C. elegans* WS model demonstrate that WRN-1 dysfunction inhibit fat-metabolism-related molecular pathways, such as mitochondrial β-oxidation, peroxisomal β-oxidation, lipolysis, glycolysis, fatty acid transport, as well as fatty acid desaturation and elongation. Moreover, significant changes are detectable between young and adult worms, showing a predominant role of aging in metabolic dysfunction.

Aging leads also to stem cells dysfunction. The *wrn-1 (gk99)* worms have a smaller germline stem cell population compared to wild type worms. However, *C. elegans* is not a good model for studying stem cells behavior, since stem cell population consist on only 27 cells. Thus we focus on intestinal stem cells (ISC) population in *Drosophila melanogaster*. ISC in $Wrnexo^{RNAi}$ flies have a lower proliferation potency compared to wild type flies. However the number of ISC is completely the same in both groups, but ISC in $Wrnexo^{RNAi}$ flies are too weak to proliferate.

Collectively, this first set of data underlines a role for WRN in mitochondrial health and stem cells behavior.

This thesis also unveils a role for NAD^+ in a possible therapeutic approach in WS. As already mentioned, NAD^+ controls hundreds of key processes from energy metabolism to cell survival, rising and falling depending on food intake, exercise, and the time of day.

NAD^+ levels steadily decline with age, resulting in altered metabolism and increased disease susceptibility. Indeed, NAD^+ depletion has been linked to hallmarks of aging [8]. Recent evidence demonstrates that boosting NAD^+ may counter aging as well as age-related pathological conditions in animal models [178, 370, 371]. As expected, NAD^+ levels in WS cells and *wrn-1 (gk99)* worms are lower compared to control line and NAD^+ precursors administration increases its levels. In order to deepen the relationship between WRN and NAD^+ depletion, we analyzed the expression of enzymes involved in NAD^+ synthesis. According to these data, we identified WRN as a transcriptional factor regulating NMNAT1 expression. Thus, WRN depletion strongly correlates with an unbalance of NAD^+ biosynthesis. NR treatment corrects these defects, even if the exact molecular mechanism is still unclear. In addition, other molecular mechanisms contribute to NAD^+ depletion in WS, such as DNA-damaged induced PARP activation and an age-dependent increase of the NAD^+-consuming CD38 [372]. Moreover, according to our genome expression analysis, WRN seems to impact metabolism, autophagy, cellular stress responses, development and aging in *wrn-1 (gk99)* worms and NAD^+ replenishment restores many of these pathways at the transcript level. For example, NR administration is able to improve fat metabolism through transcriptomic and proteomic modulation of enzymes involved in fat metabolism-related pathways. NR also increases *dct-1* and *unc-1* expression in *wrn-1 (gk99)* worms, thus indicating an impaired mitophagy which is restored by NAD^+ replenishment.

We also prove that NAD^+ replenishment, through NR and NMN administration, improves both lifespan and healthspan in *wrn-1 (gk99)* worms and $WRNexo^{RNAi}$ flies.

Surprisingly, we pinpoint a novel role of NAD^+ in stem cells dysfunction. Indeed, NR affects stem cells viability and proliferation potency in both our animal models. However, further studies are needed to clarify the molecular mechanism of NAD^+ in stem cells maintenance. Quiescence and stemness of stem cells are also regulated by autophagy /mitophagy. Indeed, recent results demonstrate that autophagy actively suppresses haematopoietic stem-cell metabolism by clearing active, healthy mitochondria to maintain quiescence and stemness, and becomes increasingly necessary with age to preserve the regenerative capacity of old haematopoietic stem cells [373].

Lastly, NR improves DNA repair through reduction of RAD-51 cells in mitotic region in *wrn-1 (gk99)* worms.

Altogether, these data indicate both WRN-exo and WRN-helicase are necessary for organismal lifespan and healthspan, including stem cell function, and provide further evidence that WRN is involved in all hallmarks of aging.

As already mentioned, NAD^+ is a co-factor for several proteins, such as the sirtuins (SIRT1 to SIRT7), CD38, sterile alpha and TIR motif-containing 1 (SARM1), and Poly (ADP-ribose) polymerase (PARPs). Moreover, there are several linkages between NAD^+ and mitophagy. The NAD^+-dependent deacetylase SIRT1 can upregulate autophagy/mitophagy through multiple pathways: by deacetylating the autophagy machinery proteins Atg5, Atg7, and Atg8 (LC3) [59]; by increasing the expression of Beclin1, a key member of the autophagy initiation PI3K III nucleation complex [374]; by deacetylating LC3 at K49 and K51 in the nucleus, enabling its nucleocytoplasmic transportation and binds on Atg7 for autophagy [375]; and by increasing the expression of autophagic proteins Rab7, LC3, Atg12, BNIP3 through deacetylation and acetylation of the transcriptional factors FOXO1 and FOXO3 [376-378]. Rab7, a small GTPase, interacts with the UVRAG-Vps16 complex to enhance the maturation of autophagosomes and endosomes [379]. The NAD^+-SIRT1 pathway may also increase mitophagy through stimulation of autophosphorylation and activation of ataxia telangiectasia mutated (ATM) which induces mitophagy via a LKB1-AMPK-TSC2 pathway [106, 380, 381]. There are three mitochondrial sirtuins, SIRT3, SIRT4, and SIRT5. Recently, it has been shown that NAD^+ replenishment induces the mitochondrial SIRT3-PGAM5-FUNDC1-dependent mitophagy [382]. Nuclear SIRT6 and SIRT7 induce autophagy through inhibition of mTOR [383, 384]. While the NAD^+-consuming enzyme CD38 plays a necessary role in autophagic fusion with lysosomes [385], a new discovered NAD^+-consuming enzyme SARM1 facilitates mitophagy via formation of a PINK1-SARM1- tumor necrosis factor receptor–associated factor 6 (TRAF6) complex to stabilize PINK1 on depolarized mitochondria [386]. Interestingly, SARM1 is required for activation of an injury-induced axon degeneration [387], thus SARM1 may be involved in both neuroprotection and neuronal death. NAD^+ also induces expression of the anti-inflammatory cytokine IL-10 which induces mitophagy through mTOR inhibiton [170, 173, 388]. However, NAD^+ is also involved with the TCA cycle, OXPHOS, and β-oxidation, so how these metabolic pathways interact with mitophagy are elusive. Noticeably, increased NAD^+ may also inhibit autophagy/mitophagy through SIRT2 [389], SIRT4 [390], SIRT5 [391], and PARPs [103]. It has been recently reported that NAD^+-dependent SIRT1 regulates mitophagy through a DAF-16 – DCT1 pathway [106]. As a key metabolic sensor/regulator, AMPK is linked to NAD^+ metabolism, SIRT1 activity, and the phosphorylation of the autophagy/mitophagy protein ULK1 at Ser555 [101, 104]. Here we also demonstrate that WRN regulates mitophagy through the NAD^+/Sirtuins-AMPK-ULK1 pathway, which correlates with both mitochondrial quality and stem cells maintenance. A possible balance of robust NAD^+-dependent mitophagy induction and a mild NAD^+-

dependent mitophagy inhibition presents a still robust mitophagy induction *(Fang EF, Autophagy, submitted).*

In summary, we identify mitochondrial health as a new target and we suggest NAD^+ as an arguable, powerful and beneficial therapy in WS. Currently, clinical trials of NAD^+ precursors on age-related diseases, such as diabetes, neurodegenerative diseases, and premature aging diseases, such as Cockayne syndrome, Xeroderma pigmentosum group A, and Ataxia telangiectasia are in progress [7]. However, despite extensive researches on NAD^+ implications in health and disease, clinical trials are required to assess the safety of NAD^+ precursors in patients with age-related diseases.

To easily recapitulate our data we propose a working model (**Fig. 23**). We suggest *WRN* mutation leads to cellular NAD^+ reduction through the down-regulation of the NAD^+ synthetic enzyme NMNAT1 and upregulation of cellular NAD^+ consumption (e.g., by PARPs). Cellular NAD^+ depletion can impair mitophagy through p-AMPK and p-ULK1 reduction (two upstream proteins which regulate autophagy/mitophagy), resulting in accumulation of damaged mitochondria. In combination with the defects in this NAD^+-AMPK-ULK1-mitophagy pathway and other WRN-dependent cellular processes, such as DNA repair, they drive defective metabolism and accelerated aging. Restoration of cellular NAD^+ through NAD^+ precursors, such as NR (nicotinamide riboside) and NMN (nicotinamide mononucleotide) alleviates *WRN mutation*-induced pathological features in both *C. elegans* and *Drosophila* models of WS and in primary human cells from WS patients. Our study suggests a novel therapeutic option for WS.

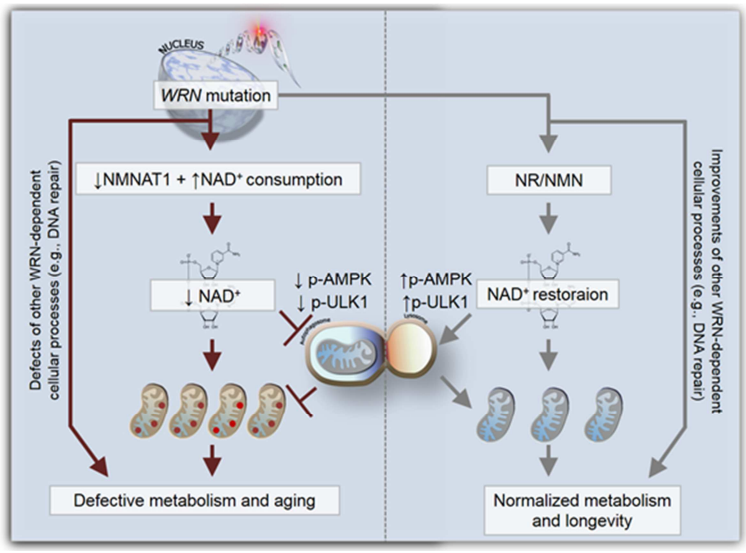

Fig. 23. Final working model.

We propose *WRN* mutation leads to cellular NAD^+ reduction through the down-regulation of the NAD^+ synthetic enzyme NMNAT1 and upregulation of cellular NAD^+ consumption (e.g., by PARPs). Cellular NAD^+ depletion can impair mitophagy through p-AMPK and p-ULK1 reduction (two upstream proteins which regulate autophagy/mitophagy), resulting in accumulation of damaged mitochondria. In combination with the defects in this NAD^+-AMPK-ULK1-mitophagy pathway and other WRN-dependent cellular processes, such as DNA repair, they drive defective metabolism and accelerated aging. Restoration of cellular NAD^+ through NAD^+ precursors, such as NR (nicotinamide riboside) and NMN (nicotinamide mononucleotide) alleviate *WRN mutation*-induced pathological features in both *C. elegans* and *Drosophila* models of WS and in primary human cells from WS patients. Our study suggests a novel therapeutic option for WS.

CONCLUSIONS

Age is the primary cause of most of human disease and interventional strategies aimed to achieve healthy aging and delay age-related diseases are the main focus of many researchers. Werner syndrome is a human premature aging disease used as model to simplify the analysis of the normal aging process.

This study proposes NAD^+ depletion as a major driver of accelerated aging in two WS animal models (*C. elegans* and *Drosophila*), pinpointing its importance in longevity. It sheds light on a new therapeutic possibility of boosting NAD^+ in aging and age-related diseases with the final purpose of delaying aging and improving quality of life, especially in WS patients. NAD^+ replenishment in WS models improves both lifespan and healthspan and also ameliorate some aging features, including mitochondrial function and turnover and stem cells maintenance.

NAD^+ could be considered an anti-aging factor but further studies are needed to reveal unknown regulatory mechanisms linking NAD^+, WRN and aging.

Supplementary figures

Samples	Age	Sex	Progeroid changes	Cataract	Metabolism	Notes
Primary fibroblasts						
WS01	30	F	pigmented and atrophic skin	Yes	hyperlipidemia type V	From Coriell institute #AG03141 2476C>T
Healthy01 (HT01)	30	F	no	no	no	From Coriell institute #AG09599
WS02-Japan	58	F	Gray hair, 20s Bird-like face	bilateral, 36yo	Abnormal glucose diabetes 58yo	Diagnosed 57 years old; homo c.1105 C>T
WS03-Japan	50	F	Gray hair Bird-like face	bilateral, n.a	n.a.	Diagnosed 50 years old; homo c.3139-1 G>C
WS04-Japan	52	M	Gray hair, 20s Bird-like face	bilateral, 30s	Abnormal glucose; Diabetes, 46 yo dyslipidemia, 46 yo.	Diagnosed 52 years old; hetero c.3139-1 G>C; c.1105 C>T; Amputation, right leg 50 yo;
WS05-Japan	42	M	Gray hair, 10s Bird-like face	bilateral, 33yo	Abnormal glucose; Diabetes (30s) dyslipidemia (age n.a.)	Homo c.3139-1 G>C
Healthy02-Japan	32	F	no	no	no	
Healthy03-Japan	33	F	no	no	no	
Healthy04-Japan	31	F	no	no	no	
Healthy05-Japan	29	M	no	no	no	

Table S1. Detailed information of primary fibroblasts used in this study.

Except WS01 and its matched HT01 which were from Coriell Institute, all the other samples were from Chiba University, Japan.

Samples	Age	Sex	Progeroid changes	Cataract	Metabolism	Notes
Blood samples						
WS02-Japan	58	F	Gray hair, 20s Bird-like face	bilateral, 36yo	Abnormal glucose diabetes 58yo	Diagnosed 57 years old; homo c.1105 C>T
WS03-Japan	50	F	Gray hair Bird-like face	bilateral, n.a	n.a.	Diagnosed 50 years old; homo c.3139-1 G>C
WS04-Japan	52	M	Gray hair, 20s Bird-like face	bilateral, 30s	Abnormal glucose; Diabetes, 46 yo dyslipidemia, 46 yo.	Diagnosed 52 years old; hetero c.3139-1 G>C; c.1105 C>T; Amputation, right leg 50 yo;
WS05-Japan	42	M	Gray hair, 10s Bird-like face	bilateral, 33yo	Abnormal glucose; Diabetes (30s) dyslipidemia (age n.a.)	Homo c.3139-1 G>C
WS06-Japan	38	M	-	bilateral, n.a	Diabetes	3139-1G>C/1720+1 G>A
WS07-Japan	41	M	Skin atrophy Bird-like face	bilateral, n.a	No diabetes	3139-1 G>C/3139-1 G>C
WS08-Japan	37	F	Gray hair Muscle atrophy Skin atrophy	bilateral, n.a	No diabetes	3139-1 G>C/3139-1 G>C
WS09-Japan	30s	M	Skin atrophy Bird-like face	bilateral, n.a	Pre-diabetes dyslipidemia	3139-1 G>C/2959 C>T
WS10-Japan	37	F	Gray hair/alopecia	bilateral, n.a	No diabetes	3139-1 G>C/3139-1 G>C
WS11-Japan	41	M	Skin atrophy Bird-like face	bilateral, n.a	Diabetes	3139-1 G>C/3139-1 G>C
Healthy02-Japan	29	M	no	no	no	
Healthy03-Japan	32	F	no	no	no	
Healthy04-Japan	33	F	no	no	no	
Healthy05-Japan	31	F	no	no	no	
Healthy06-Japan	29	M	no	no	no	
Healthy07-Japan	30	M	no	no	no	
Healthy08-Japan	35	F	no	no	no	
Healthy09-Japan	44	M	no	no	no	
Healthy10-Japan	29	F	no	no	no	
Healthy11-Japan	41	M	no	no	no	
Healthy12-Japan	31	M	no	no	no	
Healthy13-Japan	37	M	no	no	no	

Table S2. Detailed information of blood plasma samples used in this study.

All the samples were from Chiba University, Japan.

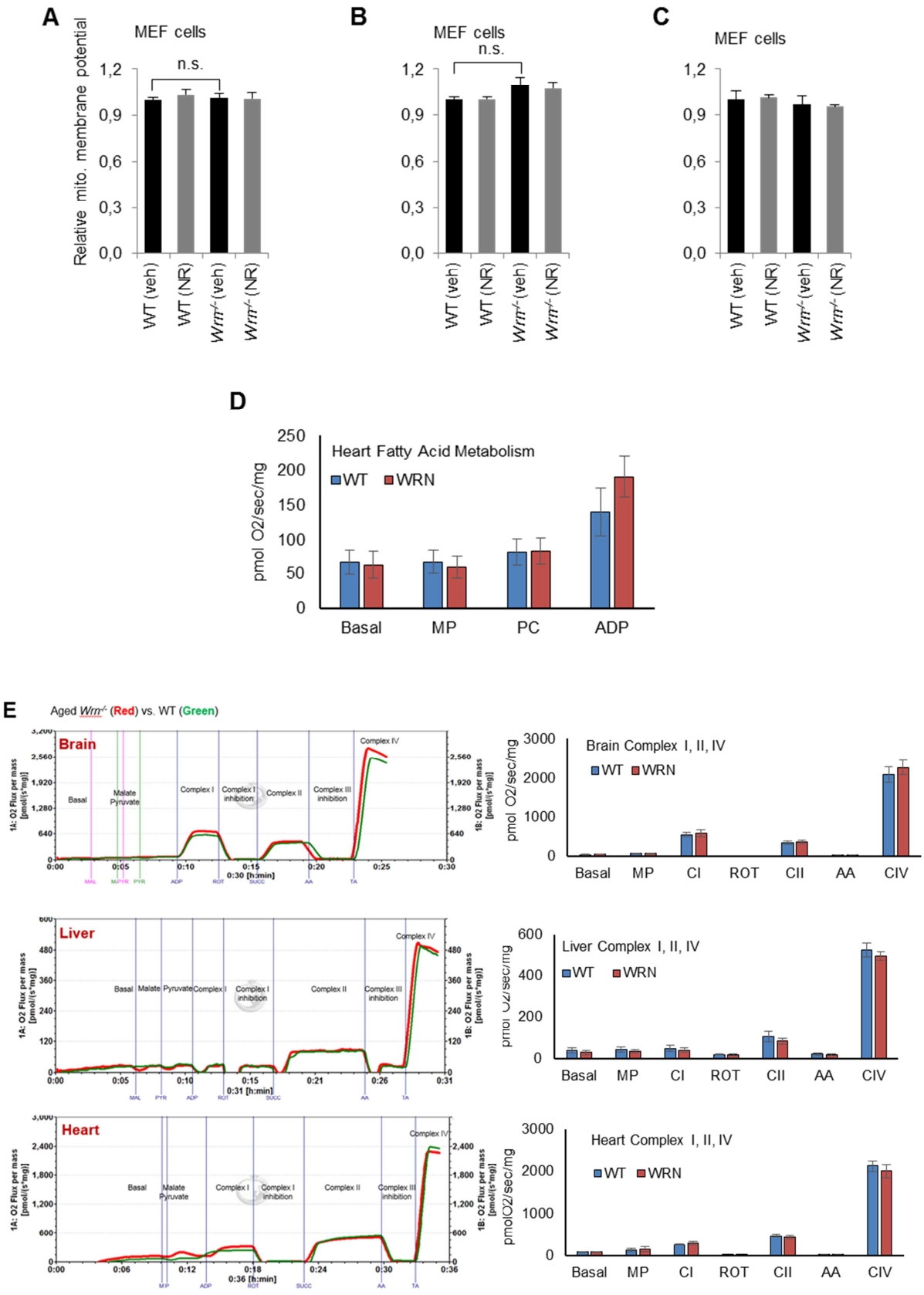

Fig. S1. Changes of mitochondrial function in mouse and *C. elegans* models of WS.

(A-C) Flow cytometry analysis of relative values of mitochondrial membrane potential (A), mitochondrial content (B), and mitochondrial ROS (C) in WT and *Wrn*$^{-/-}$ MEFs treated with/without NR (1 mM, 24 h). Data are shown in mean ± S.E.M (n = 3 biological repeats). n.s., p>0.05.

(D) No changes of fatty acid metabolism in the mitochondria extraction from heart tissues between the WT and the *Wrn*$^{-/-}$ mice. Data are shown in mean ± S.E.M. (n = 3 mice).

(E) Oroboros analysis showing no difference of mitochondrial function in the brain, liver, or heart tissues between aged *Wrn*$^{-/-}$ mice (15-17.5 months) and WT littermates.

Student *t* test or Two-way ANOVA followed by Tukey's post hoc tests: n.s., $p>0.05$ *, $p<0.05$, **, $p<0.01$, ***, $p<0.001$

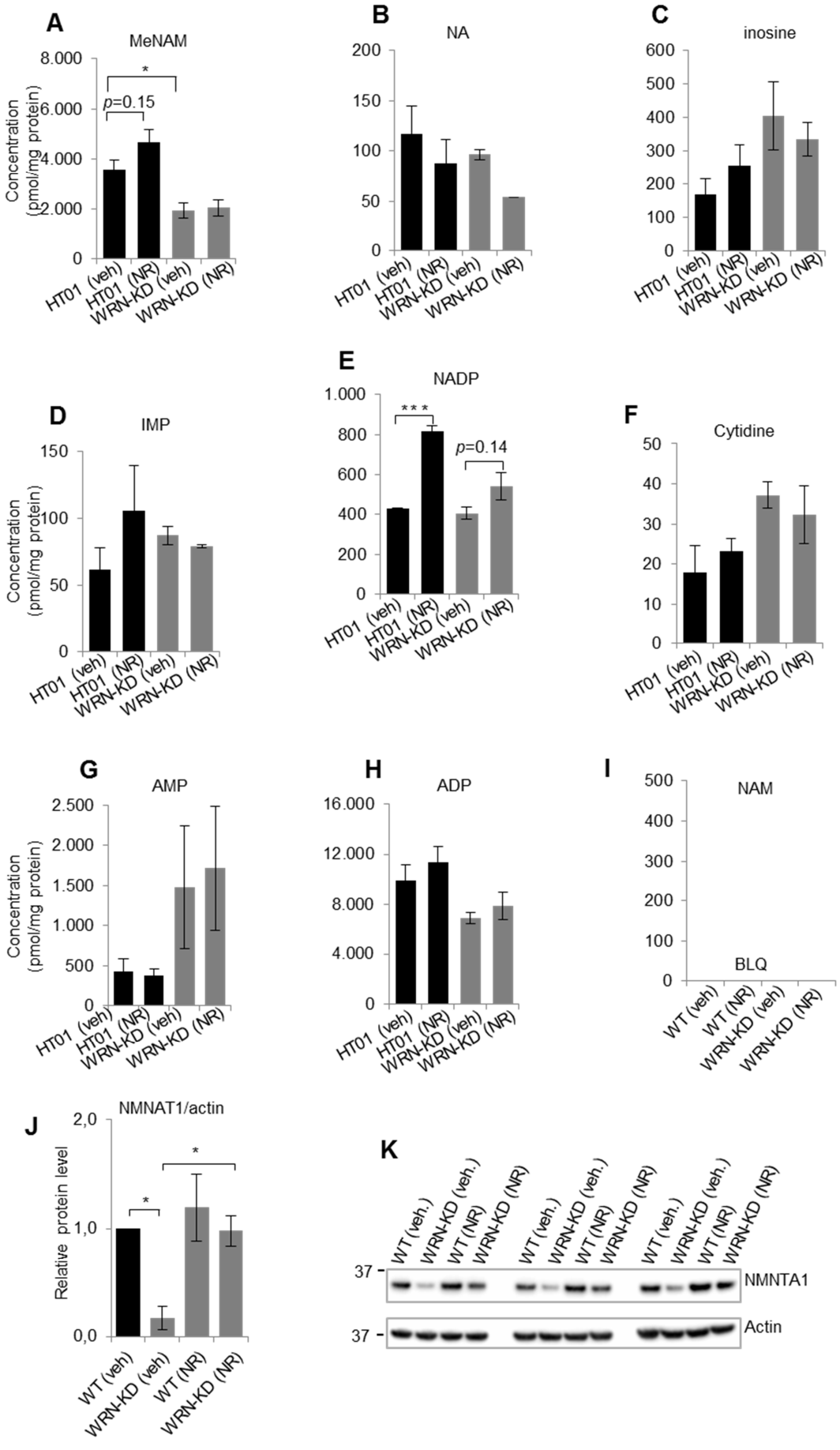
A
MeNAM
Concentration (pmol/mg protein)
8.000
6.000
4.000
2.000
0
*
p=0.15
HT01 (veh)
HT01 (NR)
WRN-KD (veh)
WRN-KD (NR)
B
NA
200
150
100
50
0
C
inosine
600
500
400
300
200
100
0
D
IMP
150
100
50
0
E
NADP
1.000
800
600
400
200
0
***
p=0.14
F
Cytidine
50
40
30
20
10
0
G
AMP
2.500
2.000
1.500
1.000
500
0
H
ADP
16.000
12.000
8.000
4.000
0
I
NAM
500
400
300
200
100
0
BLQ
WT (veh)
WT (NR)
WRN-KD (veh)
WRN-KD (NR)
J
NMNAT1/actin
Relative protein level
2,0
1,0
0,0
K
37
NMNTA1
Actin

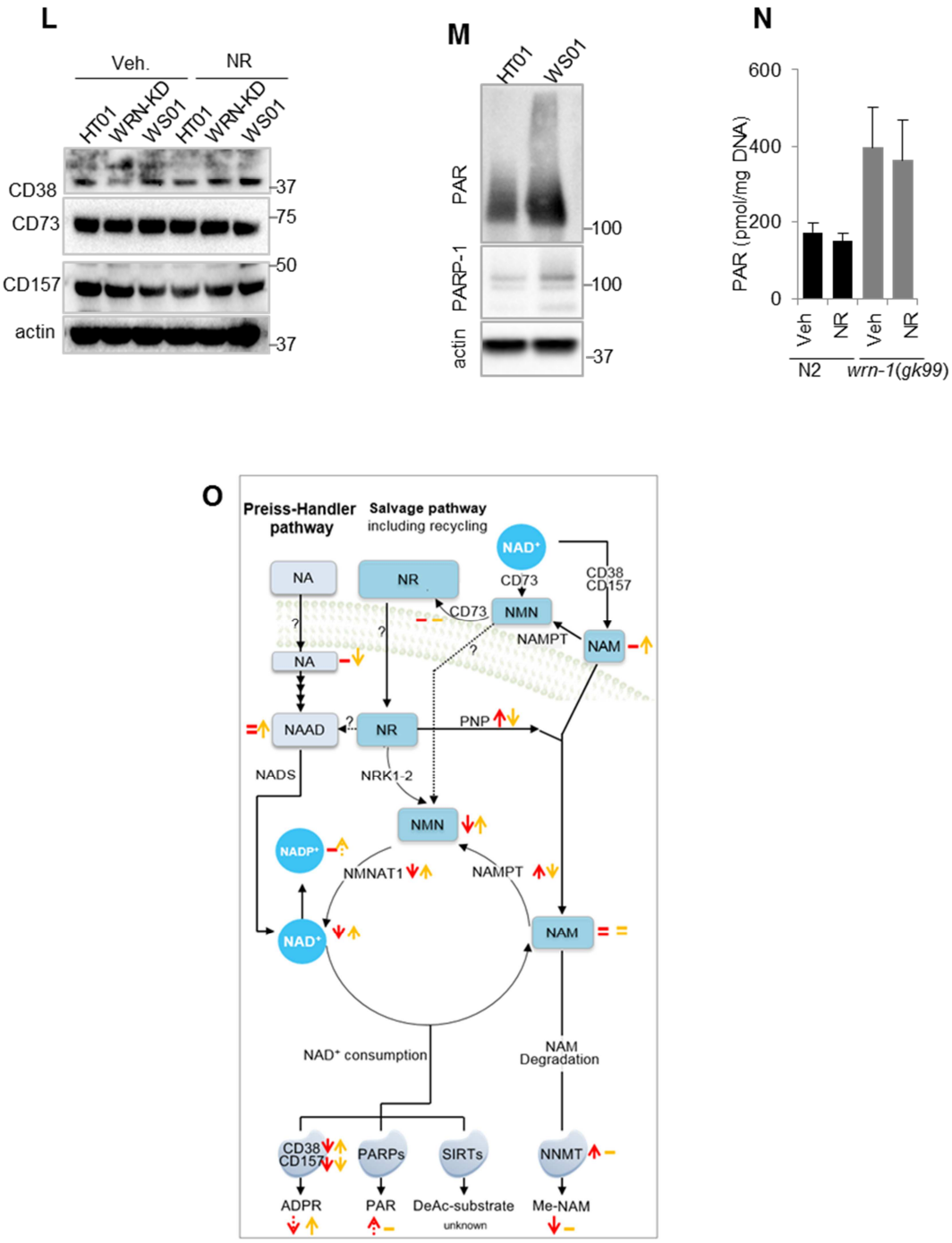

Fig. S2. Changes of NAD$^+$ metabolic profiles, NAD$^+$ metabolism-related enzymes, and mRNA level of nmnat1 in designated human cells with/without NA treatment.

(A-I) Liquid chromatography-mass spectrometry (LC-MS) data showing changes of methylated nicotinamide (MeNAM), nicotinic acid (NA), inosine, IMP, nicotinamide adenine dinucleotide phosphate (NADP), cytidine, adenosine monophosphate (AMP), adenosine diphosphate (ADP), and nicotinamide (NAM) in HT01 and WRN-KD cells before and after NR treatment (1 mM, 24 h). Data are shown in mean ± S.E.M (n = 3 samples/group).

(J) Quantification of protein expression levels from Fig. 7A. n = 3 biological repeats.

(K) Western blotting showing changes of expression levels of designated proteins. n = 3 biological repeats.

(L) Western blotting showing changes of expression levels of proteins involved in NAD$^+$ consumption in designated conditions.

(M) Western blotting showing changes of designated proteins in the HT01 and the WS01 cells.

(N) Mass spectrometry data showing changes of PAR levels in the N2 and the wrn-1(gk99) worms with/without NR treatment (1 mM from L4 stage).

(O) A summary of the changes of the NAD^+ metabolites as well as NAD^+ synthesis- or consumption-related enzymes. Red, WRN-KD (veh) vs. HT01 (veh); Orange, WRN-KD (NR) vs. WRN-KD (veh); Solid arrows, with difference; dashed arrows, with a trend of difference; one bar, no difference; two bars, undetectable. The summary was based on the data from Fig. 6-7-8 and Fig. S2, as well other results in this study.

Two-way ANOVA followed by Tukey's post hoc tests: n.s., $p>0.05$, *, $p<0.05$, **, $p<0.01$, ***, $p<0.001$.

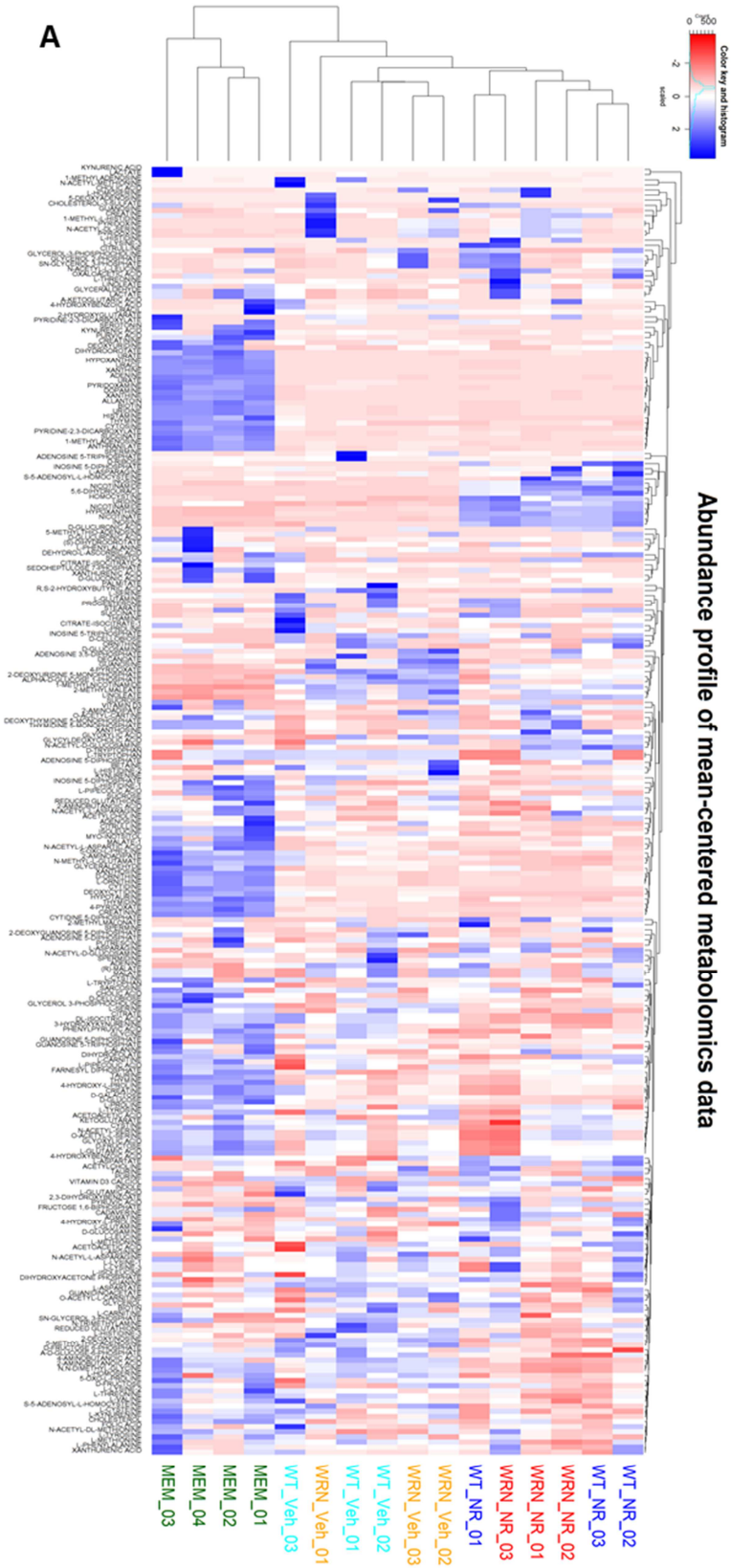
A
Color key and histogram
scaled
Abundance profile of mean-centered metabolomics data
WT_NR_02
WT_NR_03
WT_NR_01
WRN_NR_02
WRN_NR_01
WRN_NR_03
WRN_Veh_02
WRN_Veh_03
WT_Veh_02
WT_Veh_01
WRN_Veh_01
WT_Veh_03
MEM_01
MEM_02
MEM_04
MEM_03

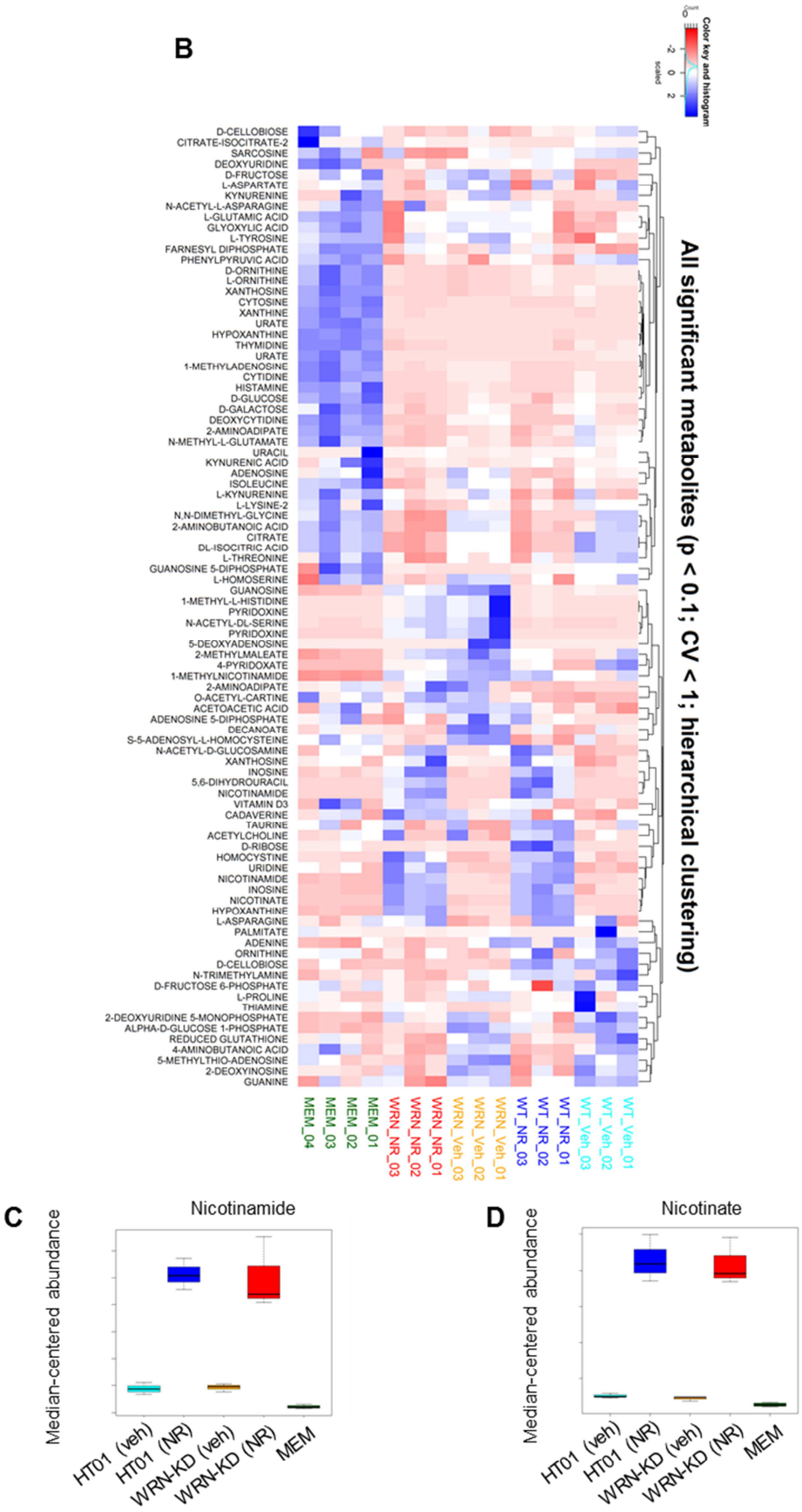

Fig. S3. Changes of extra-cellular NAD^+ metabolites.

Extracellular metabolic profiles were examined for media incubated in the HT01 and the WRN-KD cells treated with NR (1mM) or Mock. Growth media (MEM media, no FBS, incubated at 37 °C for 24 h) were used as internal background control.

(A) Targeted liquid chromatography-mass spectrometry (LC-MS) based metabolomics data showing all the detected metabolites (n=3 separate cultures/group).

(B) Data from (A) for those metabolites which exhibited significance (n=3 separate c*ul*tures//group).

(C-D) Relative levels of nicotinamide and nicotinate in different conditions (n=3 separate cultures//group) (also presented in the heat maps above).

A

Condition	Mean lifespan (Mean ± SEM)	P-Value to *wrn-1* veh
N2 veh	20.6 ± 0.25	
N2 (NR)	22,0 ± 0.23	<0.001
N2 (NMN)	22,4 ± 0,25	<0.001
wrn-1 (veh)	13.9 ± 0.43	<0.001
wrn-1 (NR)	18.1 ± 0.48	<0.001
wrn-1 (NMN)	19.8 ± 0.45	<0.001
wrn-1 (SRT1720)	16.5 ± 0.46	<0.001
wrn-1 (Ola)	15.0 ± 0,44	<0.05

B

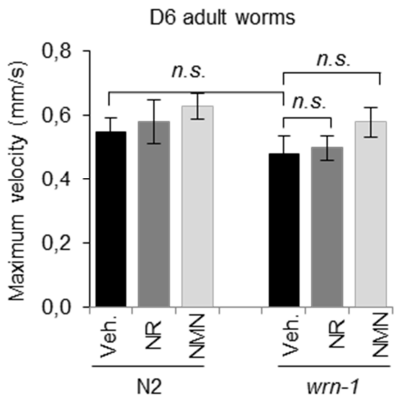

C

Condition	Mean lifespan (Mean ± SEM)	p-value to *wrn-1* (veh)
N2 (veh)	19.0 ± 0.5	<0.01
wrn-1 (veh)	16.8 ± 0.2	-
wrn-1 (NR)	20.3 ± 0.5	<0.001
wrn-1 (NMN)	21.3 ± 0.4	<0.001
wrn-1 (NAD^+)	20.8 ± 0.4	<0.001
wrn-1 (NAM)	17.9 ± 0.7	>0.05

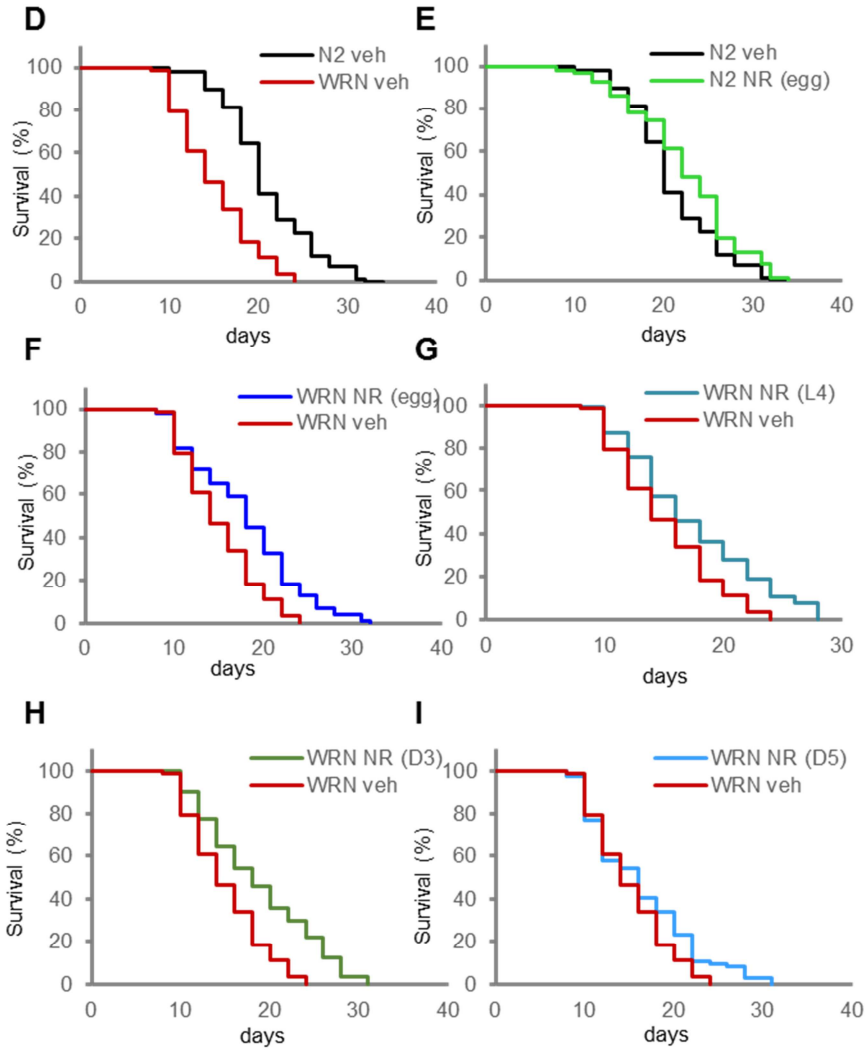

J

Condition (Starting point of treatment)	Mean lifespan (Mean ± SEM, Days)	p-value to N2 veh
N2 veh	21.0 ± 0.53	-
N2 NR (egg)	22.4 ± 0.64	0.012
wrn-1 veh	15.0 ± 0.46	< 0.0001

Condition	Mean lifespan (Mean ± SEM, Days)	p-value to *wrn-1* veh.
wrn-1 veh	15.0 ± 0.46	-
wrn-1 NR (egg)	18.0 ± 0.61	0.0007
wrn-1 NR (L4)	17.3 ± 0.57	< 0.0001
wrn-1 NR (D3)	18.3 ± 0.70	< 0.0001
wrn-1 NR (D5)	16.3 ± 0.70	0.040

Fig. S4. Changes of lifespan in the N2 and *wrn-1* worms with NR exposure at different stages of life or with different NAD^+ precursors.

(A) Changes of lifespan in N2 and the *wrn-1(gk99)* worms in different conditions. For all the experiments, worms from L4 stage were exposed to vehicle control, the NAD^+ precursors NR and NMN (both at 1 mM), a SIRT1activator SRT1720 (10 μM), or a PARP inhibitor Olaparib (500 nM).

(B) Changes of maximum velocity between adult D6 N2 and the *wrn-1(gk99)* worms in different conditions. Data are shown in mean ± S.E.M (n = 20-30 worms in each condition).

(C) Effects of NAD^+ itself and different NAD^+ precursors on the lifespan of the *wrn-1(gk99)* worms. All the treatments (1 mM) were started from L4 larva stage.

(D-J) Effects of NR treatment at different stages of the worm life on the worm lifespan. NR was given at 1 mM at different stages.

All the lifespan studies were repeated 2-7 times. Two-way ANOVA followed by Tukey's *post hoc* tests was used for data analysis.

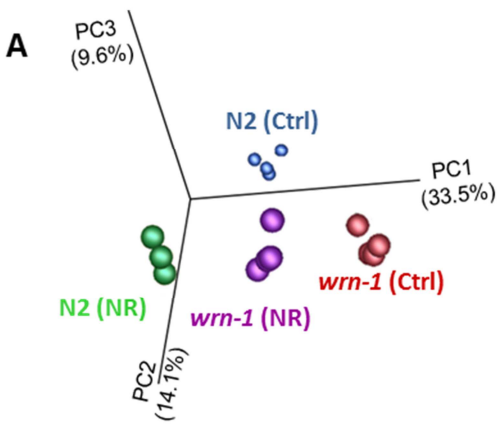
A
PC3
(9.6%)
N2 (Ctrl)
PC1
(33.5%)
N2 (NR)
wrn-1 (NR)
wrn-1 (Ctrl)
PC2
(14.1%)

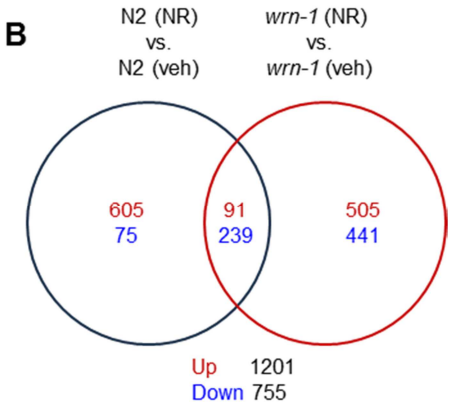
B
N2 (NR)
vs.
N2 (veh)
wrn-1 (NR)
vs.
wrn-1 (veh)
605
75
91
239
505
441
Up 1201
Down 755

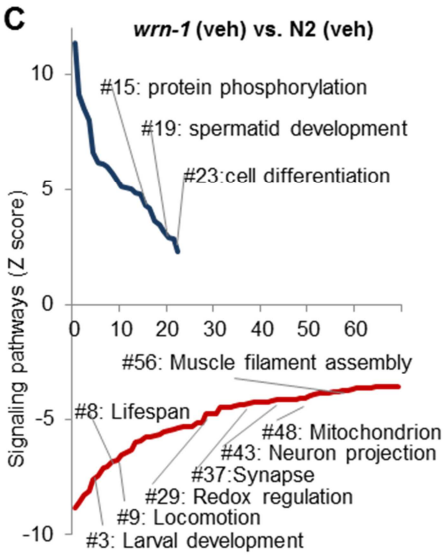
C
wrn-1 (veh) vs. N2 (veh)
Signaling pathways (Z score)
#15: protein phosphorylation
#19: spermatid development
#23:cell differentiation
#56: Muscle filament assembly
#8: Lifespan
#48: Mitochondrion
#43: Neuron projection
#37:Synapse
#29: Redox regulation
#9: Locomotion
#3: Larval development

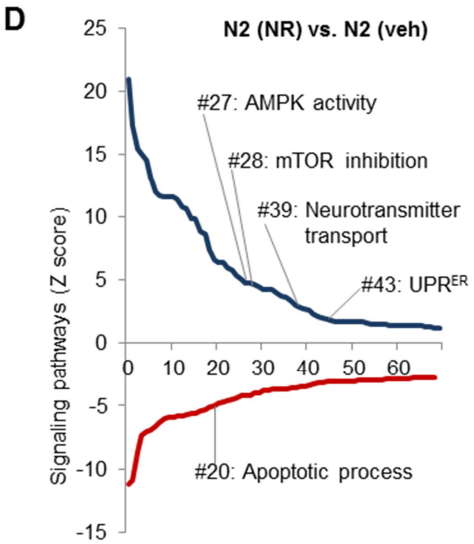
D
N2 (NR) vs. N2 (veh)
Signaling pathways (Z score)
#27: AMPK activity
#28: mTOR inhibition
#39: Neurotransmitter transport
#43: UPRER
#20: Apoptotic process

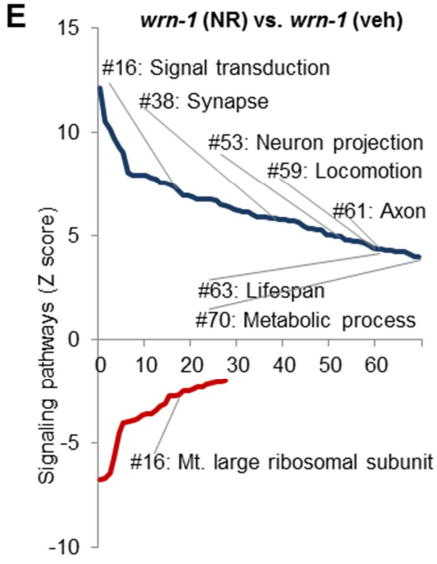
E
wrn-1 (NR) vs. wrn-1 (veh)
Signaling pathways (Z score)
#16: Signal transduction
#38: Synapse
#53: Neuron projection
#59: Locomotion
#61: Axon
#63: Lifespan
#70: Metabolic process
#16: Mt. large ribosomal subunit


F
AMP-ACTIVATED PROTEIN KINASE COMPLEX
NEGATIVE REGULATION OF TOR SIGNALING CASCADE
AMP-ACTIVATED PROTEIN KINASE ACTIVITY
CELLULAR RESPONSE TO GLUCOSE STARVATION
PEPTIDE CATABOLIC PROCESS
CELLULAR METABOLIC PROCESS
MITOCHONDRION ORGANIZATION
MITOCHONDRIAL TRANSLATION
MITOCHONDRIAL LARGE RIBOSOMAL SUBUNIT
OXIDOREDUCTASE ACTIVITY....
OXIDOREDUCTASE ACTIVITY.....
DAUER ENTRY
INOSITOL LIPID-MEDIATED SIGNALING
CHOLESTEROL HOMEOSTASIS
RESPONSE TO FOOD
CARBOHYDRATE PHOSPHORYLATION
RESPONSE TO OXIDATIVE STRESS
PROTON TRANSPORT
CELLULAR LIPID METABOLIC PROCESS
POSITIVE REGULATION OF GROWTH RATE
OXIDOREDUCTASE ACTIVITY...
LIPID BINDING
HYDROLASE ACTIVITY...
TREHALOSE METABOLIC PROCESS
GLYCOGEN METABOLIC PROCESS
PROTEIN CATABOLIC PROCESS
METABOLIC PROCESS
OXIDOREDUCTASE ACTIVITY
OXIDATION-REDUCTION PROCESS
POSITIVE REG OF MULTICELLULAR ORGANISM GROWTH
GROWTH

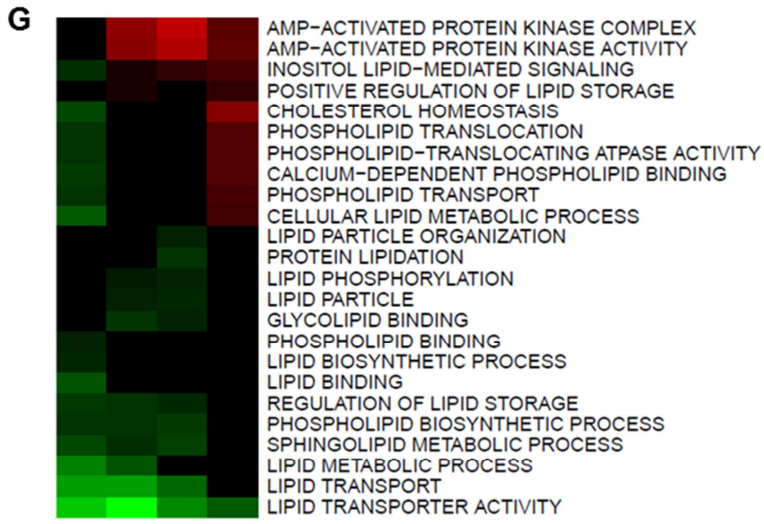

Fig. S5. NAD$^+$ replenishment normalizes the transcriptomic profiles of WRN.

The *wrn-1(gk99)* and the N2 worms were treated with NR (1 mM) from the L4 stage, followed by changing to fresh drug plate on adult Day4. The worms were collected on adult D7 for transcriptomic analysis.

(A) Principal component analysis (PCA) revealed separation between N2 (veh) and *wrn-1(gk99)* (veh), while NR treatment led to a normalization of the *wrn-1(gk99)* transcriptomic profile closer to the N2 (veh).

(B) Venn diagram of transcriptomic results showing that NR induced changes of genes between [N2 (NR) vs. N2 (veh.)] vs. [*wrn-1* (NR) vs. *wrn-1* (veh.)].

(C-E) Gene-set-enrichment analysis demonstrates upregulated and downregulated signaling pathways (GO pathways) in the D7 N2 and the *wrn-1(gk99)* worms treated with/without NR (1 mM from L4). The GO terms were ranked on the basis of enrichment scores. The upregulated GO pathways and downregulated GO pathways summarized separated, with a whole list of changes GO terms shown in Table S3.

(F) Heat map data showing changes of the GO terms related to mitochondrial function among 4 different comparisons.

(G) Heat map data showing changes of the GO terms related to lipid metabolism among 4 different comparisons.

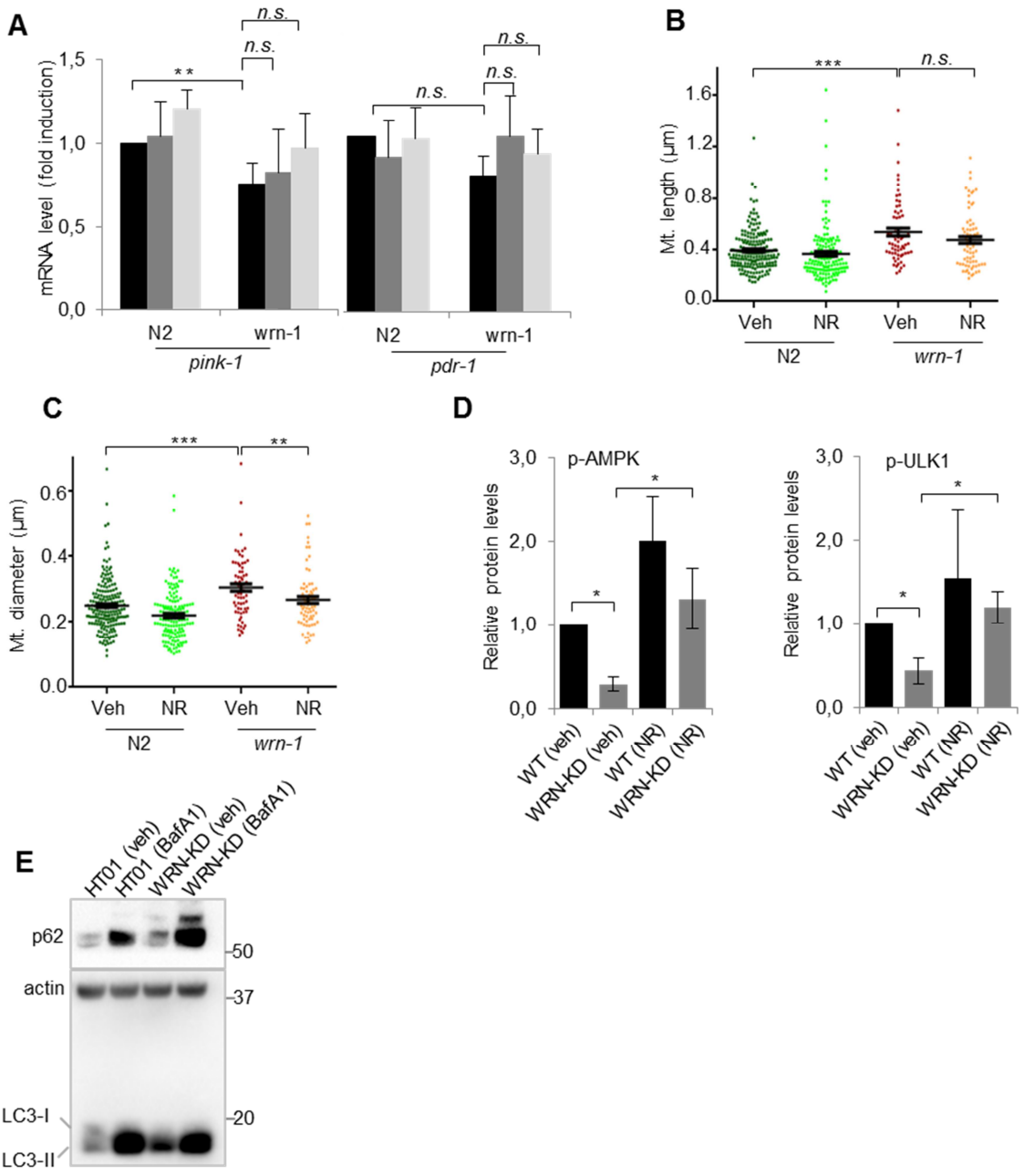

Fig. S6. Changes of mitophagy and mitochondrial fusion-fission related genes, as well as mitochondrial morphology/function in N2 and the *wrn-1*(*gk99*) worms in different conditions.

(A) The mRNA levels of *pink-1* and *pdr-1* in the NR and NMN-treated N2 and the *wrn-1(gk99)* worms. Data are shown in mean ± S.E.M (n = 3 biological repeats).

(B-C). Adult D7 worms in different conditions were collected for electron microscopy, and the length as well as diameter of mitochondria in different groups were quantified. Data are shown in mean ± S.E.M (n = 100-250 mitochondria in each condition).

(D) Quantification of protein expression levels from Fig. 19.

(E) Representative western blot data showing higher basal level of macro autophagy in the WRN-KD cells, as well as no defect of autophagic machinery. Bafilomycin A1 (BafA1), a lysosome inhibitor (100 nM, overnight).

Two-way ANOVA followed by Tukey's post hoc tests was used for data analysis with n.s., $p>0.05$ *, $p<0.05$, **, $p<0.01$, ***, $p<0.001$.

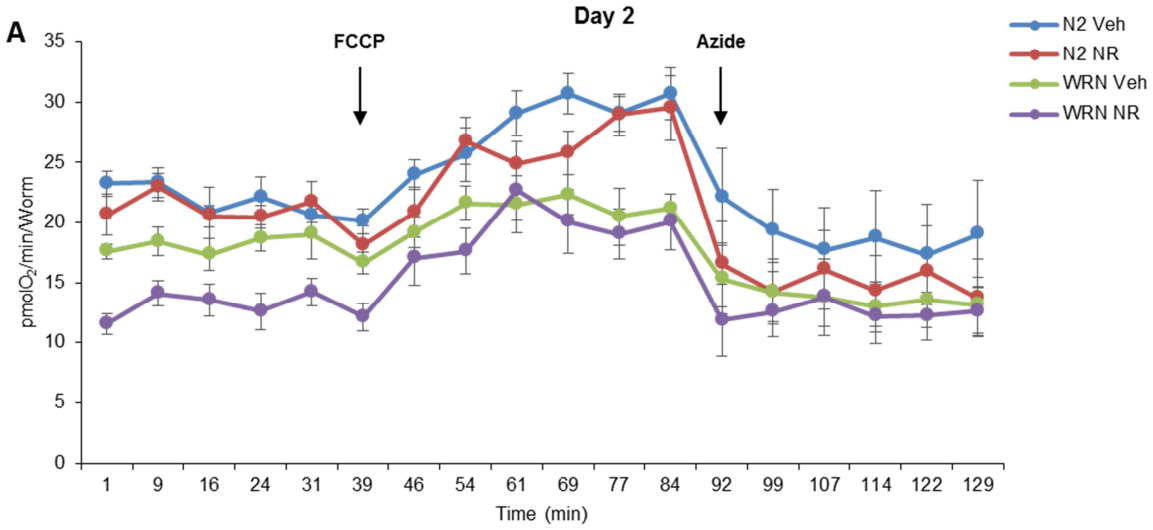
A
Day 2
FCCP
Azide
N2 Veh
N2 NR
WRN Veh
WRN NR
pmolO_2/min/Worm
0
5
10
15
20
25
30
35
1
9
16
24
31
39
46
54
61
69
77
84
92
99
107
114
122
129
Time (min)

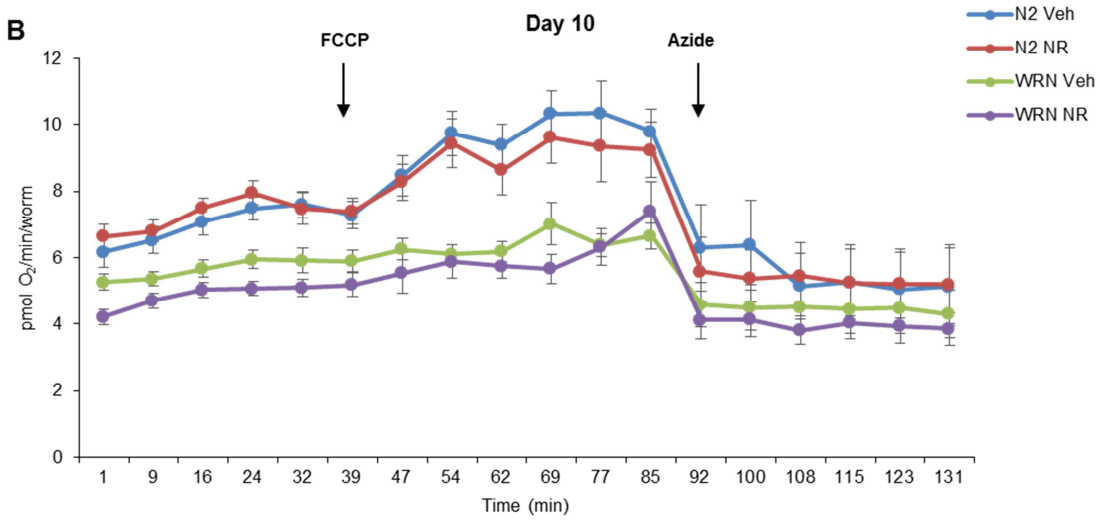
B
Day 10
FCCP
Azide
N2 Veh
N2 NR
WRN Veh
WRN NR
pmol O_2/min/worm
0
2
4
6
8
10
12
1
9
16
24
32
39
47
54
62
69
77
85
92
100
108
115
123
131
Time (min)

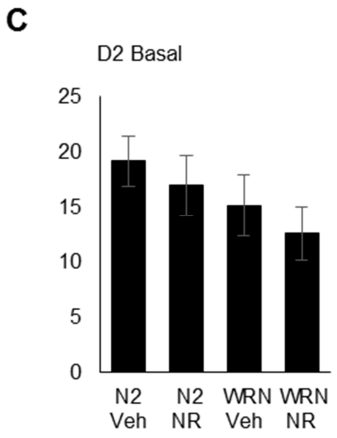
C
D2 Basal
0
5
10
15
20
25
N2 Veh
N2 NR
WRN Veh
WRN NR

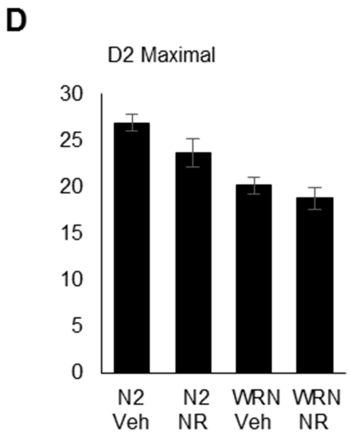
D
D2 Maximal
0
5
10
15
20
25
30
N2 Veh
N2 NR
WRN Veh
WRN NR

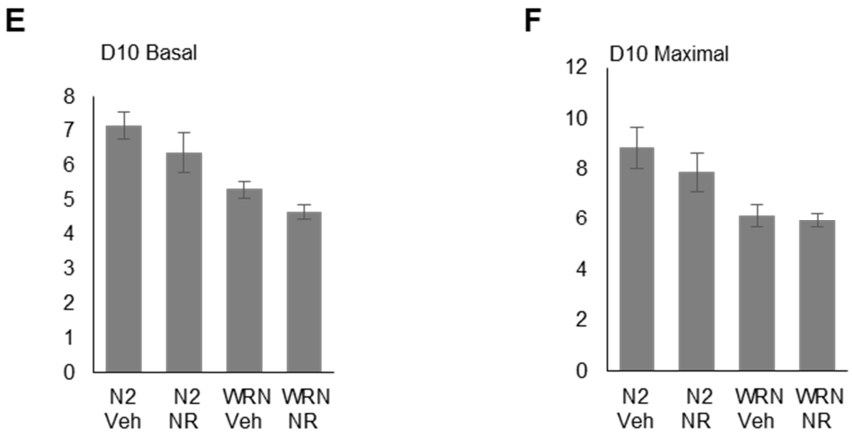

Fig. S7. Effect of NR treatment on the oxygen consumption rate in young and old *wrn-1* worms.

Wild type N2 and *wrn-1*(*gk99*) worms were exposed with/without NR (1 mM) from L4 stage until experiment. On adult day 2 or adult day 10, oxygen consumption rates were examined using the XFe96. Data are shown in mean ± S.E.M (n = 3 biological repeats).

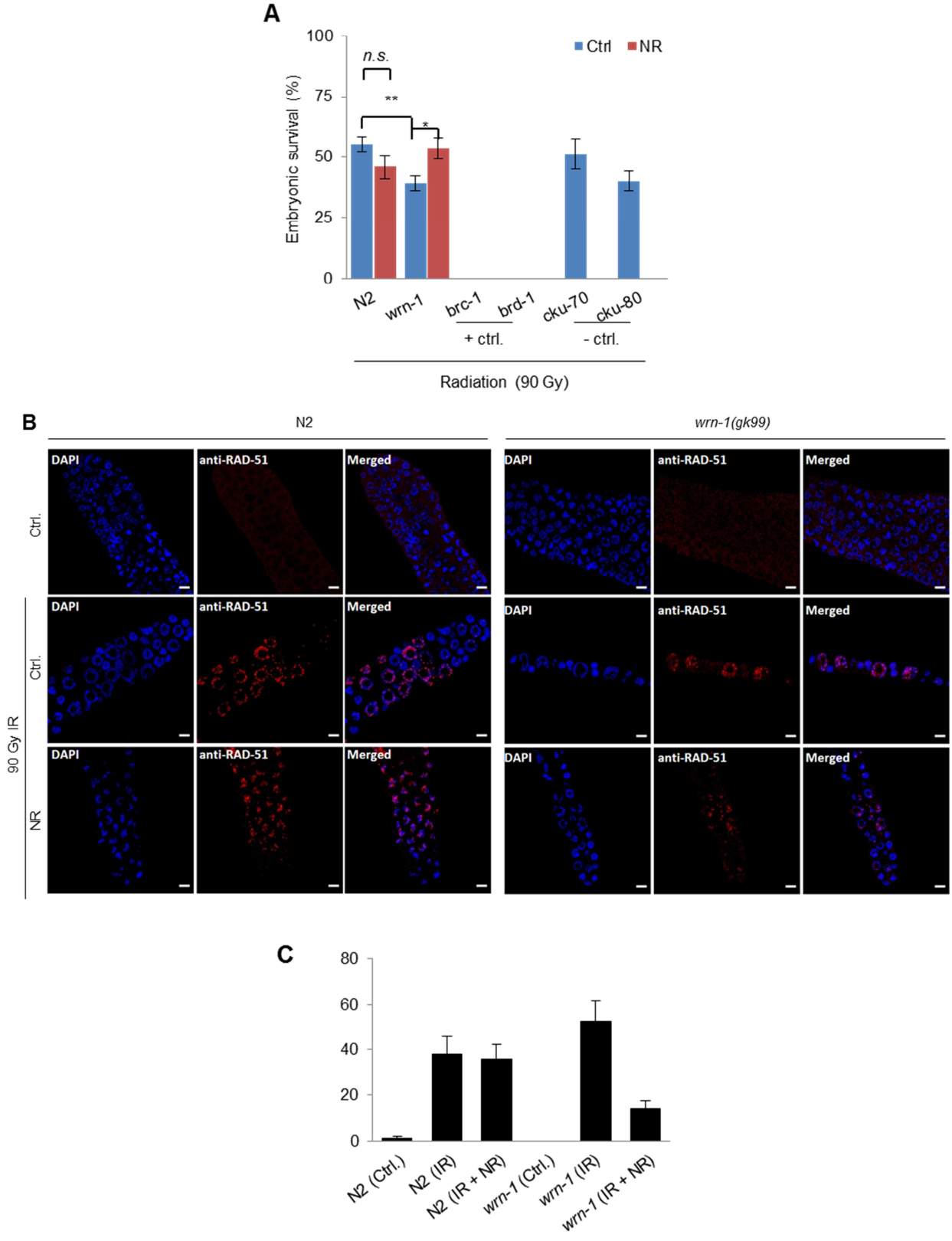

Fig. S8. Effects of PARP1, sirtuins on the healthspan of *wrn-1* worms.

(A) Embryonic homologous recombination (HR) capacity was measured by scoring the percent survival of early stage embryos after irradiation with 90 Gy. Two HR mutants, *brc-1(tm1145)* and *brd-1(dw1)*, were used as positive controls, while two NHEJ mutants, *cku-70(tm1524)* and *cku-80(ok861)*, were negative controls. The

results were from 4 biological replicates, including 400 – 900 worms for each condition. Data shown are mean ± SEM.

(B-C) Changes of RAD-51 signals in the mitotic region of designated groups of worms. Worms were exposed to 90 Gy ionizing radiation and germlines were isolated 24 hrs post-irradiation. Immunostaining of DAPI and RAD51 in the germlines were performed using standard protocols.

REFERENCES

1. Niccoli, T. and L. Partridge, *Ageing as a risk factor for disease.* Curr Biol, 2012. **22**(17): p. R741-52.
2. Klass, M.R., *A method for the isolation of longevity mutants in the nematode Caenorhabditis elegans and initial results.* Mech Ageing Dev, 1983. **22**(3-4): p. 279-86.
3. Lopez-Otin, C., et al., *The hallmarks of aging.* Cell, 2013. **153**(6): p. 1194-217.
4. Rubinsztein, D.C., G. Marino, and G. Kroemer, *Autophagy and aging.* Cell, 2011. **146**(5): p. 682-95.
5. Sun, N., R.J. Youle, and T. Finkel, *The Mitochondrial Basis of Aging.* Mol Cell, 2016. **61**(5): p. 654-666.
6. Fivenson, E.M., et al., *Mitophagy in neurodegeneration and aging.* Neurochemistry international, 2017. **109**: p. 202-209.
7. Fang, E.F., et al., *NAD+ in Aging: Molecular Mechanisms and Translational Implications.* Trends in Molecular Medicine, 2017. **23**(10): p. 899-916.
8. Aman, Y., et al., *Therapeutic potential of boosting NAD+ in aging and age-related diseases.* Translational Medicine of Aging, 2018. **2**: p. 30-37.
9. Moskalev, A.A., et al., *The role of DNA damage and repair in aging through the prism of Koch-like criteria.* Ageing Research Reviews, 2013. **12**(2): p. 661-684.
10. Hoeijmakers, J.H., *DNA damage, aging, and cancer.* N Engl J Med, 2009. **361**(15): p. 1475-85.
11. Jones, D.L. and T.A. Rando, *Emerging models and paradigms for stem cell ageing.* Nat Cell Biol, 2011. **13**(5): p. 506-12.
12. Rossi, D.J., et al., *Deficiencies in DNA damage repair limit the function of haematopoietic stem cells with age.* Nature, 2007. **447**(7145): p. 725-9.
13. Rube, C.E., et al., *Accumulation of DNA damage in hematopoietic stem and progenitor cells during human aging.* PLoS One, 2011. **6**(3): p. e17487.
14. Gregg, S.Q., et al., *A mouse model of accelerated liver aging caused by a defect in DNA repair.* Hepatology, 2012. **55**(2): p. 609-21.
15. Murga, M., et al., *A mouse model of ATR-Seckel shows embryonic replicative stress and accelerated aging.* Nat Genet, 2009. **41**(8): p. 891-8.
16. Wallace, D.C., *Mitochondrial DNA mutations in disease and aging.* Environ Mol Mutagen, 2010. **51**(5): p. 440-50.

17. Ameur, A., et al., *Ultra-deep sequencing of mouse mitochondrial DNA: mutational patterns and their origins.* PLoS Genet, 2011. **7**(3): p. e1002028.
18. Wallace, D.C., *A mitochondrial paradigm of metabolic and degenerative diseases, aging, and cancer: a dawn for evolutionary medicine.* Annu Rev Genet, 2005. **39**: p. 359-407.
19. Cabanillas, R., et al., *Nestor-Guillermo progeria syndrome: a novel premature aging condition with early onset and chronic development caused by BANF1 mutations.* Am J Med Genet A, 2011. **155a**(11): p. 2617-25.
20. De Sandre-Giovannoli, A., et al., *Lamin a truncation in Hutchinson-Gilford progeria.* Science, 2003. **300**(5628): p. 2055.
21. Eriksson, M., et al., *Recurrent de novo point mutations in lamin A cause Hutchinson-Gilford progeria syndrome.* Nature, 2003. **423**(6937): p. 293-8.
22. Armanios, M. and E.H. Blackburn, *The telomere syndromes.* Nat Rev Genet, 2012. **13**(10): p. 693-704.
23. Savage, S.A., et al., *TINF2, a component of the shelterin telomere protection complex, is mutated in dyskeratosis congenita.* Am J Hum Genet, 2008. **82**(2): p. 501-9.
24. Zhong, F., et al., *Disruption of telomerase trafficking by TCAB1 mutation causes dyskeratosis congenita.* Genes Dev, 2011. **25**(1): p. 11-6.
25. Walne, A.J., et al., *TINF2 mutations result in very short telomeres: analysis of a large cohort of patients with dyskeratosis congenita and related bone marrow failure syndromes.* Blood, 2008. **112**(9): p. 3594-600.
26. Martinez, P. and M.A. Blasco, *Role of shelterin in cancer and aging.* Aging Cell, 2010. **9**(5): p. 653-66.
27. Armanios, M., et al., *Short telomeres are sufficient to cause the degenerative defects associated with aging.* Am J Hum Genet, 2009. **85**(6): p. 823-32.
28. Herrera, E., et al., *Disease states associated with telomerase deficiency appear earlier in mice with short telomeres.* Embo j, 1999. **18**(11): p. 2950-60.
29. Blasco, M.A., et al., *Telomere shortening and tumor formation by mouse cells lacking telomerase RNA.* Cell, 1997. **91**(1): p. 25-34.
30. Tomas-Loba, A., et al., *Telomerase reverse transcriptase delays aging in cancer-resistant mice.* Cell, 2008. **135**(4): p. 609-22.
31. Jaskelioff, M., et al., *Telomerase reactivation reverses tissue degeneration in aged telomerase-deficient mice.* Nature, 2010. **469**: p. 102.
32. Talens, R.P., et al., *Epigenetic variation during the adult lifespan: cross-sectional and longitudinal data on monozygotic twin pairs.* Aging Cell, 2012. **11**(4): p. 694-703.

33. Fraga, M.F. and M. Esteller, *Epigenetics and aging: the targets and the marks.* Trends Genet, 2007. **23**(8): p. 413-8.
34. Han, S. and A. Brunet, *Histone methylation makes its mark on longevity.* Trends in cell biology, 2012. **22**(1): p. 42-49.
35. Greer, E.L., et al., *Members of the H3K4 trimethylation complex regulate lifespan in a germline-dependent manner in C. elegans.* Nature, 2010. **466**(7304): p. 383-7.
36. Siebold, A.P., et al., *Polycomb Repressive Complex 2 and Trithorax modulate Drosophila longevity and stress resistance.* Proc Natl Acad Sci U S A, 2010. **107**(1): p. 169-74.
37. Jin, C., et al., *Histone demethylase UTX-1 regulates C. elegans life span by targeting the insulin/IGF-1 signaling pathway.* Cell Metab, 2011. **14**(2): p. 161-72.
38. Herranz, D., et al., *Sirt1 improves healthy ageing and protects from metabolic syndrome-associated cancer.* Nat Commun, 2010. **1**: p. 3.
39. Brown, K., et al., *SIRT3 reverses aging-associated degeneration.* Cell Rep, 2013. **3**(2): p. 319-27.
40. Kanfi, Y., et al., *The sirtuin SIRT6 regulates lifespan in male mice.* Nature, 2012. **483**(7388): p. 218-21.
41. Mostoslavsky, R., et al., *Genomic instability and aging-like phenotype in the absence of mammalian SIRT6.* Cell, 2006. **124**(2): p. 315-29.
42. Tsurumi, A. and W.X. Li, *Global heterochromatin loss: a unifying theory of aging?* Epigenetics, 2012. **7**(7): p. 680-8.
43. Harries, L.W., et al., *Human aging is characterized by focused changes in gene expression and deregulation of alternative splicing.* Aging Cell, 2011. **10**(5): p. 868-78.
44. Powers, E.T., et al., *Biological and chemical approaches to diseases of proteostasis deficiency.* Annu Rev Biochem, 2009. **78**: p. 959-91.
45. Zhang, C. and A.M. Cuervo, *Restoration of chaperone-mediated autophagy in aging liver improves cellular maintenance and hepatic function.* Nat Med, 2008. **14**(9): p. 959-65.
46. Houtkooper, R.H., R.W. Williams, and J. Auwerx, *Metabolic networks of longevity.* Cell, 2010. **142**(1): p. 9-14.
47. Johnson, S.C., P.S. Rabinovitch, and M. Kaeberlein, *mTOR is a key modulator of ageing and age-related disease.* Nature, 2013. **493**(7432): p. 338-45.
48. Fontana, L., L. Partridge, and V.D. Longo, *Extending healthy life span--from yeast to humans.* Science, 2010. **328**(5976): p. 321-6.

49. Colman, R.J., et al., *Caloric restriction delays disease onset and mortality in rhesus monkeys.* Science, 2009. **325**(5937): p. 201-4.
50. Mattison, J.A., et al., *Impact of caloric restriction on health and survival in rhesus monkeys from the NIA study.* Nature, 2012. **489**(7415): p. 318-21.
51. Mair, W., et al., *Lifespan extension induced by AMPK and calcineurin is mediated by CRTC-1 and CREB.* Nature, 2011. **470**(7334): p. 404-8.
52. Rodgers, J.T., et al., *Nutrient control of glucose homeostasis through a complex of PGC-1alpha and SIRT1.* Nature, 2005. **434**(7029): p. 113-8.
53. Doonan, R., et al., *Against the oxidative damage theory of aging: superoxide dismutases protect against oxidative stress but have little or no effect on life span in Caenorhabditis elegans.* Genes Dev, 2008. **22**(23): p. 3236-41.
54. Mesquita, A., et al., *Caloric restriction or catalase inactivation extends yeast chronological lifespan by inducing H2O2 and superoxide dismutase activity.* Proc Natl Acad Sci U S A, 2010. **107**(34): p. 15123-8.
55. Van Raamsdonk, J.M. and S. Hekimi, *Deletion of the mitochondrial superoxide dismutase sod-2 extends lifespan in Caenorhabditis elegans.* PLoS Genet, 2009. **5**(2): p. e1000361.
56. Hekimi, S., J. Lapointe, and Y. Wen, *Taking a "good" look at free radicals in the aging process.* Trends Cell Biol, 2011. **21**(10): p. 569-76.
57. Sahin, E. and R.A. DePinho, *Axis of ageing: telomeres, p53 and mitochondria.* Nat Rev Mol Cell Biol, 2012. **13**(6): p. 397-404.
58. Bernardes de Jesus, B., et al., *Telomerase gene therapy in adult and old mice delays aging and increases longevity without increasing cancer.* EMBO Mol Med, 2012. **4**(8): p. 691-704.
59. Lee, I.H., et al., *A role for the NAD-dependent deacetylase Sirt1 in the regulation of autophagy.* Proc Natl Acad Sci U S A, 2008. **105**(9): p. 3374-9.
60. Giralt, A. and F. Villarroya, *SIRT3, a pivotal actor in mitochondrial functions: metabolism, cell death and aging.* Biochem J, 2012. **444**(1): p. 1-10.
61. Castello, L., et al., *Alternate-day fasting reverses the age-associated hypertrophy phenotype in rat heart by influencing the ERK and PI3K signaling pathways.* Mech Ageing Dev, 2011. **132**(6-7): p. 305-14.
62. Safdar, A., et al., *Endurance exercise rescues progeroid aging and induces systemic mitochondrial rejuvenation in mtDNA mutator mice.* Proc Natl Acad Sci U S A, 2011. **108**(10): p. 4135-40.

63. Kujoth, G.C., et al., *Mitochondrial DNA mutations, oxidative stress, and apoptosis in mammalian aging.* Science, 2005. **309**(5733): p. 481-4.
64. Hayflick, L., *The limited in vitro lifetime of human diploid cell strains.* Experimental Cell Research, 1965. **37**(3): p. 614-636.
65. Collado, M., M.A. Blasco, and M. Serrano, *Cellular senescence in cancer and aging.* Cell, 2007. **130**(2): p. 223-33.
66. Cao, L., et al., *Senescence, aging, and malignant transformation mediated by p53 in mice lacking the Brca1 full-length isoform.* Genes Dev, 2003. **17**(2): p. 201-13.
67. Matheu, A., et al., *Delayed ageing through damage protection by the Arf/p53 pathway.* Nature, 2007. **448**(7151): p. 375-9.
68. Oh, J., Y.D. Lee, and A.J. Wagers, *Stem cell aging: mechanisms, regulators and therapeutic opportunities.* Nature medicine, 2014. **20**(8): p. 870-880.
69. Rando, T.A. and H.Y. Chang, *Aging, rejuvenation, and epigenetic reprogramming: resetting the aging clock.* Cell, 2012. **148**(1-2): p. 46-57.
70. Abramovich, A., K.K. Muradian, and V.E. Fraifeld, *Have we reached the point for in vivo rejuvenation?* Rejuvenation Res, 2008. **11**(2): p. 489-92.
71. Takahashi, K. and S. Yamanaka, *Induced pluripotent stem cells in medicine and biology.* Development, 2013. **140**(12): p. 2457-61.
72. Wahlestedt, M., et al., *An epigenetic component of hematopoietic stem cell aging amenable to reprogramming into a young state.* Blood, 2013. **121**(21): p. 4257-64.
73. Conboy, I.M., et al., *Rejuvenation of aged progenitor cells by exposure to a young systemic environment.* Nature, 2005. **433**(7027): p. 760-4.
74. Castilho, R.M., et al., *mTOR mediates Wnt-induced epidermal stem cell exhaustion and aging.* Cell Stem Cell, 2009. **5**(3): p. 279-89.
75. Chen, C., et al., *mTOR regulation and therapeutic rejuvenation of aging hematopoietic stem cells.* Sci Signal, 2009. **2**(98): p. ra75.
76. Yilmaz, O.H., et al., *mTORC1 in the Paneth cell niche couples intestinal stem-cell function to calorie intake.* Nature, 2012. **486**(7404): p. 490-5.
77. Laplante, M. and D.M. Sabatini, *mTOR signaling in growth control and disease.* Cell, 2012. **149**(2): p. 274-93.
78. Russell, S.J. and C.R. Kahn, *Endocrine regulation of ageing.* Nat Rev Mol Cell Biol, 2007. **8**(9): p. 681-91.
79. Salminen, A., K. Kaarniranta, and A. Kauppinen, *Inflammaging: disturbed interplay between autophagy and inflammasomes.* Aging (Albany NY), 2012. **4**(3): p. 166-75.

80. Yao, H., et al., *SIRT1 protects against emphysema via FOXO3-mediated reduction of premature senescence in mice.* J Clin Invest, 2012. **122**(6): p. 2032-45.
81. Gillum, M.P., et al., *SirT1 regulates adipose tissue inflammation.* Diabetes, 2011. **60**(12): p. 3235-45.
82. Xie, J., X. Zhang, and L. Zhang, *Negative regulation of inflammation by SIRT1.* Pharmacol Res, 2013. **67**(1): p. 60-7.
83. Loffredo, F.S., et al., *Growth differentiation factor 11 is a circulating factor that reverses age-related cardiac hypertrophy.* Cell, 2013. **153**(4): p. 828-39.
84. Ottaviani, E., et al., *Gut microbiota as a candidate for lifespan extension: an ecological/evolutionary perspective targeted on living organisms as metaorganisms.* Biogerontology, 2011. **12**(6): p. 599-609.
85. Strong, R., et al., *Nordihydroguaiaretic acid and aspirin increase lifespan of genetically heterogeneous male mice.* Aging Cell, 2008. **7**(5): p. 641-50.
86. Rothwell, P.M., et al., *Effect of daily aspirin on long-term risk of death due to cancer: analysis of individual patient data from randomised trials.* Lancet, 2011. **377**(9759): p. 31-41.
87. Cuervo, A.M., *Autophagy: in sickness and in health.* Trends Cell Biol, 2004. **14**(2): p. 70-7.
88. Levine, B. and G. Kroemer, *Autophagy in the pathogenesis of disease.* Cell, 2008. **132**(1): p. 27-42.
89. Chu, C.T., *Eaten alive: autophagy and neuronal cell death after hypoxia-ischemia.* Am J Pathol, 2008. **172**(2): p. 284-7.
90. Gelino, S. and M. Hansen, *Autophagy - An Emerging Anti-Aging Mechanism.* J Clin Exp Pathol, 2012. **Suppl 4**.
91. Madeo, F., N. Tavernarakis, and G. Kroemer, *Can autophagy promote longevity?* Nat Cell Biol, 2010. **12**(9): p. 842-6.
92. Palikaras, K. and N. Tavernarakis, *Mitophagy in neurodegeneration and aging.* Front Genet, 2012. **3**: p. 297.
93. Ryan, B.J., et al., *Mitochondrial dysfunction and mitophagy in Parkinson's: from familial to sporadic disease.* Trends Biochem Sci, 2015. **40**(4): p. 200-10.
94. Khalil, B., et al., *PINK1-induced mitophagy promotes neuroprotection in Huntington's disease.* Cell Death Dis, 2015. **6**: p. e1617.
95. Ye, X., et al., *Parkin-mediated mitophagy in mutant hAPP neurons and Alzheimer's disease patient brains.* Hum Mol Genet, 2015. **24**(10): p. 2938-51.

96. Pickrell, A.M. and R.J. Youle, *The roles of PINK1, parkin, and mitochondrial fidelity in Parkinson's disease.* Neuron, 2015. **85**(2): p. 257-73.
97. Lazarou, M., et al., *The ubiquitin kinase PINK1 recruits autophagy receptors to induce mitophagy.* Nature, 2015. **524**(7565): p. 309-314.
98. Palikaras, K., E. Lionaki, and N. Tavernarakis, *Coordination of mitophagy and mitochondrial biogenesis during ageing in C. elegans.* Nature, 2015. **521**(7553): p. 525-8.
99. Schiavi, A., et al., *Iron-Starvation-Induced Mitophagy Mediates Lifespan Extension upon Mitochondrial Stress in C. elegans.* Curr Biol, 2015. **25**(14): p. 1810-22.
100. Sun, N., et al., *Measuring In Vivo Mitophagy.* Mol Cell, 2015. **60**(4): p. 685-96.
101. Egan, D.F., et al., *Phosphorylation of ULK1 (hATG1) by AMP-activated protein kinase connects energy sensing to mitophagy.* Science, 2011. **331**(6016): p. 456-61.
102. Canto, C., et al., *AMPK regulates energy expenditure by modulating NAD+ metabolism and SIRT1 activity.* Nature, 2009. **458**(7241): p. 1056-60.
103. Fang, Evandro F., et al., *Defective Mitophagy in XPA via PARP-1 Hyperactivation and NAD+/SIRT1 Reduction.* Cell, 2014. **157**(4): p. 882-896.
104. Fang, E.F., et al., *Nuclear DNA damage signalling to mitochondria in ageing.* Nat Rev Mol Cell Biol, 2016. **17**(5): p. 308-21.
105. Fang, E.F. and V.A. Bohr, *NAD(+): The convergence of DNA repair and mitophagy.* Autophagy, 2017. **13**(2): p. 442-443.
106. Fang, E.F., et al., *NAD(+) Replenishment Improves Lifespan and Healthspan in Ataxia Telangiectasia Models via Mitophagy and DNA Repair.* Cell Metab, 2016. **24**(4): p. 566-581.
107. Howitz, K.T., et al., *Small molecule activators of sirtuins extend Saccharomyces cerevisiae lifespan.* Nature, 2003. **425**(6954): p. 191-6.
108. Song, Y.M., et al., *Metformin alleviates hepatosteatosis by restoring SIRT1-mediated autophagy induction via an AMP-activated protein kinase-independent pathway.* Autophagy, 2015. **11**(1): p. 46-59.
109. Bonkowski, M.S. and D.A. Sinclair, *Slowing ageing by design: the rise of NAD(+) and sirtuin-activating compounds.* Nat Rev Mol Cell Biol, 2016. **17**(11): p. 679-690.
110. Ryu, D., et al., *Urolithin A induces mitophagy and prolongs lifespan in C. elegans and increases muscle function in rodents.* Nat Med, 2016. **22**(8): p. 879-88.
111. Zhang, H., et al., *NAD(+) repletion improves mitochondrial and stem cell function and enhances life span in mice.* Science, 2016. **352**(6292): p. 1436-43.

112. Magni, G., et al., *Enzymology of NAD+ homeostasis in man.* Cell Mol Life Sci, 2004. **61**(1): p. 19-34.
113. Canto, C., K.J. Menzies, and J. Auwerx, *NAD(+) Metabolism and the Control of Energy Homeostasis: A Balancing Act between Mitochondria and the Nucleus.* Cell Metab, 2015. **22**(1): p. 31-53.
114. *The alcoholic ferment of yeast-juice. Part II.—The coferment of yeast-juice.* Proceedings of the Royal Society of London. Series B, Containing Papers of a Biological Character, 1906. **78**(526): p. 369-375.
115. Belenky, P., et al., *Nicotinamide riboside promotes Sir2 silencing and extends lifespan via Nrk and Urh1/Pnp1/Meu1 pathways to NAD+.* Cell, 2007. **129**(3): p. 473-84.
116. Yang, H., et al., *Nutrient-sensitive mitochondrial NAD+ levels dictate cell survival.* Cell, 2007. **130**(6): p. 1095-107.
117. Cambronne, X.A., et al., *Biosensor reveals multiple sources for mitochondrial NAD(+).* Science, 2016. **352**(6292): p. 1474-7.
118. Verdin, E., *NAD(+) in aging, metabolism, and neurodegeneration.* Science, 2015. **350**(6265): p. 1208-13.
119. Bender, D.A., *Biochemistry of tryptophan in health and disease.* Mol Aspects Med, 1983. **6**(2): p. 101-97.
120. Houtkooper, R.H., et al., *The secret life of NAD+: an old metabolite controlling new metabolic signaling pathways.* Endocr Rev, 2010. **31**(2): p. 194-223.
121. Yamazaki, F., et al., *Human indolylamine 2,3-dioxygenase. Its tissue distribution, and characterization of the placental enzyme.* Biochem J, 1985. **230**(3): p. 635-8.
122. Kudo, Y. and C.A. Boyd, *Human placental indoleamine 2,3-dioxygenase: cellular localization and characterization of an enzyme preventing fetal rejection.* Biochim Biophys Acta, 2000. **1500**(1): p. 119-24.
123. Ikeda, M., et al., *STUDIES ON THE BIOSYNTHESIS OF NICOTINAMIDE ADENINE DINUCLEOTIDE. II. A ROLE OF PICOLINIC CARBOXYLASE IN THE BIOSYNTHESIS OF NICOTINAMIDE ADENINE DINUCLEOTIDE FROM TRYPTOPHAN IN MAMMALS.* J Biol Chem, 1965. **240**: p. 1395-401.
124. Lau, C., M. Niere, and M. Ziegler, *The NMN/NaMN adenylyltransferase (NMNAT) protein family.* Front Biosci (Landmark Ed), 2009. **14**: p. 410-31.
125. Emanuelli, M., et al., *Molecular cloning, chromosomal localization, tissue mRNA levels, bacterial expression, and enzymatic properties of human NMN adenylyltransferase.* J Biol Chem, 2001. **276**(1): p. 406-12.

126. Yalowitz, J.A., et al., *Characterization of human brain nicotinamide 5′-mononucleotide adenylyltransferase-2 and expression in human pancreas.* Biochem J, 2004. **377**(Pt 2): p. 317-26.

127. Berger, F., et al., *Subcellular compartmentation and differential catalytic properties of the three human nicotinamide mononucleotide adenylyltransferase isoforms.* J Biol Chem, 2005. **280**(43): p. 36334-41.

128. Zhang, X., et al., *Structural characterization of a human cytosolic NMN/NaMN adenylyltransferase and implication in human NAD biosynthesis.* J Biol Chem, 2003. **278**(15): p. 13503-11.

129. Hara, N., et al., *Molecular identification of human glutamine- and ammonia-dependent NAD synthetases. Carbon-nitrogen hydrolase domain confers glutamine dependency.* J Biol Chem, 2003. **278**(13): p. 10914-21.

130. Preiss, J. and P. Handler, *Biosynthesis of diphosphopyridine nucleotide. I. Identification of intermediates.* J Biol Chem, 1958. **233**(2): p. 488-92.

131. Nikiforov, A., et al., *Pathways and subcellular compartmentation of NAD biosynthesis in human cells: from entry of extracellular precursors to mitochondrial NAD generation.* J Biol Chem, 2011. **286**(24): p. 21767-78.

132. Bieganowski, P. and C. Brenner, *Discoveries of nicotinamide riboside as a nutrient and conserved NRK genes establish a Preiss-Handler independent route to NAD+ in fungi and humans.* Cell, 2004. **117**(4): p. 495-502.

133. Revollo, J.R., A.A. Grimm, and S. Imai, *The NAD biosynthesis pathway mediated by nicotinamide phosphoribosyltransferase regulates Sir2 activity in mammalian cells.* J Biol Chem, 2004. **279**(49): p. 50754-63.

134. Uddin, G.M., et al., *Head to Head Comparison of Short-Term Treatment with the NAD(+) Precursor Nicotinamide Mononucleotide (NMN) and 6 Weeks of Exercise in Obese Female Mice.* Front Pharmacol, 2016. **7**: p. 258.

135. Fukuwatari, T., et al., *Elevation of blood NAD level after moderate exercise in young women and mice.* J Nutr Sci Vitaminol (Tokyo), 2001. **47**(2): p. 177-9.

136. Mitchell, S.J., et al., *Effects of Sex, Strain, and Energy Intake on Hallmarks of Aging in Mice.* Cell Metab, 2016. **23**(6): p. 1093-1112.

137. Dali-Youcef, N., et al., *Sirtuins: the 'magnificent seven', function, metabolism and longevity.* Ann Med, 2007. **39**(5): p. 335-45.

138. Michishita, E., et al., *Evolutionarily conserved and nonconserved cellular localizations and functions of human SIRT proteins.* Mol Biol Cell, 2005. **16**(10): p. 4623-35.

139. Verdin, E., et al., *Sirtuin regulation of mitochondria: energy production, apoptosis, and signaling.* Trends Biochem Sci, 2010. **35**(12): p. 669-75.
140. Canto, C., et al., *Interdependence of AMPK and SIRT1 for metabolic adaptation to fasting and exercise in skeletal muscle.* Cell Metab, 2010. **11**(3): p. 213-9.
141. Chen, D., et al., *Tissue-specific regulation of SIRT1 by calorie restriction.* Genes & development, 2008. **22**(13): p. 1753-1757.
142. Kim, H.J., et al., *Metabolomic analysis of livers and serum from high-fat diet induced obese mice.* J Proteome Res, 2011. **10**(2): p. 722-31.
143. Kerr, J.S., et al., *Mitophagy and Alzheimer's Disease: Cellular and Molecular Mechanisms.* Trends Neurosci, 2017. **40**(3): p. 151-166.
144. Nakagawa, T. and L. Guarente, *Sirtuins at a glance.* J Cell Sci, 2011. **124**(Pt 6): p. 833-8.
145. Ramsey, K.M., et al., *Age-associated loss of Sirt1-mediated enhancement of glucose-stimulated insulin secretion in beta cell-specific Sirt1-overexpressing (BESTO) mice.* Aging Cell, 2008. **7**(1): p. 78-88.
146. Imai, S. and L. Guarente, *NAD+ and sirtuins in aging and disease.* Trends Cell Biol, 2014. **24**(8): p. 464-71.
147. Gibson, B.A. and W.L. Kraus, *New insights into the molecular and cellular functions of poly(ADP-ribose) and PARPs.* Nat Rev Mol Cell Biol, 2012. **13**(7): p. 411-24.
148. Canto, C., A.A. Sauve, and P. Bai, *Crosstalk between poly(ADP-ribose) polymerase and sirtuin enzymes.* Mol Aspects Med, 2013. **34**(6): p. 1168-201.
149. Kraus, W.L. and M.O. Hottiger, *PARP-1 and gene regulation: progress and puzzles.* Mol Aspects Med, 2013. **34**(6): p. 1109-23.
150. Rouleau, M., et al., *PARP inhibition: PARP1 and beyond.* Nat Rev Cancer, 2010. **10**(4): p. 293-301.
151. Aksoy, P., et al., *Regulation of intracellular levels of NAD: A novel role for CD38.* Biochemical and Biophysical Research Communications, 2006. **345**(4): p. 1386-1392.
152. Malavasi, F., et al., *Evolution and function of the ADP ribosyl cyclase/CD38 gene family in physiology and pathology.* Physiol Rev, 2008. **88**(3): p. 841-86.
153. Bonkowski, M.S. and D.A. Sinclair, *Slowing ageing by design: the rise of NAD+ and sirtuin-activating compounds.* Nature Reviews Molecular Cell Biology, 2016. **17**: p. 679.
154. Yaku, K., K. Okabe, and T. Nakagawa, *NAD metabolism: Implications in aging and longevity.* Ageing Research Reviews, 2018. **47**: p. 1-17.

155. Clement, J., et al., *The Plasma NAD(+) Metabolome Is Dysregulated in "Normal" Aging.* Rejuvenation Res, 2018.
156. Balan, V., et al., *Life span extension and neuronal cell protection by Drosophila nicotinamidase.* J Biol Chem, 2008. **283**(41): p. 27810-9.
157. Riklis, E., et al., *Increased radioprotection attained by DNA repair enhancement.* Pharmacology & Therapeutics, 1988. **39**(1): p. 311-322.
158. Watson, A., et al., *Nicotinamide Phosphoribosyltransferase in Smooth Muscle Cells Maintains Genome Integrity, Resists Aortic Medial Degeneration, and Is Suppressed in Human Thoracic Aortic Aneurysm Disease.* Circ Res, 2017. **120**(12): p. 1889-1902.
159. Weidele, K., S. Beneke, and A. Bürkle, *The NAD+ precursor nicotinic acid improves genomic integrity in human peripheral blood mononuclear cells after X-irradiation.* DNA Repair, 2017. **52**: p. 12-23.
160. Ryu, D., et al., *NAD⁺ repletion improves muscle function in muscular dystrophy and counters global PARylation.* Science Translational Medicine, 2016. **8**(361): p. 361ra139-361ra139.
161. Scheibye-Knudsen, M., et al., *A High-Fat Diet and NAD+ Activate Sirt1 to Rescue Premature Aging in Cockayne Syndrome.* Cell Metabolism, 2014. **20**(5): p. 840-855.
162. North, B.J., et al., *SIRT2 induces the checkpoint kinase BubR1 to increase lifespan.* Embo j, 2014. **33**(13): p. 1438-53.
163. Katsyuba, E., et al., *De novo NAD(+) synthesis enhances mitochondrial function and improves health.* Nature, 2018. **563**(7731): p. 354-359.
164. Gong, B., et al., *Nicotinamide riboside restores cognition through an upregulation of proliferator-activated receptor-γ coactivator 1α regulated β-secretase 1 degradation and mitochondrial gene expression in Alzheimer's mouse models.* Neurobiology of Aging, 2013. **34**(6): p. 1581-1588.
165. Schöndorf, D.C., et al., *The NAD+ Precursor Nicotinamide Riboside Rescues Mitochondrial Defects and Neuronal Loss in iPSC and Fly Models of Parkinson's Disease.* Cell Reports, 2018. **23**(10): p. 2976-2988.
166. Sorrentino, V., et al., *Enhancing mitochondrial proteostasis reduces amyloid-β proteotoxicity.* Nature, 2017. **552**: p. 187.
167. Long, A.N., et al., *Effect of nicotinamide mononucleotide on brain mitochondrial respiratory deficits in an Alzheimer's disease-relevant murine model.* BMC Neurol, 2015. **15**: p. 19.

168. Wang, X., et al., *Nicotinamide mononucleotide protects against beta-amyloid oligomer-induced cognitive impairment and neuronal death.* Brain Res, 2016. **1643**: p. 1-9.

169. Liu, D., et al., *Nicotinamide forestalls pathology and cognitive decline in Alzheimer mice: evidence for improved neuronal bioenergetics and autophagy procession.* Neurobiol Aging, 2013. **34**(6): p. 1564-80.

170. Fang, E.F., et al., *Mitophagy inhibits amyloid-β and tau pathology and reverses cognitive deficits in models of Alzheimer's disease.* Nature Neuroscience, In press.

171. Mouchiroud, L., et al., *The NAD+/Sirtuin Pathway Modulates Longevity through Activation of Mitochondrial UPR and FOXO Signaling.* Cell, 2013. **154**(2): p. 430-441.

172. Misiak, M., et al., *DNA polymerase β decrement triggers death of olfactory bulb cells and impairs olfaction in a mouse model of Alzheimer's disease.* Aging Cell, 2017. **16**(1): p. 162-172.

173. Hou, Y., et al., *NAD(+) supplementation normalizes key Alzheimer's features and DNA damage responses in a new AD mouse model with introduced DNA repair deficiency.* Proc Natl Acad Sci U S A, 2018. **115**(8): p. E1876-e1885.

174. Cantó, C., et al., *The NAD+ Precursor Nicotinamide Riboside Enhances Oxidative Metabolism and Protects against High-Fat Diet-Induced Obesity.* Cell Metabolism, 2012. **15**(6): p. 838-847.

175. Trammell, S.A.J., et al., *Nicotinamide Riboside Opposes Type 2 Diabetes and Neuropathy in Mice.* Scientific Reports, 2016. **6**: p. 26933.

176. Gariani, K., et al., *Eliciting the mitochondrial unfolded protein response by nicotinamide adenine dinucleotide repletion reverses fatty liver disease in mice.* Hepatology, 2016. **63**(4): p. 1190-1204.

177. Ramsey, K.M., et al., *Age-associated loss of Sirt1-mediated enhancement of glucose-stimulated insulin secretion in beta cell-specific Sirt1-overexpressing (BESTO) mice.* Aging Cell, 2008. **7**(1): p. 78-88.

178. Yoshino, J., et al., *Nicotinamide Mononucleotide, a Key NAD+ Intermediate, Treats the Pathophysiology of Diet- and Age-Induced Diabetes in Mice.* Cell Metabolism, 2011. **14**(4): p. 528-536.

179. Gilley, J. and M.P. Coleman, *Endogenous Nmnat2 is an essential survival factor for maintenance of healthy axons.* PLoS Biol, 2010. **8**(1): p. e1000300.

180. Zhang, H., et al., *NAD⁺ repletion improves mitochondrial and stem cell function and enhances life span in mice.* Science, 2016. **352**(6292): p. 1436-1443.

181. Wiley, C. and J. Campisi, *NAD+ controls neural stem cell fate in the aging brain.* Embo j, 2014. **33**(12): p. 1289-91.

182. Stein, L.R. and S. Imai, *Specific ablation of Nampt in adult neural stem cells recapitulates their functional defects during aging.* Embo j, 2014. **33**(12): p. 1321-40.

183. Oshima, J., G.M. Martin, and F.M. Hisama, *Werner Syndrome*, in *GeneReviews((R))*, M.P. Adam, et al., Editors. 1993, University of Washington, Seattle

University of Washington, Seattle. GeneReviews is a registered trademark of the University of Washington, Seattle. All rights reserved.: Seattle (WA).

184. Werner, O., *On Cataract in Conjunction with Scleroderma*, in *Werner's Syndrome and Human Aging*, D. Salk, Y. Fujiwara, and G.M. Martin, Editors. 1985, Springer US: Boston, MA. p. 1-14.

185. Oshima, J., J.M. Sidorova, and R.J. Monnat, Jr., *Werner syndrome: Clinical features, pathogenesis and potential therapeutic interventions.* Ageing Res Rev, 2017. **33**: p. 105-114.

186. Hisama, F.M., V.A. Bohr, and J. Oshima, *WRN's tenth anniversary.* Sci Aging Knowledge Environ, 2006. **2006**(10): p. pe18.

187. Takemoto, M., et al., *Diagnostic criteria for Werner syndrome based on Japanese nationwide epidemiological survey.* Geriatr Gerontol Int, 2013. **13**(2): p. 475-81.

188. Huang, S., et al., *The spectrum of WRN mutations in Werner syndrome patients.* Hum Mutat, 2006. **27**(6): p. 558-67.

189. Goto, M., *Hierarchical deterioration of body systems in Werner's syndrome: implications for normal ageing.* Mech Ageing Dev, 1997. **98**(3): p. 239-54.

190. Epstein, C.J., et al., *Werner's syndrome a review of its symptomatology, natural history, pathologic features, genetics and relationship to the natural aging process.* Medicine (Baltimore), 1966. **45**(3): p. 177-221.

191. Lauper, J.M., et al., *Spectrum and risk of neoplasia in Werner syndrome: a systematic review.* PLoS One, 2013. **8**(4): p. e59709.

192. Martin, G.M., et al., *What Geriatricians Should Know About the Werner Syndrome.* Journal of the American Geriatrics Society, 1999. **47**(9): p. 1136-1144.

193. Hanada, K. and I.D. Hickson, *Molecular genetics of RecQ helicase disorders.* Cell Mol Life Sci, 2007. **64**(17): p. 2306-22.

194. Satoh, M., et al., *Prevalence of Werner's syndrome heterozygotes in Japan.* Lancet, 1999. **353**(9166): p. 1766.

195. Masala, M.V., et al., *Epidemiology and clinical aspects of Werner's syndrome in North Sardinia: description of a cluster.* Eur J Dermatol, 2007. **17**(3): p. 213-6.

196. Yu, C.E., et al., *Positional cloning of the Werner's syndrome gene.* Science, 1996. **272**(5259): p. 258-62.
197. Bohr, V.A., *Rising from the RecQ-age: the role of human RecQ helicases in genome maintenance.* Trends Biochem Sci, 2008. **33**(12): p. 609-20.
198. Larsen, N.B. and I.D. Hickson, *RecQ Helicases: Conserved Guardians of Genomic Integrity.* Adv Exp Med Biol, 2013. **767**: p. 161-84.
199. Croteau, D.L., et al., *Human RecQ helicases in DNA repair, recombination, and replication.* Annu Rev Biochem, 2014. **83**: p. 519-52.
200. Gorbalenya, A.E. and E.V. Koonin, *Helicases: amino acid sequence comparisons and structure-function relationships.* Current Opinion in Structural Biology, 1993. **3**(3): p. 419-429.
201. Huang, S., et al., *The premature ageing syndrome protein, WRN, is a 3'-->5' exonuclease.* Nat Genet, 1998. **20**(2): p. 114-6.
202. Gray, M.D., et al., *The Werner syndrome protein is a DNA helicase.* Nat Genet, 1997. **17**(1): p. 100-3.
203. Matsumoto, T., et al., *Impaired nuclear localization of defective DNA helicases in Werner's syndrome.* Nat Genet, 1997. **16**(4): p. 335-6.
204. Suzuki, T., et al., *Diverged nuclear localization of Werner helicase in human and mouse cells.* Oncogene, 2001. **20**(20): p. 2551-8.
205. Kitano, K., S.Y. Kim, and T. Hakoshima, *Structural basis for DNA strand separation by the unconventional winged-helix domain of RecQ helicase WRN.* Structure, 2010. **18**(2): p. 177-87.
206. Tadokoro, T., et al., *DNA binding residues in the RQC domain of Werner protein are critical for its catalytic activities.* Aging (Albany NY), 2012. **4**(6): p. 417-29.
207. von Kobbe, C., et al., *Werner syndrome protein contains three structure-specific DNA binding domains.* J Biol Chem, 2003. **278**(52): p. 52997-3006.
208. Kitano, K., N. Yoshihara, and T. Hakoshima, *Crystal structure of the HRDC domain of human Werner syndrome protein, WRN.* J Biol Chem, 2007. **282**(4): p. 2717-28.
209. Lan, L., et al., *Accumulation of Werner protein at DNA double-strand breaks in human cells.* J Cell Sci, 2005. **118**(Pt 18): p. 4153-62.
210. Muftuoglu, M., et al., *Intrinsic ssDNA annealing activity in the C-terminal region of WRN.* Biochemistry, 2008. **47**(39): p. 10247-54.
211. Friedrich, K., et al., *WRN mutations in Werner syndrome patients: genomic rearrangements, unusual intronic mutations and ethnic-specific alterations.* Hum Genet, 2010. **128**(1): p. 103-11.

212. Uhrhammer, N.A., et al., *Werner syndrome and mutations of the WRN and LMNA genes in France.* Hum Mutat, 2006. **27**(7): p. 718-9.
213. Oshima, J. and F.M. Hisama, *Search and insights into novel genetic alterations leading to classical and atypical Werner syndrome.* Gerontology, 2014. **60**(3): p. 239-46.
214. Chen, L., et al., *LMNA mutations in atypical Werner's syndrome.* Lancet, 2003. **362**(9382): p. 440-5.
215. Lebel, M. and R.J. Monnat, Jr., *Werner syndrome (WRN) gene variants and their association with altered function and age-associated diseases.* Ageing Res Rev, 2018. **41**: p. 82-97.
216. Castro, E., et al., *Polymorphisms at the Werner locus: II. 1074Leu/Phe, 1367Cys/Arg, longevity, and atherosclerosis.* Am J Med Genet, 2000. **95**(4): p. 374-80.
217. Kulminski, A.M. and I. Culminskaya, *Genomics of human health and aging.* Age (Dordr), 2013. **35**(2): p. 455-69.
218. Ye, L., et al., *Association of a polymorphic variant of the Werner helicase gene with myocardial infarction in a Japanese population.* American Journal of Medical Genetics, 1997. **68**(4): p. 494-498.
219. Sebastiani, P., et al., *Meta-analysis of genetic variants associated with human exceptional longevity.* Aging, 2013. **5**(9): p. 653-661.
220. Sebastiani, P., et al., *Genetic signatures of exceptional longevity in humans.* Science, 2010. **2010**.
221. Berube, J., et al., *The non-synonymous polymorphism at position 114 of the WRN protein affects cholesterol efflux in vitro and correlates with cholesterol levels in vivo.* Exp Gerontol, 2013. **48**(6): p. 533-8.
222. Hirai, M., et al., *WRN gene 1367 Arg allele protects against development of type 2 diabetes mellitus.* Diabetes Research and Clinical Practice, 2005. **69**(3): p. 287-292.
223. Gagne, J.P., et al., *Different non-synonymous polymorphisms modulate the interaction of the WRN protein to its protein partners and its enzymatic activities.* Oncotarget, 2016. **7**(52): p. 85680-85696.
224. Nakayama, R., et al., *Association of a missense single nucleotide polymorphism, Cys1367Arg of the WRN gene, with the risk of bone and soft tissue sarcomas in Japan.* Cancer Sci, 2008. **99**(2): p. 333-9.
225. Shen, M., et al., *Polymorphisms in DNA repair genes and risk of non-Hodgkin lymphoma among women in Connecticut.* Hum Genet, 2006. **119**(6): p. 659-68.

226. Chen, D.T., et al., *Genome-wide association study meta-analysis of European and Asian-ancestry samples identifies three novel loci associated with bipolar disorder.* Mol Psychiatry, 2013. **18**(2): p. 195-205.

227. Mead, S., et al., *Genome-wide association study in multiple human prion diseases suggests genetic risk factors additional to PRNP.* Hum Mol Genet, 2012. **21**(8): p. 1897-906.

228. Sild, M., et al., *Possible associations between successful aging and polymorphic markers in the Werner gene region.* Ann N Y Acad Sci, 2006. **1067**: p. 309-10.

229. Brosh, R.M., Jr. and V.A. Bohr, *Roles of the Werner syndrome protein in pathways required for maintenance of genome stability.* Exp Gerontol, 2002. **37**(4): p. 491-506.

230. Crabbe, L., et al., *Defective telomere lagging strand synthesis in cells lacking WRN helicase activity.* Science, 2004. **306**(5703): p. 1951-3.

231. Kamath-Loeb, A., L.A. Loeb, and M. Fry, *The Werner syndrome protein is distinguished from the Bloom syndrome protein by its capacity to tightly bind diverse DNA structures.* PLoS One, 2012. **7**(1): p. e30189.

232. Brosh, R.M., Jr., P.L. Opresko, and V.A. Bohr, *Enzymatic mechanism of the WRN helicase/nuclease.* Methods Enzymol, 2006. **409**: p. 52-85.

233. Shen, J.C. and L.A. Loeb, *Werner syndrome exonuclease catalyzes structure-dependent degradation of DNA.* Nucleic Acids Res, 2000. **28**(17): p. 3260-8.

234. Lebel, M., et al., *The Werner syndrome gene product co-purifies with the DNA replication complex and interacts with PCNA and topoisomerase I.* J Biol Chem, 1999. **274**(53): p. 37795-9.

235. Ahn, B., et al., *Regulation of WRN helicase activity in human base excision repair.* J Biol Chem, 2004. **279**(51): p. 53465-74.

236. Kusumoto, R., M. Muftuoglu, and V.A. Bohr, *The role of WRN in DNA repair is affected by post-translational modifications.* Mech Ageing Dev, 2007. **128**(1): p. 50-7.

237. Bohr, V.A., et al., *Pathways defective in the human premature aging disease Werner syndrome.* Biogerontology, 2002. **3**(1-2): p. 89-94.

238. Shamanna, R.A., et al., *Recent Advances in Understanding Werner Syndrome.* F1000Research, 2017. **6**: p. 1779-1779.

239. Maierhofer, A., et al., *Accelerated epigenetic aging in Werner syndrome.* Aging (Albany NY), 2017. **9**(4): p. 1143-1152.

240. Opresko, P.L., et al., *The Werner syndrome helicase and exonuclease cooperate to resolve telomeric D loops in a manner regulated by TRF1 and TRF2.* Mol Cell, 2004. **14**(6): p. 763-74.

241. Crabbe, L., et al., *Telomere dysfunction as a cause of genomic instability in Werner syndrome.* Proc Natl Acad Sci U S A, 2007. **104**(7): p. 2205-10.
242. Wyllie, F.S., et al., *Telomerase prevents the accelerated cell ageing of Werner syndrome fibroblasts.* Nat Genet, 2000. **24**(1): p. 16-7.
243. Cheng, W.H., et al., *Collaboration of Werner syndrome protein and BRCA1 in cellular responses to DNA interstrand cross-links.* Nucleic Acids Res, 2006. **34**(9): p. 2751-60.
244. Yasuda, H., et al., *Biguanide, but not thiazolidinedione, improved insulin resistance in Werner syndrome.* J Am Geriatr Soc, 2010. **58**(1): p. 181-2.
245. Yokote, K., et al., *Dysadipocytokinemia in werner syndrome and its recovery by treatment with pioglitazone.* Diabetes Care, 2004. **27**(10): p. 2562-3.
246. Yokote, K. and Y. Saito, *Extension of the life span in patients with Werner syndrome.* J Am Geriatr Soc, 2008. **56**(9): p. 1770-1.
247. Talaei, F., V.M. van Praag, and R.H. Henning, *Hydrogen sulfide restores a normal morphological phenotype in Werner syndrome fibroblasts, attenuates oxidative damage and modulates mTOR pathway.* Pharmacol Res, 2013. **74**: p. 34-44.
248. Zhu, X., et al., *Epigenetic Regulation of Werner Syndrome Gene in Age-Related Cataract.* J Ophthalmol, 2015. **2015**: p. 579695.
249. Goto, M., et al., *Multiplex cytokine analysis of Werner syndrome.* Intractable & Rare Diseases Research, 2015. **4**(4): p. 190-197.
250. Grandori, C., et al., *Werner syndrome protein limits MYC-induced cellular senescence.* Genes Dev, 2003. **17**(13): p. 1569-74.
251. Lu, H., et al., *Senescence induced by RECQL4 dysfunction contributes to Rothmund-Thomson syndrome features in mice.* Cell Death Dis, 2014. **5**: p. e1226.
252. Zhang, W., et al., *Aging stem cells. A Werner syndrome stem cell model unveils heterochromatin alterations as a driver of human aging.* Science (New York, N.Y.), 2015. **348**(6239): p. 1160-1163.
253. Lautrup, S., et al., *Studying Werner syndrome to elucidate mechanisms and therapeutics of human aging and age-related diseases*. 2019.
254. Oshima, J., et al., *Regulation of c-fos expression in senescing Werner syndrome fibroblasts differs from that observed in senescing fibroblasts from normal donors.* J Cell Physiol, 1995. **162**(2): p. 277-83.
255. Salk, D., et al., *Cytogenetic aspects of Werner syndrome.* Adv Exp Med Biol, 1985. **190**: p. 541-6.

256. Salk, D., et al., *Growth characteristics of Werner syndrome cells in vitro.* Adv Exp Med Biol, 1985. **190**: p. 305-11.
257. Melcher, R., et al., *Spectral karyotyping of Werner syndrome fibroblast cultures.* Cytogenet Cell Genet, 2000. **91**(1-4): p. 180-5.
258. Chang, H.H.Y., et al., *Non-homologous DNA end joining and alternative pathways to double-strand break repair.* Nat Rev Mol Cell Biol, 2017. **18**(8): p. 495-506.
259. Shamanna, R.A., et al., *WRN regulates pathway choice between classical and alternative non-homologous end joining.* Nat Commun, 2016. **7**: p. 13785.
260. Blander, G., et al., *DNA damage-induced translocation of the Werner helicase is regulated by acetylation.* J Biol Chem, 2002. **277**(52): p. 50934-40.
261. Li, K., et al., *Regulation of WRN protein cellular localization and enzymatic activities by SIRT1-mediated deacetylation.* J Biol Chem, 2008. **283**(12): p. 7590-8.
262. Kusumoto-Matsuo, R., et al., *Serines 440 and 467 in the Werner syndrome protein are phosphorylated by DNA-PK and affects its dynamics in response to DNA double strand breaks.* Aging (Albany NY), 2014. **6**(1): p. 70-81.
263. Kusumoto, R., et al., *Werner protein cooperates with the XRCC4-DNA ligase IV complex in end-processing.* Biochemistry, 2008. **47**(28): p. 7548-56.
264. Cooper, M.P., et al., *Ku complex interacts with and stimulates the Werner protein.* Genes Dev, 2000. **14**(8): p. 907-12.
265. Li, B. and L. Comai, *Requirements for the nucleolytic processing of DNA ends by the Werner syndrome protein-Ku70/80 complex.* J Biol Chem, 2001. **276**(13): p. 9896-902.
266. Wang, H., et al., *Biochemical evidence for Ku-independent backup pathways of NHEJ.* Nucleic Acids Res, 2003. **31**(18): p. 5377-88.
267. Bennardo, N., et al., *Alternative-NHEJ is a mechanistically distinct pathway of mammalian chromosome break repair.* PLoS Genet, 2008. **4**(6): p. e1000110.
268. Lachapelle, S., et al., *Proteome-wide identification of WRN-interacting proteins in untreated and nuclease-treated samples.* J Proteome Res, 2011. **10**(3): p. 1216-27.
269. Cheng, W.H., et al., *Linkage between Werner syndrome protein and the Mre11 complex via Nbs1.* J Biol Chem, 2004. **279**(20): p. 21169-76.
270. Karmakar, P., et al., *Werner protein is a target of DNA-dependent protein kinase in vivo and in vitro, and its catalytic activities are regulated by phosphorylation.* J Biol Chem, 2002. **277**(21): p. 18291-302.

271. Sallmyr, A., A.E. Tomkinson, and F.V. Rassool, *Up-regulation of WRN and DNA ligase IIIalpha in chronic myeloid leukemia: consequences for the repair of DNA double-strand breaks.* Blood, 2008. **112**(4): p. 1413-23.
272. Li, B. and L. Comai, *Functional interaction between Ku and the werner syndrome protein in DNA end processing.* J Biol Chem, 2000. **275**(37): p. 28349-52.
273. Grundy, G.J., et al., *The Ku-binding motif is a conserved module for recruitment and stimulation of non-homologous end-joining proteins.* 2016. **7**: p. 11242.
274. Keijzers, G., et al., *The role of RecQ helicases in non-homologous end-joining.* Crit Rev Biochem Mol Biol, 2014. **49**(6): p. 463-72.
275. Sturzenegger, A., et al., *DNA2 cooperates with the WRN and BLM RecQ helicases to mediate long-range DNA end resection in human cells.* J Biol Chem, 2014. **289**(39): p. 27314-26.
276. Cejka, P., *DNA End Resection: Nucleases Team Up with the Right Partners to Initiate Homologous Recombination.* J Biol Chem, 2015. **290**(38): p. 22931-8.
277. Iannascoli, C., et al., *The WRN exonuclease domain protects nascent strands from pathological MRE11/EXO1-dependent degradation.* Nucleic Acids Res, 2015. **43**(20): p. 9788-803.
278. Shamanna, R.A., et al., *Camptothecin targets WRN protein: mechanism and relevance in clinical breast cancer.* Oncotarget, 2016. **7**(12): p. 13269-84.
279. Pinto, C., et al., *Human DNA2 possesses a cryptic DNA unwinding activity that functionally integrates with BLM or WRN helicases.* 2016. **5**.
280. Sidorova, J.M., et al., *Distinct functions of human RECQ helicases WRN and BLM in replication fork recovery and progression after hydroxyurea-induced stalling.* DNA Repair (Amst), 2013. **12**(2): p. 128-39.
281. Sidorova, J.M., et al., *The RecQ helicase WRN is required for normal replication fork progression after DNA damage or replication fork arrest.* Cell Cycle, 2008. **7**(6): p. 796-807.
282. Kamath-Loeb, A.S., et al., *Werner syndrome protein interacts functionally with translesion DNA polymerases.* Proc Natl Acad Sci U S A, 2007. **104**(25): p. 10394-9.
283. Rodriguez-Lopez, A.M., et al., *Asymmetry of DNA replication fork progression in Werner's syndrome.* Aging Cell, 2002. **1**(1): p. 30-9.
284. Murfuni, I., et al., *Perturbed replication induced genome wide or at common fragile sites is differently managed in the absence of WRN.* Carcinogenesis, 2012. **33**(9): p. 1655-63.

285. Pirzio, L.M., et al., *Werner syndrome helicase activity is essential in maintaining fragile site stability.* J Cell Biol, 2008. **180**(2): p. 305-14.

286. Trego, K.S., et al., *The DNA repair endonuclease XPG interacts directly and functionally with the WRN helicase defective in Werner syndrome.* Cell Cycle, 2011. **10**(12): p. 1998-2007.

287. O'Sullivan, R.J. and J. Karlseder, *Telomeres: protecting chromosomes against genome instability.* Nat Rev Mol Cell Biol, 2010. **11**(3): p. 171-81.

288. Palm, W. and T. de Lange, *How shelterin protects mammalian telomeres.* Annu Rev Genet, 2008. **42**: p. 301-34.

289. Edwards, D.N., D.K. Orren, and A. Machwe, *Strand exchange of telomeric DNA catalyzed by the Werner syndrome protein (WRN) is specifically stimulated by TRF2.* Nucleic Acids Res, 2014. **42**(12): p. 7748-61.

290. Opresko, P.L., *Telomere ResQue and preservation--roles for the Werner syndrome protein and other RecQ helicases.* Mech Ageing Dev, 2008. **129**(1-2): p. 79-90.

291. Machwe, A., L. Xiao, and D.K. Orren, *TRF2 recruits the Werner syndrome (WRN) exonuclease for processing of telomeric DNA.* Oncogene, 2004. **23**(1): p. 149-56.

292. Rossi, M.L., A.K. Ghosh, and V.A. Bohr, *Roles of Werner syndrome protein in protection of genome integrity.* DNA Repair (Amst), 2010. **9**(3): p. 331-44.

293. Ibrahim, B., et al., *Absence of premature senescence in Werner's syndrome keratinocytes.* Exp Gerontol, 2016. **83**: p. 139-47.

294. Laud, P.R., et al., *Elevated telomere-telomere recombination in WRN-deficient, telomere dysfunctional cells promotes escape from senescence and engagement of the ALT pathway.* Genes Dev, 2005. **19**(21): p. 2560-70.

295. Londono-Vallejo, J.A., et al., *Alternative lengthening of telomeres is characterized by high rates of telomeric exchange.* Cancer Res, 2004. **64**(7): p. 2324-7.

296. Benayoun, B.A., E.A. Pollina, and A. Brunet, *Epigenetic regulation of ageing: linking environmental inputs to genomic stability.* Nat Rev Mol Cell Biol, 2015. **16**(10): p. 593-610.

297. Peters, A.H., et al., *Loss of the Suv39h histone methyltransferases impairs mammalian heterochromatin and genome stability.* Cell, 2001. **107**(3): p. 323-37.

298. Jiao, R., et al., *The Werner syndrome protein is required for recruitment of chromatin assembly factor 1 following DNA damage.* Oncogene, 2007. **26**(26): p. 3811-22.

299. Smith, S. and B. Stillman, *Purification and characterization of CAF-I, a human cell factor required for chromatin assembly during DNA replication in vitro.* Cell, 1989. **58**(1): p. 15-25.

300. Li, Y., et al., *Vitamin C alleviates aging defects in a stem cell model for Werner syndrome.* Protein & cell, 2016. **7**(7): p. 478-488.
301. Norwood, T.H., et al., *Cellular aging in Werner's syndrome: a unique phenotype?* J Invest Dermatol, 1979. **73**(1): p. 92-6.
302. Goto, M., et al., *Werner syndrome: a changing pattern of clinical manifestations in Japan (1917~2008).* Biosci Trends, 2013. **7**(1): p. 13-22.
303. Rodier, F. and J. Campisi, *Four faces of cellular senescence.* J Cell Biol, 2011. **192**(4): p. 547-56.
304. Rodier, F., et al., *DNA-SCARS: distinct nuclear structures that sustain damage-induced senescence growth arrest and inflammatory cytokine secretion.* J Cell Sci, 2011. **124**(Pt 1): p. 68-81.
305. Yamauchi, T., et al., *The fat-derived hormone adiponectin reverses insulin resistance associated with both lipoatrophy and obesity.* Nat Med, 2001. **7**(8): p. 941-6.
306. Mori, S., et al., *Enhanced intra-abdominal visceral fat accumulation in patients with Werner's syndrome.* Int J Obes Relat Metab Disord, 2001. **25**(2): p. 292-5.
307. Daimon, M., et al., *Decreased serum levels of adiponectin are a risk factor for the progression to type 2 diabetes in the Japanese Population: the Funagata study.* Diabetes Care, 2003. **26**(7): p. 2015-20.
308. Maity, J., et al., *Transient overexpression of Werner protein rescues starvation induced autophagy in Werner syndrome cells.* Biochim Biophys Acta, 2014. **1842**(12 Pt A): p. 2387-94.
309. Chang, S., et al., *Essential role of limiting telomeres in the pathogenesis of Werner syndrome.* Nat Genet, 2004. **36**(8): p. 877-82.
310. Lee, S.J., et al., *A Werner syndrome protein homolog affects C. elegans development, growth rate, life span and sensitivity to DNA damage by acting at a DNA damage checkpoint.* Development, 2004. **131**(11): p. 2565-75.
311. Ryu, J.S. and H.S. Koo, *Roles of Caenorhabditis elegans WRN Helicase in DNA Damage Responses, and a Comparison with Its Mammalian Homolog: A Mini-Review.* Gerontology, 2016. **62**(3): p. 296-303.
312. Ketting, R.F., et al., *Mut-7 of C. elegans, required for transposon silencing and RNA interference, is a homolog of Werner syndrome helicase and RNaseD.* Cell, 1999. **99**(2): p. 133-41.
313. Hyun, M., V.A. Bohr, and B. Ahn, *Biochemical characterization of the WRN-1 RecQ helicase of Caenorhabditis elegans.* Biochemistry, 2008. **47**(28): p. 7583-93.

314. Marciniak, R.A., et al., *Nucleolar localization of the Werner syndrome protein in human cells.* Proc Natl Acad Sci U S A, 1998. **95**(12): p. 6887-92.
315. Ryu, J.S. and H.S. Koo, *The Caenorhabditis elegans WRN helicase promotes double-strand DNA break repair by mediating end resection and checkpoint activation.* FEBS Lett, 2017. **591**(14): p. 2155-2166.
316. Dallaire, A., et al., *Down regulation of miR-124 in both Werner syndrome DNA helicase mutant mice and mutant Caenorhabditis elegans wrn-1 reveals the importance of this microRNA in accelerated aging.* Aging (Albany NY), 2012. **4**(9): p. 636-47.
317. Dallaire, A., et al., *Expression profile of Caenorhabditis elegans mutant for the Werner syndrome gene ortholog reveals the impact of vitamin C on development to increase life span.* BMC Genomics, 2014. **15**: p. 940.
318. Massip, L., et al., *Vitamin C restores healthy aging in a mouse model for Werner syndrome.* FASEB J, 2010. **24**(1): p. 158-72.
319. Li, Y., et al., *Vitamin C alleviates aging defects in a stem cell model for Werner syndrome.* Protein Cell, 2016. **7**(7): p. 478-88.
320. Cox, L.S., et al., *Modeling Werner Syndrome in Drosophila melanogaster: hyper-recombination in flies lacking WRN-like exonuclease.* Ann N Y Acad Sci, 2007. **1119**: p. 274-88.
321. Saunders, R.D., et al., *Identification and characterization of a Drosophila ortholog of WRN exonuclease that is required to maintain genome integrity.* Aging Cell, 2008. **7**(3): p. 418-25.
322. Kusano, K., M.E. Berres, and W.R. Engels, *Evolution of the RECQ family of helicases: A drosophila homolog, Dmblm, is similar to the human bloom syndrome gene.* Genetics, 1999. **151**(3): p. 1027-39.
323. Machwe, A., et al., *The Werner and Bloom syndrome proteins help resolve replication blockage by converting (regressed) holliday junctions to functional replication forks.* Biochemistry, 2011. **50**(32): p. 6774-88.
324. Bolterstein, E., et al., *The Drosophila Werner exonuclease participates in an exonuclease-independent response to replication stress.* Genetics, 2014. **197**(2): p. 643-52.
325. Opresko, P.L., J.P. Calvo, and C. von Kobbe, *Role for the Werner syndrome protein in the promotion of tumor cell growth.* Mech Ageing Dev, 2007. **128**(7-8): p. 423-36.

326. Pichierri, P., et al., *Werner's syndrome protein is required for correct recovery after replication arrest and DNA damage induced in S-phase of cell cycle.* Mol Biol Cell, 2001. **12**(8): p. 2412-21.

327. Szekely, A.M., et al., *Werner protein protects nonproliferating cells from oxidative DNA damage.* Mol Cell Biol, 2005. **25**(23): p. 10492-506.

328. Huang, S., et al., *Characterization of the human and mouse WRN 3′→5′ exonuclease.* Nucleic Acids Research, 2000. **28**(12): p. 2396-2405.

329. Massip, L., et al., *Increased insulin, triglycerides, reactive oxygen species, and cardiac fibrosis in mice with a mutation in the helicase domain of the Werner syndrome gene homologue.* Exp Gerontol, 2006. **41**(2): p. 157-68.

330. Lebel, M., et al., *Genetic cooperation between the Werner syndrome protein and poly(ADP-ribose) polymerase-1 in preventing chromatid breaks, complex chromosomal rearrangements, and cancer in mice.* Am J Pathol, 2003. **162**(5): p. 1559-69.

331. Aumailley, L., et al., *Metabolic and Phenotypic Differences between Mice Producing a Werner Syndrome Helicase Mutant Protein and Wrn Null Mice.* PLoS One, 2015. **10**(10): p. e0140292.

332. Chang, S., *A mouse model of Werner Syndrome: what can it tell us about aging and cancer?* Int J Biochem Cell Biol, 2005. **37**(5): p. 991-9.

333. Lebel, M. and P. Leder, *A deletion within the murine Werner syndrome helicase induces sensitivity to inhibitors of topoisomerase and loss of cellular proliferative capacity.* Proc Natl Acad Sci U S A, 1998. **95**(22): p. 13097-102.

334. Lebel, M., R.D. Cardiff, and P. Leder, *Tumorigenic effect of nonfunctional p53 or p21 in mice mutant in the Werner syndrome helicase.* Cancer Res, 2001. **61**(5): p. 1816-9.

335. Wang, L., et al., *Cellular Werner phenotypes in mice expressing a putative dominant-negative human WRN gene.* Genetics, 2000. **154**(1): p. 357-62.

336. Zhang, W., et al., *A Werner syndrome stem cell model unveils heterochromatin alterations as a driver of human aging.* Science (New York, N.Y.), 2015. **348**(6239): p. 1160-1163.

337. Shimamoto, A., et al., *Reprogramming suppresses premature senescence phenotypes of Werner syndrome cells and maintains chromosomal stability over long-term culture.* PLoS One, 2014. **9**(11): p. e112900.

338. Cheung, H.H., et al., *Telomerase protects werner syndrome lineage-specific stem cells from premature aging.* Stem Cell Reports, 2014. **2**(4): p. 534-46.

339. Wang, S., et al., *Ectopic hTERT expression facilitates reprograming of fibroblasts derived from patients with Werner syndrome as a WS cellular model.* Cell Death Dis, 2018. **9**(9): p. 923.

340. Shimamoto, A., K. Yokote, and H. Tahara, *Werner Syndrome-specific induced pluripotent stem cells: recovery of telomere function by reprogramming.* Front Genet, 2015. **6**: p. 10.

341. Wu, Z., et al., *Differential stem cell aging kinetics in Hutchinson-Gilford progeria syndrome and Werner syndrome.* Protein Cell, 2018. **9**(4): p. 333-350.

342. Chen, L. and J. Oshima, *Werner Syndrome.* J Biomed Biotechnol, 2002. **2**(2): p. 46-54.

343. Makrecka-Kuka, M., G. Krumschnabel, and E. Gnaiger, *High-Resolution Respirometry for Simultaneous Measurement of Oxygen and Hydrogen Peroxide Fluxes in Permeabilized Cells, Tissue Homogenate and Isolated Mitochondria.* Biomolecules, 2015. **5**(3): p. 1319-38.

344. Roman, G., et al., *P[Switch], a system for spatial and temporal control of gene expression in Drosophila melanogaster.* Proc Natl Acad Sci U S A, 2001. **98**(22): p. 12602-7.

345. Mathur, D., et al., *A transient niche regulates the specification of Drosophila intestinal stem cells.* Science (New York, N.Y.), 2010. **327**(5962): p. 210-213.

346. Jensen, M.B., et al., *PGAM5 promotes lasting FoxO activation after developmental mitochondrial stress and extends lifespan in Drosophila.* Elife, 2017. **6**.

347. Brenner, S., *The genetics of Caenorhabditis elegans.* Genetics, 1974. **77**(1): p. 71-94.

348. Fang, E.F., et al., *NAD+ Replenishment Improves Lifespan and Healthspan in Ataxia Telangiectasia Models via Mitophagy and DNA Repair.* Cell Metab, 2016. **24**(4): p. 566-581.

349. Koopman, M., et al., *A screening-based platform for the assessment of cellular respiration in Caenorhabditis elegans.* Nat Protoc, 2016. **11**(10): p. 1798-816.

350. Fang, E.F., et al., *Tomatidine enhances lifespan and healthspan in C-elegans through mitophagy induction via the SKN-1/Nrf2 pathway.* Scientific Reports, 2017. **7**.

351. Kassahun, H., et al., *Constitutive MAP-kinase activation suppresses germline apoptosis in NTH-1 DNA glycosylase deficient C. elegans.* DNA Repair, 2018. **61**: p. 46-55.

352. O'Rourke, E.J., et al., *C. elegans major fats are stored in vesicles distinct from lysosome-related organelles.* Cell Metab, 2009. **10**(5): p. 430-5.

353. Yen, K., et al., *A comparative study of fat storage quantitation in nematode Caenorhabditis elegans using label and label-free methods.* PLoS One, 2010. **5**(9).

354. Martello, R., et al., *Quantification of cellular poly(ADP-ribosyl)ation by stable isotope dilution mass spectrometry reveals tissue- and drug-dependent stress response dynamics.* ACS Chem Biol, 2013. **8**(7): p. 1567-75.

355. Zubel, T., et al., *Quantitation of Poly(ADP-Ribose) by Isotope Dilution Mass Spectrometry.* Methods Mol Biol, 2017. **1608**: p. 3-18.

356. Trammell, S.A., et al., *Nicotinamide riboside is uniquely and orally bioavailable in mice and humans.* Nat Commun, 2016. **7**: p. 12948.

357. Sousa, C.M., et al., *Pancreatic stellate cells support tumour metabolism through autophagic alanine secretion.* Nature, 2016. **536**(7617): p. 479-83.

358. Livak, K.J. and T.D. Schmittgen, *Analysis of relative gene expression data using real-time quantitative PCR and the 2(-Delta Delta C(T)) Method.* Methods, 2001. **25**(4): p. 402-8.

359. Song, T., et al., *The NAD+ synthesis enzyme nicotinamide mononucleotide adenylyltransferase (NMNAT1) regulates ribosomal RNA transcription.* J Biol Chem, 2013. **288**(29): p. 20908-17.

360. Mouchiroud, L., et al., *The NAD(+)/Sirtuin Pathway Modulates Longevity through Activation of Mitochondrial UPR and FOXO Signaling.* Cell, 2013. **154**(2): p. 430-41.

361. Trammell, S.A., et al., *Nicotinamide riboside is uniquely and orally bioavailable in mice and humans.* 2016. **7**: p. 12948.

362. Qin, Z. and E.J. Hubbard, *Non-autonomous DAF-16/FOXO activity antagonizes age-related loss of C. elegans germline stem/progenitor cells.* Nat Commun, 2015. **6**: p. 7107.

363. Deng, H., A.A. Gerencser, and H. Jasper, *Signal integration by Ca(2+) regulates intestinal stem-cell activity.* Nature, 2015. **528**(7581): p. 212-7.

364. Egan, D.F., et al., *Phosphorylation of ULK1 (hATG1) by AMP-activated protein kinase connects energy sensing to mitophagy.* Science (New York, N.Y.), 2011. **331**(6016): p. 456-461.

365. Saha, B., et al., *Rapamycin decreases DNA damage accumulation and enhances cell growth of WRN-deficient human fibroblasts.* Aging Cell, 2014. **13**(3): p. 573-5.

366. Glick, D., et al., *BNip3 regulates mitochondrial function and lipid metabolism in the liver.* Mol Cell Biol, 2012. **32**(13): p. 2570-84.

367. Ma, D.K., et al., *Acyl-CoA Dehydrogenase Drives Heat Adaptation by Sequestering Fatty Acids.* Cell, 2015. **161**(5): p. 1152-1163.

368. Saintigny, Y., et al., *Homologous recombination resolution defect in werner syndrome.* Molecular and cellular biology, 2002. **22**(20): p. 6971-6978.
369. Johnson, N.M., B.B. Lemmens, and M. Tijsterman, *A role for the malignant brain tumour (MBT) domain protein LIN-61 in DNA double-strand break repair by homologous recombination.* PLoS Genet, 2013. **9**(3): p. e1003339.
370. Yoshino, J., J.A. Baur, and S.-i. Imai, *NAD+ Intermediates: The Biology and Therapeutic Potential of NMN and NR.* Cell Metabolism, 2018. **27**(3): p. 513-528.
371. Mitchell, S.J., et al., *Nicotinamide Improves Aspects of Healthspan, but Not Lifespan, in Mice.* Cell Metab, 2018. **27**(3): p. 667-676.e4.
372. Camacho-Pereira, J., et al., *CD38 Dictates Age-Related NAD Decline and Mitochondrial Dysfunction through an SIRT3-Dependent Mechanism.* Cell Metab, 2016. **23**(6): p. 1127-1139.
373. Ho, T.T., et al., *Autophagy maintains the metabolism and function of young and old stem cells.* Nature, 2017. **543**(7644): p. 205-210.
374. Ou, X., et al., *SIRT1 positively regulates autophagy and mitochondria function in embryonic stem cells under oxidative stress.* Stem Cells, 2014. **32**(5): p. 1183-94.
375. Huang, R., et al., *Deacetylation of nuclear LC3 drives autophagy initiation under starvation.* Mol Cell, 2015. **57**(3): p. 456-66.
376. Kume, S., et al., *Calorie restriction enhances cell adaptation to hypoxia through Sirt1-dependent mitochondrial autophagy in mouse aged kidney.* J Clin Invest, 2010. **120**(4): p. 1043-55.
377. Sengupta, A., J.D. Molkentin, and K.E. Yutzey, *FoxO transcription factors promote autophagy in cardiomyocytes.* J Biol Chem, 2009. **284**(41): p. 28319-31.
378. Hariharan, N., et al., *Deacetylation of FoxO by Sirt1 Plays an Essential Role in Mediating Starvation-Induced Autophagy in Cardiac Myocytes.* Circ Res, 2010. **107**(12): p. 1470-82.
379. Zhan, L., et al., *Autophagosome maturation mediated by Rab7 contributes to neuroprotection of hypoxic preconditioning against global cerebral ischemia in rats.* Cell Death Dis, 2017. **8**(7): p. e2949.
380. Dobbin, M.M., et al., *SIRT1 collaborates with ATM and HDAC1 to maintain genomic stability in neurons.* Nat Neurosci, 2013. **16**(8): p. 1008-15.
381. Alexander, A., et al., *ATM signals to TSC2 in the cytoplasm to regulate mTORC1 in response to ROS.* Proc Natl Acad Sci U S A, 2010. **107**(9): p. 4153-8.

382. Ma, S., F. Cao, and J. Ren, *NAD+ Precursor Nicotinamide Riboside Alleviates Alcoholic Cardiomyopathy via Mitophagy Induction: A Novel SIRT3-PGAM5-FUNDC1 Axis.* Circulation, 2018. **136**(Suppl_1).

383. Takasaka, N., et al., *Autophagy induction by SIRT6 through attenuation of insulin-like growth factor signaling is involved in the regulation of human bronchial epithelial cell senescence.* J Immunol, 2014. **192**(3): p. 958-68.

384. Xu, D.H., et al., *Long noncoding RNA MEG3 inhibits proliferation and migration but induces autophagy by regulation of Sirt7 and PI3K/AKT/mTOR pathway in glioma cells.* J Cell Biochem, 2018.

385. Xiong, J., et al., *Autophagy maturation associated with CD38-mediated regulation of lysosome function in mouse glomerular podocytes.* J Cell Mol Med, 2013. **17**(12): p. 1598-607.

386. Murata, H., et al., *SARM1 and TRAF6 bind to and stabilize PINK1 on depolarized mitochondria.* Mol Biol Cell, 2013. **24**(18): p. 2772-84.

387. Osterloh, J.M., et al., *dSarm/Sarm1 is required for activation of an injury-induced axon death pathway.* Science, 2012. **337**(6093): p. 481-4.

388. Ip, W.K.E., et al., *Anti-inflammatory effect of IL-10 mediated by metabolic reprogramming of macrophages.* Science, 2017. **356**(6337): p. 513-519.

389. Gal, J., Y. Bang, and H.J. Choi, *SIRT2 interferes with autophagy-mediated degradation of protein aggregates in neuronal cells under proteasome inhibition.* Neurochem Int, 2012. **61**(7): p. 992-1000.

390. Lang, A., et al., *SIRT4 interacts with OPA1 and regulates mitochondrial quality control and mitophagy.* Aging (Albany NY), 2017. **9**(10): p. 2163-2189.

391. Polletta, L., et al., *SIRT5 regulation of ammonia-induced autophagy and mitophagy.* Autophagy, 2015. **11**(2): p. 253-70.

Acknowledgments

I acknowledge the important contribution of collaborators who contributed on ideas and data generation of this project: Evandro F. Fang, Vilhelm A. Bohr, Yujun Hou, Martin Borch Jensen, Beimeng Yang, Henok Kassahun, Rojyar Khezri, Tyler G. Demarest, David Figueroa, Marya Morevati, Ho-Joon Lee, Hisaya Kato, Tanima SenGupta, Jong-Hyuk Lee, Deborah Filippelli, Mustafa Nazir Okur, Aswin Mangerich, Deborah L. Croteau, Yoshiro Maezawa, Costas A. Lyssiotis, Jun Tao, Koutaro Yokote, Tor Erik Rusten, Mark P. Mattson, Heinrich Jasper, Hilde Nilsen.